Behavior of gold (III) chloride during the precipitation of iron (III)/arsenic (V) in aqueous media under atmospheric and pressure conditions

Derek Blais

Department of Mining and Materials Engineering
McGill University, Montreal, Canada
August 2010

A thesis submitted to McGill University
in partial fulfillment of the requirements of the degree of
Master of Engineering

Abstract

This research has focused on the behavior of gold (III) chloride in acidic solutions containing dissolved iron (III) sulphate and arsenic (V) that have been subjected to neutralization or hydrothermal treatments. In particular, the scope of the research was the study of the co-precipitation behavior of gold (III) chloride with various iron (III) – arsenic (V) precipitates that form either in pressure oxidation and leaching autoclaves, or during the neutralization of pressure oxidation/leaching discharge solutions.

Gold (III) chloride ($5x10^{-4}$ M in 0.05 M HCl) was found to co-precipitate with ferrihydrite formed during neutralization of ferric sulphate solutions, of variable concentration, at pH 4. The amount of gold chloride that co-precipitated from solution increased with increasing temperature (22 to 90 °C) and initial iron concentration (0.075 to 0.3 M) or equivalently the surface area of the precipitate. In the presence of arsenic (V) the degree of gold chloride co-precipitation decreased due to apparent competition for adsorption on the surface of ferrihydrite. It was found that gold chloride does not adsorb onto ferric arsenate itself, but only onto co-precipitating ferrihydrite, the latter being favored at elevated temperatures and at Fe/As ratios over 1. During the heterogeneous growth of scorodite, no gold (III) chloride co-precipitated but remained in solution.

Under autoclave conditions (>200 °C) gold (III) chloride was found to co-precipitate completely during the formation of hematite, scorodite, ferric arsenate sub-hydrate (FAsH) and basic ferric arsenate sulphate (BFAS). Part of the gold chloride co-precipitated via adsorption or substitution, and the balance via reduction to a metallic state. The latter, based on thermodynamic analyses performed with the OLI software package - may be attributed to inadequate concentration of excess chloride. However, during the precipitation of natrojarosite at 200 °C there was no co-precipitation of gold chloride via adsorption or reduction.

Résumé

Cette étude porte sur le comportement du chlorure d'or (III) en solution acide contenant du sulfate de fer (III) et de l'arsenic (V) sous forme de solutés soumis à des traitements de neutralisation ou bien de type hydrothermique. En particulier, le champ d'application de la recherche liée à cette étude s'étend au comportement de co-précipitation du chlorure d'or (III) avec des précipités de fer (III) – arsenic (V) qui se forment soit par oxidation sous pression et/ou dans des autoclaves de lixiviation, soit lors de la neutralisation de solutions récupérées après oxidation sous pression/lixiviation.

Les résultats de cette étude indiquent que le chlorure d'or (III) ($5x10^{-4}$ M dans 0.05 M HCl) se co-précipite avec la ferrihydrite formée pendant la neutralisation des solutions de sulfate de fer à concentration variable et à pH 4. La quantité de chlorure d'or co-précipitée à partir de la solution augmente avec la température (22 à 90 °C) et la concentration initiale en fer de la solution (0.075 à 0.3 M) mais également avec l'aire de surface du précipité. En présence d'arsenic (V), le degré de précipitation du chlorure d'or diminue, apparemment dû au mécanisme compétitif d'adsorption de l'arsenic (V) à la surface de la ferrihydrite. L'étude indique également que le chlorure d'or ne s'adsorbe pas à l'arséniate de fer mais seulement à la ferrihydrite co-précipitée, cette dernière étant favorisée par des conditions de températures élevées et de taux de Fe/As supérieurs à 1. Lors de la croissance hétérogène de la scorodite, aucun chlorure d'or n'est co-précipité mais reste en solution.

L'étude réalisée en autoclave (>200 °C) à montré que le chlorure d'or se co-précipite dans son intégralité durant la formation d'hématite, de scorodite, d'arséniate ferrique sous-hydratée (FAsH) et d'arséniate et de sulfate de fer à caractère basique (BFAS). Une partie du chlorure d'or se co-précipite par adsorption ou substitution et le restant par réduction en or métallique. D'après des analyses thermodynamiques réalisées à l'aide du logiciel OLI, la réduction de l'or à l'état métallique pourrait s'expliquer par la présence inadéquate d'un excès d'ions chlorures. Cependant, lors de la précipitation de

la natrojarosite à 200 °C, la co-précipitation du chlorure d'or par adsorption ou par réduction n'a pas été observée.

Acknowledgements

I would like to take this opportunity to give my deepest thanks to Professor George Demopoulos for all he has done for me over the past two years. I have had the opportunity to work with some of the kindest and smartest people I have met, I am grateful for being offered a position within the Hydrometallurgy group. I also thank him for the countless help and guidance he has provided both in scholastic terms, editorial work on my thesis and on a personal level. The project would not have been completed without the invested interest and support of Dr. Peter Kondos and Barrick Gold. Their sponsorship was greatly appreciated throughout my degree. The editing of the thesis encountered numerous issues with software, the process would have been much longer and near impossible without the help of my friend Letao Wang who spent many hours learning how to code Word just to recover my files, thank you! Also, thanks goes, to Nalini Singh, for her labour in editing my thesis, during the final stages, of my thesis.

My thanks also goes out to Monique Riendeau for her help with solids characterization and other techniques, Ranjan Roy and Andrew Golsztajn for their help performing and developing methods for ICP-AES as well as the entire technical staff in the Materials Engineering department at McGill University. Moreover, I would like to send my heartfelt thanks to Barbara Hanley for her help on every issue or problem I have ever encountered while doing my Masters. She goes above and beyond the call of duty when helping graduate students, our lives would all be a lot harder if not for her. Finally, on a scholastic level I would like to thank the hydrometallurgy group who operates under the tutelage of Dr. George Demopoulos. We are a very close group and their help in terms of aid with characterization techniques, experimental set-ups and everything else helped facilitate the completion of my degree. Moreover, I thank Dr. Levente Becze for mentoring me and helping me get my ducks in a row, research wise, when I first started my degree.

Writing acknowledgements is a difficult task as there are so many people around who help us in so many ways and I feel as if this section allows me the opportunity to write a testimonial, a tribute, to all that they are, and all they have done for me. My family, those born by blood and those gained through the process of life, have always been a pillar of loyalty and a beacon of hope helping me to find my way through the fog of life. When I first started at McGill University I was a good student but I was young and did not have the best work habits or personal habits for that matter. After my first work term I had lost a considerable amount of weight and had become a more serious student who took pride in what he did. During the course of my Masters degree I found it within myself to go through a similar change by juggling work responsibilities with personal health and growth. This radical transformation over the years would not have been possible without the support of family and friends, God, Renaud (who would always tell it like it is, that honesty has always been helpful in gaining objectivity), gym partners, the makers of Chunky Soup, the letter “U” and finally personal dedication to a goal. Andrea, you helped me through one of the hardest times I’ve been through, my shining star guiding me along, making me a better person, thank you, I love you. It is possible to achieve personal and professional goals simultaneously while realizing that the things that truly matter in life are our well-being and the loved ones we keep around us. I decided not to list all of my loved ones name by name but by reading this you know I mean you! Yes, you! I thank you for standing by my side and I know that you’ll keep standing by my side in times of need, right or wrong.

Table of contents

List of figures

List of tables

List of symbols/Nomenclature

FAsH	Ferric arsenate sub-hydrate
BFAS	Basic ferric arsenate sulphate
POX	Pressure oxidation
BFS	Basic ferric sulphate
OLI	OLI StreamAnalyzer software package version 3.0
AR	*Aqua regia*
Physisorption	Physical adsorption
Chemisorption	Chemical Adsorption
RPT	Repeat (ie. repeat experiment)

Chapter 1: Introduction

The recovery of gold from ores and concentrates has evolved over the years with processing routes becoming increasingly complex. Given the high value of gold, any reduction in losses during recovery operations constitutes an important economic benefit. One such loss that needs to be addressed is the potential solubilization of gold during pressure oxidation (POX) of refractory sulphidic gold feedstocks. For example, Agnico Eagle Mines [1] recently reported a loss in gold recovery due to the formation of a gold chloride complex. Gold is known to form complexes in solution, such as gold (III) chloride, if an excess of chloride ions are present. The fate of such soluble gold chloride during pressure oxidation and the subsequent neutralization of the acidic discharge slurry will determine if gold is lost or recovered in the downstream cyanidation operation. Thus it is of interest to know under what conditions gold chloride may stay soluble or co-precipitate along primary (formed in the autoclave) or secondary (formed during neutralization) precipitates. Furthermore, the mode of co-precipitated gold, such as: adsorption on iron compounds, like goethite and hematite[2, 3]; substitution in one of the precipitated phases; or finally chemical reduction to metallic state would have consequences in terms of gold recovery.

For these reasons the behavior of gold (III) chloride in acidic iron (III) sulphate/arsenate solutions during hydrothermal or neutralization treatment was investigated. In particular two types of experiments were carried out. The first involved atmospheric pressure precipitation of iron (III) (with and without arsenate) by neutralization to pH 4 in the presence of gold chloride (100 mg/L Au as $HAuCl_4$). This investigation involved examination of solution composition (iron(III) concentration, Fe/As molar ratio, Cl/Au molar ratio) and temperature (20-90 °C). The second series involved autoclave experiments under various conditions favoring the formation of crystalline iron (III) and arsenate phases and monitoring the behavior of gold chloride over the temperature range of 200-250 °C. The obtained results from the two series of experiments are presented in Chapters 4 and 5, respectively. Chapter 2 is a literature review covering a

brief description of the POX process followed by discussion of the formation of different iron (III) and arsenate precipitates. In the same chapter, the behavior of gold (III) chloride in terms of stability (resistance to reduction) in solution is analyzed with the aid of the OLI thermodynamic package to set the scene for the experimental investigations undertaken. The adsorption of gold chloride on iron oxides is also covered. Chapter 3 discusses the experimental methodology for executing the various precipitation experiments and provides a record of all analytical techniques employed during the course of this research. The global conclusions drawn from this research are found in Chapter 6.

Chapter 2: Literature review and theory

2.1 Gold recovery

Originally gold extraction was performed using simple gravity separation of crushed ores. Gravity separation exploits differences in specific gravity between gold and the host ore to affect the recovery of coarse metallic gold particles. Cyanidation on the other hand is used for the recovery of fine or ultrafine but liberated gold grains [4] . During cyanidation gold forms a complex, $Au(CN)_2^-$, which is stable in solution. The gold-bearing cyanide leach solution is commonly contacted with activated carbon where the complex adsorbs to the surface of carbon. It is subsequently recovered by elution and electrowinning. Some ores, deemed refractory, are resistant to direct cyanidation because gold occurs within the crystal structure of sulphidic host minerals requiring pretreatment prior to cyanidation [5]. In addition to gold ores, gold is also recovered as by-product from copper sulphide concentrates.

2.1.1 Nature of refractory gold

Gold found in sulphide minerals, such as pyrite and arsenopyrite, represents an important source of gold in industry [4]. As the arsenic content increases in these types of ore so too does the amount of gold, which is found in localized regions throughout the mineral structure. Much of the gold found within these minerals is termed “invisible” gold as it is impossible to view using optical microscopic techniques [6]. However, using advanced characterization techniques, such as Mössbauer spectroscopy, gold rich regions may be identified and the chemical state of gold can be ascertained. It has been reported [7] that at magnifications over 750,000 times, gold rich areas in aresnopyrite reveal no micro-precipitates. This suggests the presence of chemically bonded gold within the arsenopyrite mineral structure and similar results show chemically bonded gold in certain pyrite ores [7]. Thus, it is possible that gold can be incorporated into the structure of forming iron and arsenic products as well as undergo reduction to metallic state given the presence of impurities or reducing agents [8].

2.1.2 Processing of refractory gold ores

To affect the recovery of refractory gold the host sulphidic minerals, arsenopyrite and pyrite, need to be oxidized prior to cyanidation in order to liberate the trapped gold. Traditionally, this oxidative treatment involved roasting of a concentrate. However, economic and environmental factors have led to the development of hydrometallurgical oxidation processes for achieving the same. Among these are pressure oxidation and biooxidation [9]. Pressure oxidation carried out at temperatures 190-240 °C is by far the most successful refractory gold processing technology. Upon pressure oxidation the gold reports to the residue from which it is recovered by cyanidation following washing and neutralization. Similarly to pressure oxidation gold present in copper concentrates may report to the residue from which it can be recovered, as is the case of the CESL process [10, 11].

2.2 Pressure oxidation

The pressure oxidation treatment of refractory gold-bearing minerals involves a number of processing steps as seen in Figure 1. Slurried crushed/ground ore, or concentrate, is fed into a multi compartment autoclave where it is made to react with oxygen. Oxidized iron, arsenic and sulphur (as sulphate) are released temporarily into solution where most ions later form precipitates “in-situ”. Depending on the operating conditions a wide range of precipitates may form.

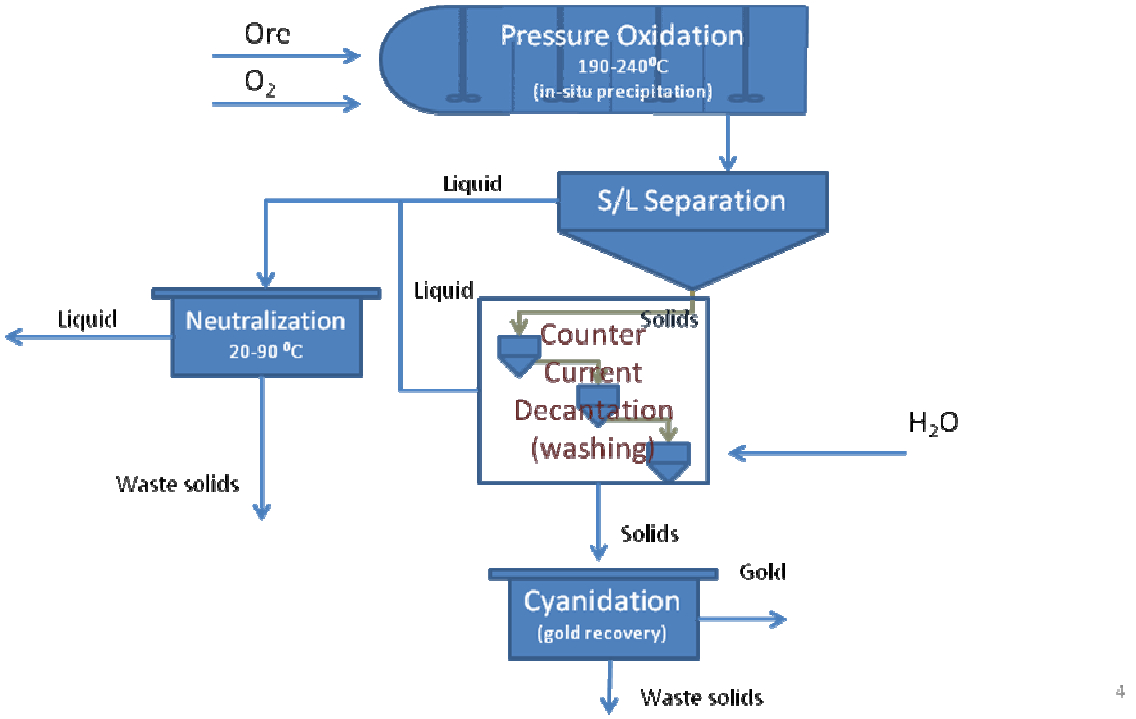

Figure 1: General flowsheet for the recovery of refractory gold via pressure oxidation

Pressure oxidation may be conducted in either acidic or alkaline media. Acidic media remains the prominent route used in industry, whereas alkaline oxidation may be applied industrially in special cases. For proper oxidation the autoclave operating temperature should be above 180 °C to ensure complete oxidation of all sulphides present to the sulphate form of sulphur. Elemental sulphur forming at lower temperatures is undesirable as it interferes with the oxidation process and the downstream recovery of gold by cyanidation [12]. After pressure oxidation the solids and liquids are separated and the solids are sent to cyanidation to recover the gold, which was liberated during pressure oxidation (POX). The liquid, which still contains dissolved iron and arsenic, is neutralized to completely precipitate all the metals from solution. As in POX, stable gold complexes can react with compounds that form during neutralization.

2.3 Precipitation during POX

2.3.1 Supersaturation theory

Before discussing the possible precipitates formed within the POX autoclave or neutralization tanks, a brief reference to supersaturation theory is made [13]. The nucleation and growth of a compound by precipitation is governed by the prevailing supersaturation environment. At high supersaturation fast homogeneous nucleation occurs while growth requires seed crystals and a low supersaturation. The produced compounds may be amorphous, crystalline, metastable or stable. According to Stranski's law or the Oswald rule of stages [14], the least stable phase shall precipitate preferentially if the supersaturation is high enough, i.e. if homogeneous nucleation dominates [14]. The initially forming compound is metastable and may transform into various phases (such as iron oxides and oxyhydroxides in the present system) over time, depending on the solution chemistry and kinetics.

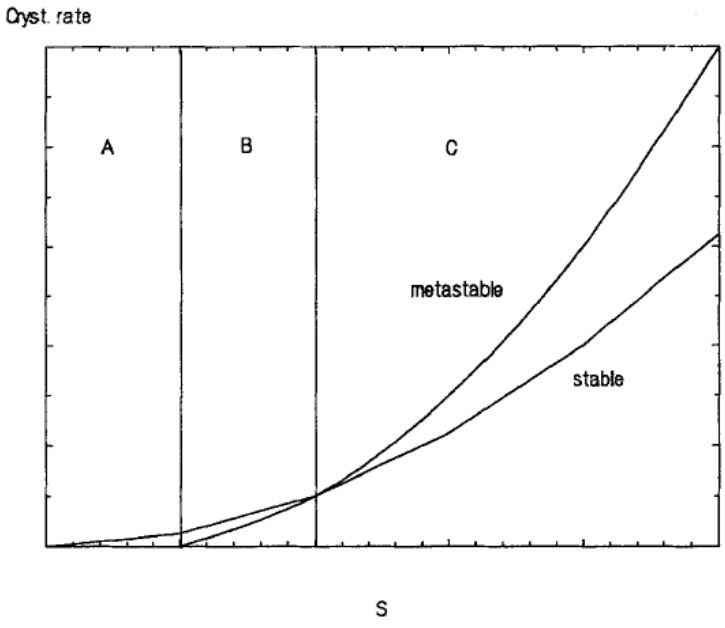

Figure 2: Crystallization rate versus super saturation ratio [14]

At low supersaturation levels and in the presence of seed it is possible to avoid the precipitation of metastable phases altogether. As the level of supersaturation increases, there is competition between the possible precipitate phases as shown in Figure 2 [14].

Thus during in-situ precipitation if the release of ions into solution due to oxidation is slow, the metastable phases may not form.

2.3.2 Pyrite oxidation and in-situ precipitates

Pyrite may undergo two competing reactions upon oxidation however under POX conditions reaction 1 is dominant [9]:

$$FeS_2 + \frac{7}{2}O_2 + H_2O \rightarrow FeSO_4 + H_2SO_4 \quad (1)$$

$$FeS_2 + 2O_2 \rightarrow FeSO_4 + S^\circ \quad (2)$$

Upon the formation of ferrous ions there is a subsequent oxidation to ferric via the following reaction:

$$FeSO_4 + \frac{1}{2}O_2 + H_2SO_4 \rightarrow Fe_2(SO_4)_3 + H_2O \quad (3)$$

As ferric ions are produced they are subjected to hydrolysis reactions which, depending on the solution chemistry and operating conditions, may form several in-situ precipitates such as: hematite, basic ferric sulphate (BFS) and several types of jarosites that may be stable or metastable.

As the temperature is increased, the kinetics favouring the rate of hydrolysis into higher ordered crystal structures increases and less of the initial metastable phase forms [15]. In the temperature range of 150-250 °C ferric sulphate may hydrolyze to basic ferric sulphate or hematite as seen in Equations 4 and 5 respectively. In general the formation of hematite is favoured by temperature elevation, lowering of ferric concentration, lower acid concentration and the presence of excess sulphate in the form of metal sulphates [15].

$$Fe_2(SO_4)_3 + 2H_2O \rightarrow Fe(OH)SO_4 + 2H_2SO_4 \quad (4)$$

$$Fe_2(SO_4)_3 + 3H_2O \rightarrow Fe_2O_3 + 3H_2SO_4 \quad (5)$$

2.3.2.1 The effect of sulphate ions on iron precipitation

It has been reported, as far back as the 1920s, that at 200 °C hematite is only stable (in a SO_3-H_2O) below SO_3 concentrations of 5.58% [16]. If this is exceeded basic ferric sulphate will form. This amount of SO_3 is attributable to the total sulphate content, meaning both the sulphuric acid and sulphate from any salts present [17]. These results were confirmed by modern day researchers who found the critical amount of SO_3 to be 5.93% [18]. As the amount of SO_3 affects the final products, one may look at the initial free acidity to determine the value at which the hematite stability region ends. As the temperature of the system increases, the stability region of hematite grows [18]. Although an increase in total sulphate content causes a transition from the stability region of hematite to the stability region of basic ferric sulphate - it is interesting to note that the presence of soluble metal sulphate salts, such as $MgSO_4$ or $ZnSO_4$, actually aid in increasing the stability region of hematite [17, 19]. This phenomenon has been explained by Tozawa *et al.* to result from the formation of the bisulphate ion (Equation 6) that reduces the free proton concentration; shifting the hematite equilibrium to high free acid concentrations. [17, 20].

$$HSO_4^- \rightarrow SO_4^{2-} + H^+ \quad (6)$$

2.3.2.2 The effects of temperature and ferric sulphate concentration

Voight and Gobler have reported on the effect of temperature on hematite formation by performing tests between 100 and 300 °C for times of 1,6 and 24 hours [21] in which the iron concentration was kept at 1 M. At 150 °C the only phase that was found to form was hydronium jarosite. Even after 100 hours no other phases formed. With a residence time of 6 hours, a temperature of 200 °C was required to see the formation of basic ferric sulphate, while 250 °C was the required temperature for the production of hematite. The same results were obtained when the residence time was increased to 24

hours, however, the basic ferric sulphate phase formed even at 300 °C. Analysis of these results by Cheng and Demopoulos [22] led to the conclusion that the produced basic ferric sulphate in Voight and Gobler's work is indeed metastable, transforming to hematite upon temperature elevation and time extension. This is said to occur via a dissolution/re-crystallization mechanism. There is a discrepancy between the results of Voight and Gobler [21] and of Umetsu *et al.* [18], which is more evidence of the attainment or not of equilibrium in the respective studies. The concentration of iron in Voight and Gobler's tests was 1 M, which is a high concentration (or equivalently supersaturation) apparently favoring homogeneous nucleation giving rise to the formation of metastable BFS. Both Umetsu *et al.* [18] and Cheng and Demopoulos [17] performed hydrolysis experiments under varying iron (III) sulphate concentrations and noted the transition from hematite to BFS formation. This is exemplified with the data reproduced in Figure 3. Similar tests were performed by Dutrizac and Chen [23] at 225 °C where similar conclusions are drawn.

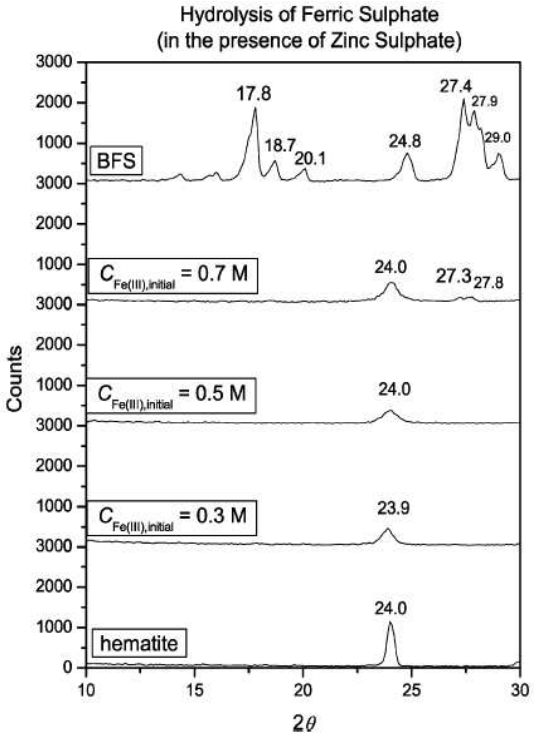

Figure 3: Effect of ferric sulphate concentration on the final product [15]

Hematite precipitation was found to be favored up until 0.3 M; after 0.5 M basic ferric sulphate dominated [24]. Apparently upon a ferric sulphate concentration increase, the excessive supersaturation leads to the formation of the metastable phase as per Stranski's law, which in this case is metastable basic ferric sulphate. These results agree with continuous reactor tests performed by Randolph *et al.* [25]. During these experiments the solids were recycled to provide seed. In doing so, the percentage of hematite in the solids was increased. This effect is due to the transformation of metastable basic ferric sulphate facilitated by the longer retention time. At the same time, this seed may have acted as nucleation sites for the heterogeneous precipitation and growth of hematite particles.

2.3.2.3 The precipitation of jarosite

During pressure oxidation of gold-bearing ores, various metal cation-impurites, like lead or sodium, may be released to the solution. In the presence of such cations it is possible that the system favors the formation of a different iron precipitate: jarosite. Jarosite occurs in many forms having the basic formula $MFe_3(SO_4)_2(OH)_6 \cdot xH_2O$ where M may be H_30^+, K^+, Na^+, Ag^+, NH_4^+, $0.5Pb^{2+}$ to name a few [26]. Jarosite is known to be the favourable iron precipitate by which iron is rejected in zinc plants [27, 28].

$$\mathbf{Fe_2(SO_4)_3 + Na_2SO_4 + 12H_2O \rightarrow 2NaFe_3(SO_4)_2(OH)_6 + 6H_2SO_4} \quad (7)$$

The formation of natrojarosite from sodium sulphate/ferric sulphate solutions is seen in Equation 7. The stability region for jarosite, seen in Figure 4, depends on the temperature and pH of the system. According to the equilibrium constant for natrojarosite (Equation 8) [26] its stability is dependent on there being a low free acid concentration as well as high concentrations of sulphate, ferric and sodium ions.

$$\mathbf{K = (aH^+)^6 * (aFe^{3+})^{-3} * (aNa^+)^{-1} * \left(aSO_4^{2-}\right)^{-2}} \quad (8)$$

In addition to equilibrium factors, the kinetics of jarosite precipitation need to be taken into account. Jarosite precipitation is known to have very slow kinetics under atmospheric conditions [29], but is accelerated under autoclave conditions and in the presence of seed [30]. Under POX conditions (>180 °C) jarosite forms, and has been known to cause the loss of silver [24, 31].

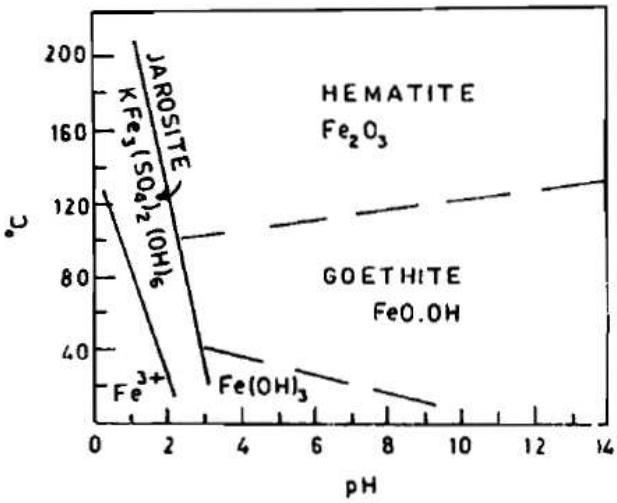

Figure 4: "Stability region" of potassium jarosite [26]

2.3.3 Arsenopyrite oxidation and in-situ precipitates

The oxidation behavior of arsenopyrite under pressure oxidation conditions has been studied by Papangelakis and Demopoulos [32, 33]. During two hour oxidation/precipitation experiments performed between 130 to 180 °C, it was observed that most of the iron released from arsenopyrite is in ferric form (i.e. most ferrous ions quickly oxidized to ferric under the applied conditions), some of the sulphur to be in elemental form (with this form decreasing with increasing temperature) and finally most of the arsenic to be in the pentavalent form [32]. Like in the case of pyrite, two competing oxidation reactions (Equations 9 and 10) were proposed to occur, one producing elemental sulphur and the other sulphate ions. At higher temperatures Equation 10 is favored.

$$4FeAsS + 13O_2 + 6H_2O \rightarrow 4H_3AsO_4 + 4Fe^{2+} + SO_4^{2-} \quad (9)$$

$$4FeAsS + 7O_2 + 8H^+ + 2H_2O \rightarrow 4H_3AsO_4 + 4Fe^{2+} + 2S^0 \quad (10)$$

Ferrous ions released during the dissolution of arsenopyrite are further oxidized to the trivalent state via a reaction with oxygen:

$$2Fe^{2+} + \frac{1}{2}O_2 + 2H^+ \rightarrow 2Fe^{3+} + H_2O \quad (11)$$

Under conditions of high solids loading, Papangelakis and Demopoulos [32] found that the oxidation products of iron and arsenic precipitated out of solution as crystalline scorodite ($FeAsO_4 \cdot 2H_2O$) as summarized in Equation 12. During the batch experiments it was observed that precipitation only occurred after the levels of ferric and arsenate ions reach appropriate supersaturation levels.

$$2H_3AsO_4 + Fe_2(SO_4)_3 + 4H_2O \rightarrow 2FeAsO_4 \cdot 2H_2O + 3H_2SO_4 \quad (12)$$

In terms of kinetics, the dissolution of arsenopyrite was reported to occur via a shrinking core model with the surface chemical reaction as the rate controlling step [33]. This may be seen as an electrochemical reaction wherein chemically adsorbed oxygen on the surface of arsenopyrite has two single-electron transfers with the mineral.

Since real refractory concentrates are composed of mixed minerals during POX precipitation, different phases may form under variable solution composition conditions The precipitation of iron (III) and arsenate phases from complex Fe(III)-As_2O_5-SO_4 solutions under hydrothermal conditions was originally studied by Swash and Monhemius [34]. These authors reported the formation of two new ferric arsenate phases, in addition to scorodite, which they labeled “Type 1” and “Type 2”. Later Dutrizac and Jambor [35] reported on similar phases that they labeled “Phase 3” and “Phase 4”. This confusion was recently cleared via a comprehensive characterization program carried out by Gomez *et al.* [36, 37]. In addition to scorodite ($FeAsO_4 \cdot 2H_2O$), ferric arsenate sub-hydrate (FAsH, $FeAsO_4 \cdot ¾ H_2O$ previously labeled as Type 1 or Phase

4) and basic ferric arsenate sulphate (BFAS, $Fe[(AsO_4)_{1-x}(SO_4)_x(OH)_x] \cdot wH_2O$, previously labeled Type 2 or Phase 3) may precipitate during pressure oxidation of refractory gold ores. The specific arsenate phase that may precipitate depends on the temperature and the iron to arsenic molar ratio as depicted in Figure 5.

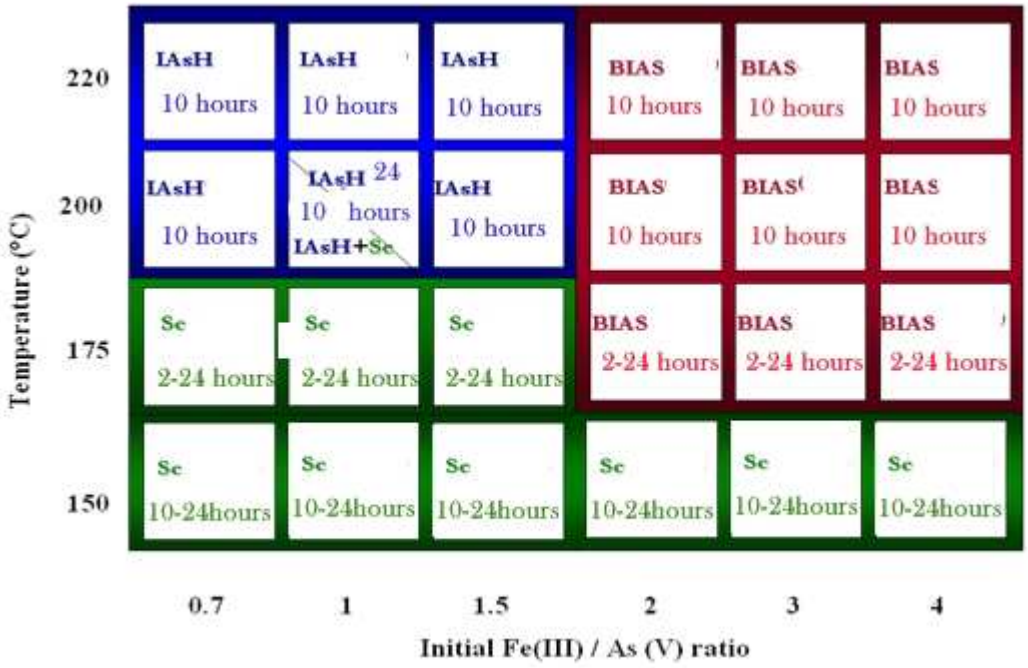

Figure 5: Temperature and molar ratio dependence for iron-arsenic precipitates in the autoclave [36]

Industrially, most pressure oxidation circuits have an iron to arsenic ratio well above 1 and given that the applied temperature is above 180 °C, BFAS is expected to be the dominant arsenate-bearing precipitated phase - as found in industrial residues analyzed by Dutrizac and Jambor [35] and Gomez *et al.* [37]. Alternatively, in the case of copper pressure leaching, as in the case of Teck's CESL process that operates at 150 °C, scorodite is expected to be the dominant arsenate phase [38]. Excess ferric iron may still of course precipitate as hematite, basic ferric sulphate or jarosite.

2.4 Precipitation during autoclave discharge solution neutralization

As per the flowsheet in Figure 1, the autoclave solution is subjected to neutralization in order to meet environmental standards. It follows that the pH must be adjusted and any harmful elements such as iron, arsenic, etc must be controlled. There are, once more, different forms into which iron and arsenic may precipitate under atmospheric pressure (and T<100 °C). These principally include ferric hydroxide/ferrihydrite, goethite and jarosite in terms of iron; and amorphous/poorly crystalline ferric arsenate, arsenate-bearing ferrihydrite or crystalline scorodite. Of these precipitates ferric hydroxide/ferrihydritee and ferric arsenate/scorodite are considered most relevant in terms of POX acidic discharge solution neutralization operations.

2.4.1 Ferric hydroxide/ferrihydrite

Ferric hydroxide (ferrihydrite) precipitation commonly occurs during neutralization of relatively low concentration ferric sulphate solutions, as is the case of acidic leach solution pre-neutralization (at around 60-80 °C) practiced in the laterite industry [39], acidic effluent treatment (typically at ambient temperature) [40] or neutral leaching of zinc calcine [24]. The produced ferrihydrite (the 2-line variety) [41] is amorphous and ultrafine (4-6 nm) [42], hence imposing dewatering challenges. The generation of ultrafine, amorphous ferrihydrite is the consequence of precipitation occurring well over the critical supersaturation limit [13]. As the supersaturation is increased so too is the driving force: homogeneous nucleation occurs more rapidly and there is less time for growth of particles. As a result the surface area of ferrihydrite tends to be high as it consists of nanosized particles. Owing to its large surface area it tends to remove impurity ions (both cations and anions) via adsorption [13, 24]. If neutralization is properly carried out, for example via staged pH elevation and recycling/seeding, well grown ferrihydrite (2-line or even 6-line variety [42]) may be obtained [13, 40]. Impurity-free ferrihydrite transforms into goethite or hematite over time as it is a metastable hydrous iron oxide [43]. Transformation of iron oxides typically occurs via a dissolution/re-crystallization mechanism that obeys the Oswald rule of stages [14].

2.4.2 Ferric Arsenate, scorodite and As-bearing ferrihydrite

The high temperature autoclave precipitation section dealt with the in-situ formation of scorodite. At lower temperatures during neutralization of the discharge solution, any arsenate species in solution may co-precipitate along with iron as arsenate-adsorbed on ferrihydrite [44, 45] and/or poorly crystalline ferric arsenate [46]. Alternatively, at temperatures above 70 °C and under controlled supersaturation (regulated by neutralization) conditions, crystalline scorodite may form [47].

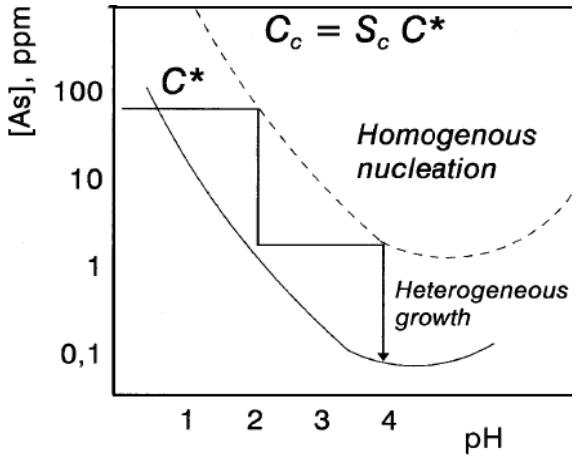

Figure 6: Controlled precipitation of crystalline scorodite (atmospheric) [48]

The controlled precipitation of scorodite can be described with the aid of Figure 6. In order to form crystalline scorodite, precipitation must occur within the heterogeneous precipitation zone at low supersaturation (seen between the solid and dotted line in Figure 6). This is achieved via a step-wise increase of pH using MgO or $Ca(OH)_2$ of which lime is the industrially preferred base [48]. Following scorodite precipitation, the residual arsenic is removed from solution at higher pH via adsorption of arsenate ions onto the surface of ferrihydrite that forms from the excess iron (initial ferric/arsenate molar ratio > 1) [49]. It is interesting to note that arsenate-adsorbed on ferrihydrite has been observed to transform to ferric arsenate under certain conditions [45, 50].

2.5 Behavior of Gold (III) chloride

Chloride ions may enter a POX circuit as a component of the ore, but more commonly it does so as a constituent of the plant water. In the presence of chloride ions the chemically bonded gold released during POX may solubilize (at least partially) hence it is interesting to review the relevant chemistry of gold complexes. Gold can form complexes in the form of aurous (Au^{+}) or auric (Au^{3+}). A prevalent aurous complex commonly seen is gold (I) cyanide $Au(CN)_2^-$, however in the presence of halides, such as chloride, gold may form complexes as well [51]. Gold (III) chloride is more stable than gold (I) chloride and is the focus of discussion as background to the experimental work described in the Results and Discussion chapters. The chemistry of gold (III) chloride is reviewed with the aid of the thermodynamic software program OLI (OLI StreamAnalyzer version 3.0 www.olisystems.com).

2.5.1 Reduction/oxidation and complexation of gold

Gold is a noble metal, which means that it prefers to remain in its solid elemental state as opposed to an oxidized form as a compound or dissolved ion. Its high stability as metal is manifested by the respective standard reduction potentials involving the aurous (Au^{+}) and auric (Au^{3+}) ions.

$$Au^{3+} + 3e^- \rightarrow Au_{(s)} \qquad e^o = 1.498V \tag{13}$$

$$Au^{+} + e^- \rightarrow Au_{(s)} \qquad e^o = 1.692\ V \tag{14}$$

These reduction potentials are above the standard reduction potential of O_2 the oxidant used in POX, so the oxidation of gold is not thermodynamically feasible under these conditions:

$$\frac{1}{2}O_2 + 2e^- + 2H^+ \rightarrow H_2O \qquad e^o = 1.23\ V \tag{15}$$

Figure 7 shows the eh-pH (Pourbaix) diagram for the gold-water system at 25 °C with the activities of the species set to 10^{-4}. From this diagram we see that gold cannot be oxidized by oxygen. Alternatively it may be stated that free gold ions are unstable and convert to metallic gold within the stability region of water.

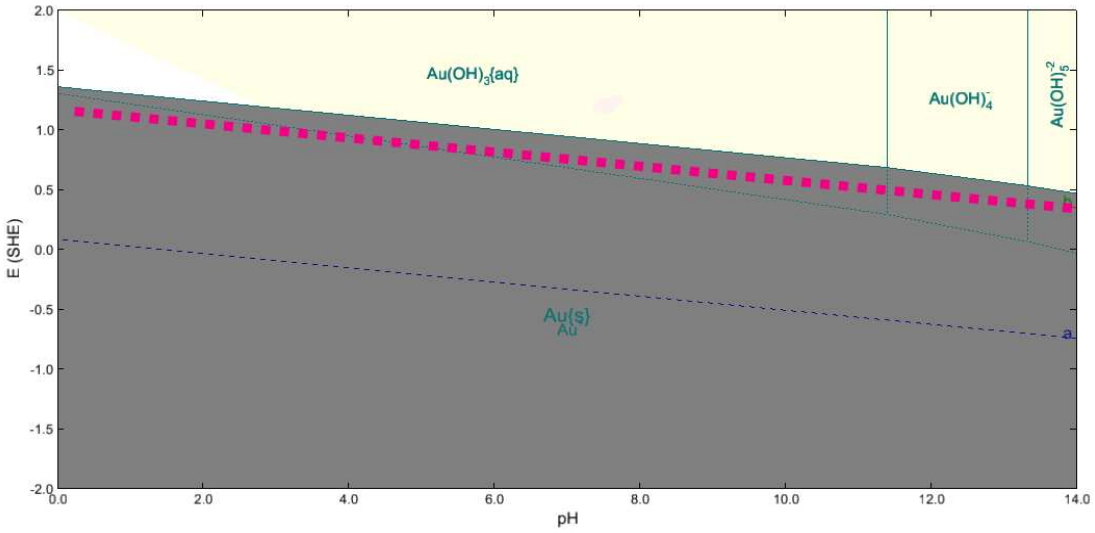

Figure 7: Pourbaix diagram of gold-water system constructed with the aid of OLI (Version 3.0) at 25 °C and species activities of 10^{-4}

However, the stability of gold is greatly affected in the presence of complexing agents. In fact, the great effectiveness of cyanidation is owed to the formation of the strong gold(I) cyanide complex [4].

Similarly gold may form complexes with chloride, bromide or iodide ions. The standard potentials for these auro-halogen complexes are listed below [52].

$$AuCl_4^- + 3e^- \rightarrow 4Cl^- + Au_{(s)} \quad e^o = 1.002\ V \tag{16}$$

$$AuBr_4^- + 3e^- \rightarrow 4Br^- + Au_{(s)} \quad e^o = 0.854\ V \tag{17}$$

$$AuI_4^- + 3e^- \rightarrow 4I^- + Au_{(s)} \quad e^o = 0.56\ V \tag{18}$$

Equations 16 through 18 show a decrease in the standard reduction potential of gold as it is complexed with various halides. By considering the $AuCl_4^-$/Au couple it becomes evident that its standard reduction potential lies below that of oxygen for the pH region below 4, which implies that gold can be oxidized by oxygen. Alternatively, it may be said that thermodynamically speaking, the gold (III) tetrachlorocomplex ($AuCl_4^-$) is stable, or that gold is soluble under these conditions.

2.5.1.1 Calculating the gold (III) chloride solubility in the $AuCl_3$-H_2O system

Calculating the maximum gold (III) chloride solubility, as the $AuCl_4^-$ complex, provides insight of extent to which gold may be present as a complex in solution at various temperatures. Using the OLI software package (StreamAnalyzer Version 3.0) the solubility of gold chloride was surveyed as a function of temperature for a different initial $AuCl_3$ concentration. This was first performed for the simple system of $AuCl_3$-H_2O. In order to ensure that there was no evaporation of water at high temperatures, the formation of the water vapor phase was suppressed. If this is not done then there will not be any water left at high temperatures. The calculated solubilities are plotted in Figure 8 where the y-axis shows the soluble fraction of $AuCl_3$ as $AuCl_4^-$ (in moles) while the figure legend displays the initial moles of $AuCl_3$ input to the system.

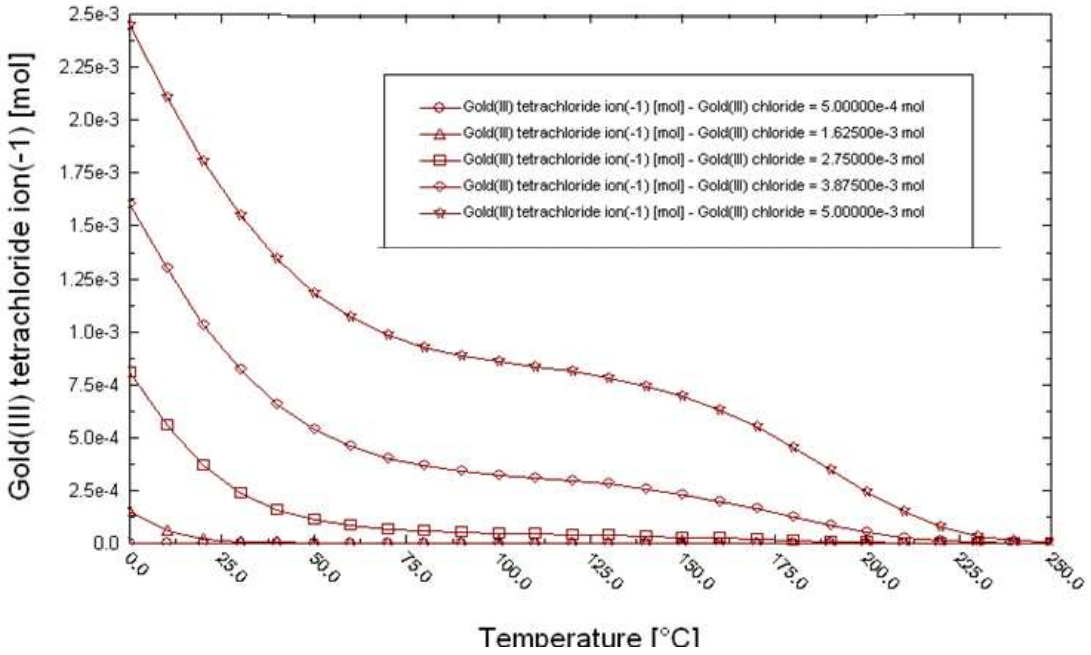

Figure 8: Amount of gold tetrachloride in solution between 0 and 250 °C with varying initial amounts of $AuCl_3$ ($5x10^{-4}$ to $5x10^{-3}$)

As in the case of stoichiometric $AuCl_3$ in water, only a fraction of it is soluble, this fraction decreases with decreasing concentration (activity) and decreases with increasing temperature. Thus at $5x10^{-4}$ mol of $AuCl_3$ (corresponding to approximately 100 mg/L Au) essentially no soluble complex appears, even at 25 °C. By increasing the initial amount of $AuCl_3$ to $5x10^{-3}$ moles, approximately half of the gold reports as a soluble complex at 25 °C. At 250 °C, independent of the initial amount of $AuCl_3$, it can be seen that there is no gold left in solution.

Since it was determined that most of gold precipitates out of solution in the $AuCl_3$-H_2O system, it is important to know in what form it is precipitating. In order to determine the nature of precipitated gold under the same conditions, OLI was used again to analyze the $AuCl_3$-H_2O system. The gold chloride input for this calculation was set to $5x10^{-4}$ moles. The results for this analysis are shown in Figure 9.

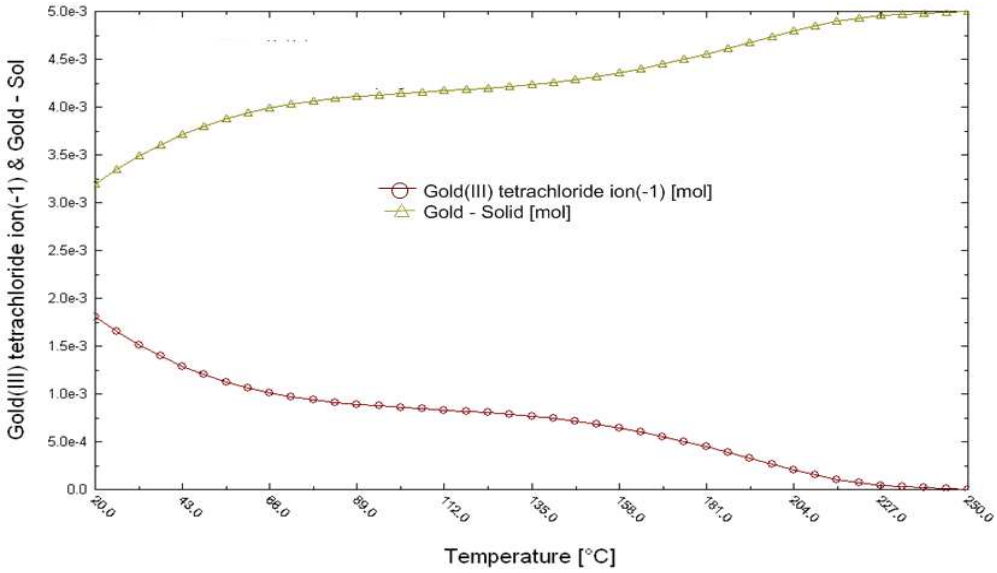

Figure 9: Thermodynamic prediction of gold products in the $AuCl_3$-H_2O system with an initial amount of $AuCl_3$ of $5x10^{-4}$ moles as a function of temperature

It can be seen that the precipitated gold is metallic in nature, which suggests that $AuCl_3$ is thermodynamically unstable being reduced from auric (Au (III) state) to metallic gold (Au (0) state). The reduction of stoichiometric "$AuCl_3$" to metallic gold apparently occurs in this pure $AuCl_3$-H_2O system via a reaction with water:

$$AuCl_3 + \frac{3}{2}H_2O \rightarrow Au + \frac{3}{4}O_2 + 3HCl \quad (19)$$

2.5.1.2 Calculating the gold (III) chloride solubility: the effect of excess chloride ions

The standard reduction potential for gold (III) chloride is:

$$AuCl_4^- + 3HCl + 3e^- \rightarrow Au_{(s)} + 4Cl^- \quad e^o = 1.002\ V \quad (20)$$

Using the above reaction we can calculate the equilibrium constant of the reaction by taking the activity of the products over that of the reactants Equation 21 and then combining it with the Nernst equation (Equation 22):

$$K = \left(\frac{a(Cl^-)^4 \times aAu}{aAuCl_4^-} \right) \tag{21}$$

$$e = e^{=} - \frac{RT}{nF} \ln\left(\frac{a(Cl^-)^4 \times aAu}{aAuCl_4^-} \right) \tag{22}$$

The activity of chloride ions has a great impact on whether gold will remain in solution. The Nernst equation seen in Equation 22 dictates that (using a concentration of $5x10^{-4}$ M for $AuCl_4^-$) as the chloride concentration increases we should obtain a reduction potential of 1.02 for a concentration of 0.075 M Cl^- and 1.2V for 0.0005 M of Cl^-. This example demonstrates that by having an excess of free chloride ions the oxidation of gold becomes easier and the gold tetrachloride complex becomes more stable, i.e. the gold chloride solubility increases.

The effect of excess chloride ions (in the form of HCl) on the stability (or equivalently solubility) of the gold tetrachloride complex is illustrated in Figure 10.

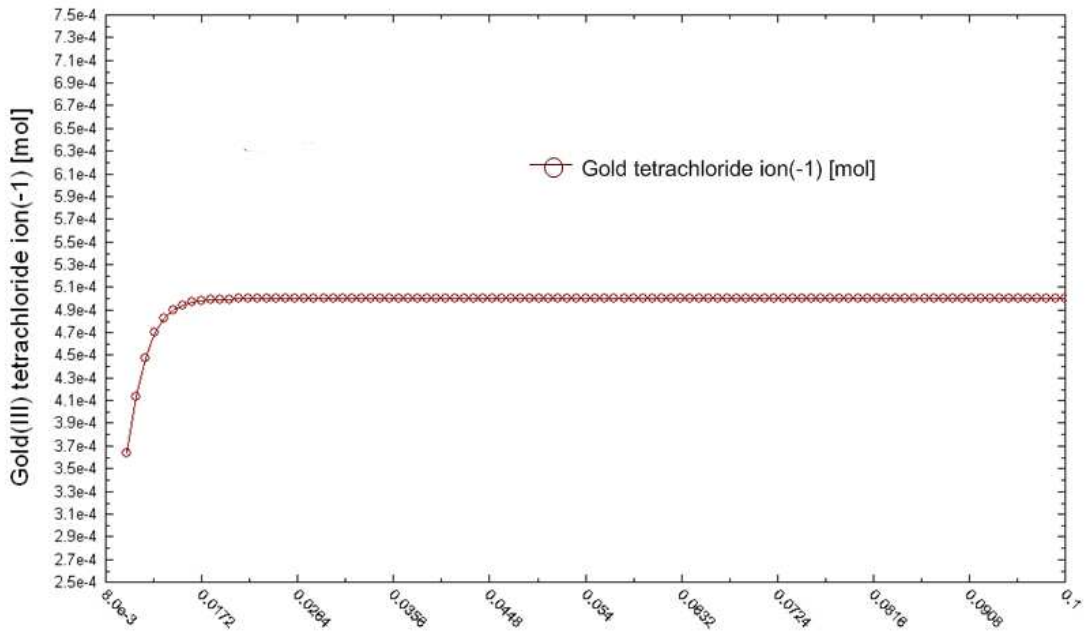

Figure 10: Stability of gold chloride concentration with excess chloride ions at 25 °C

At zero or low chloride ion excess there is virtually no gold tetrachloride in solution, which is similar to the results obtained in Figure 8 when no hydrogen chloride was added. As the concentration increases a plateau is reached which indicates that all of the gold (III) chloride ($AuCl_3$) is in solution. The molar ratio of $Cl^-/AuCl_3$ required for this gold concentration ($5x10^{-4}$ M) to be fully soluble is approximately 4 times at 25 °C. As a result of the presence of excess chloride ions, gold can be oxidized by oxygen or alternatively it can be said that gold chloride becomes soluble. This is illustrated in the Pourbaix diagram in Figure 11 built with the aid of OLI for the case of 10^{-4} molal gold and 10^{-2} molal HCl.

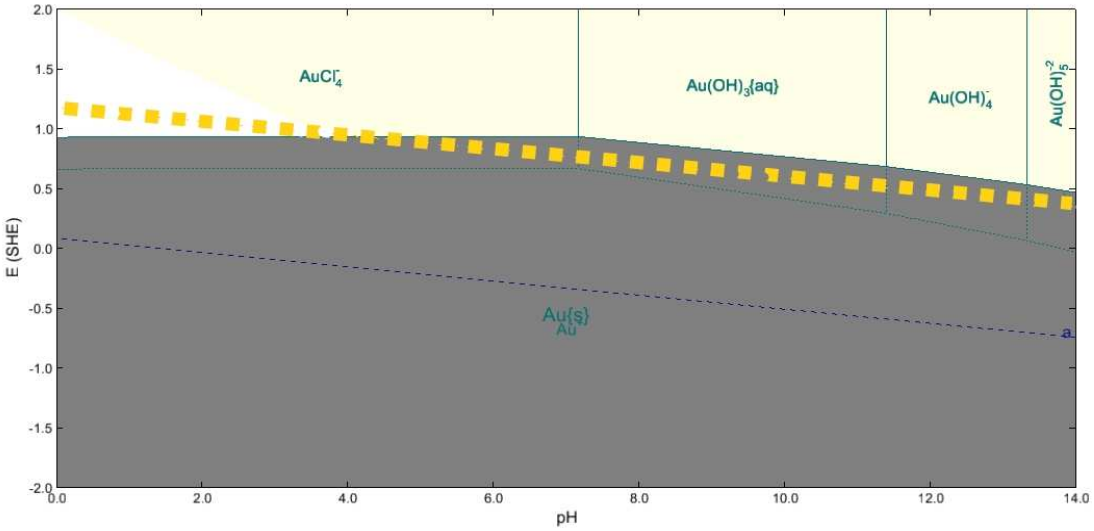

Figure 11: Pourbaix diagram of gold-chloride-water system at 25 °C with activities of 10^{-4} for Au and for 10^{-2} Cl

It has been shown in Figure 8 that temperature decreases the solubility of gold (III) chloride in the absence of excess chloride via a reduction of gold chloride by water seen in Equation 19. Thus the system was examined as a function of excess chloride ion concentration and temperature from 25 °C to the upper limit of POX temperatures (250 °C). The results are shown in Figure 12.

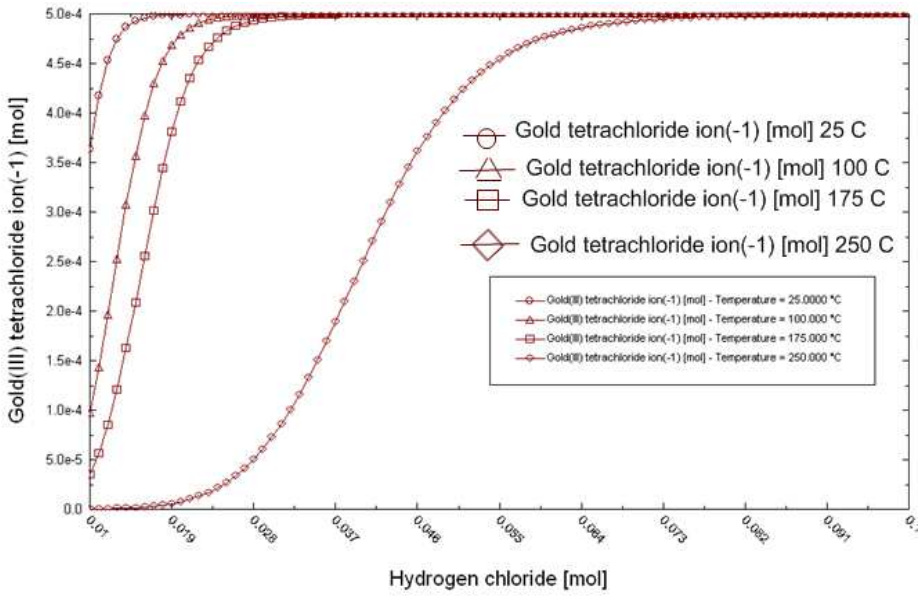

Figure 12: The effect of excess chloride (as HCl) on the stability/solubility of the gold tetrachloride complex at various temperatures (initial amount of Au being $5x10^{-4}$ moles)

It can be seen that as the temperature increases an increasingly higher chloride ion concentration is required to stabilize the gold tetrachloride ion in solution. At 250 °C a chloride concentration excess of almost 150 times is required to keep gold in solution. This is also seen in Figure 13 which shows very similar curves to Figure 12, but instead shows the decrease in soluble gold complex during hypothetical temperature raises in an autoclave with a solution having an initial gold concentration equal to $5x10^{-4}$ molal and different free chloride ion (as HCl) concentrations.

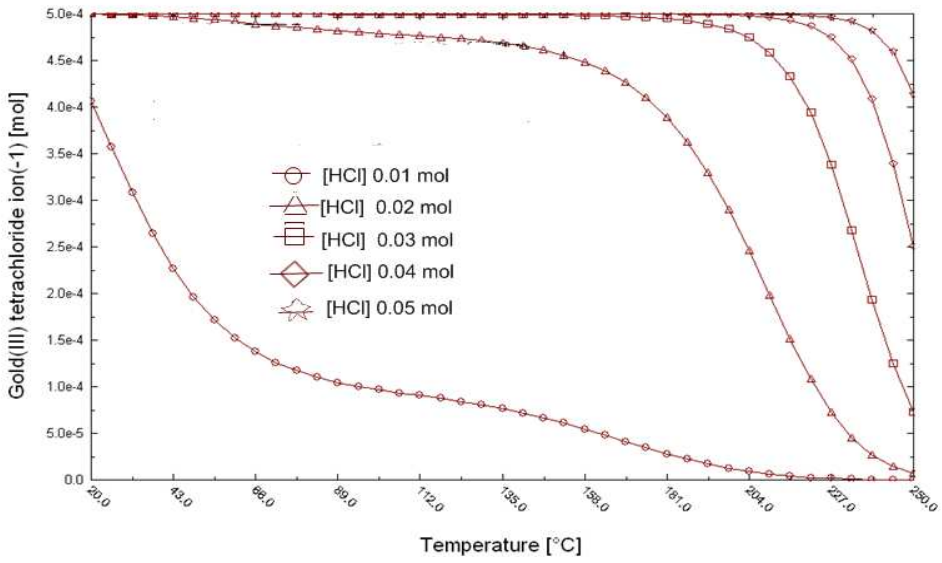

Figure 13: The effect of temperature on gold (III) chloride complex concentration for various added amounts of excess chloride (as HCl)

As demonstrated earlier for the $AuCl_3$-H_2O system, OLI also confirmed that the gold which precipitates from $AuCl_3$-HCl-H_2O solutions, independent of the initial amount, is in metallic form as per Equation 19. This is exemplified with the data of Figure 14 obtained with Cl/Au molar ratio equal to 40

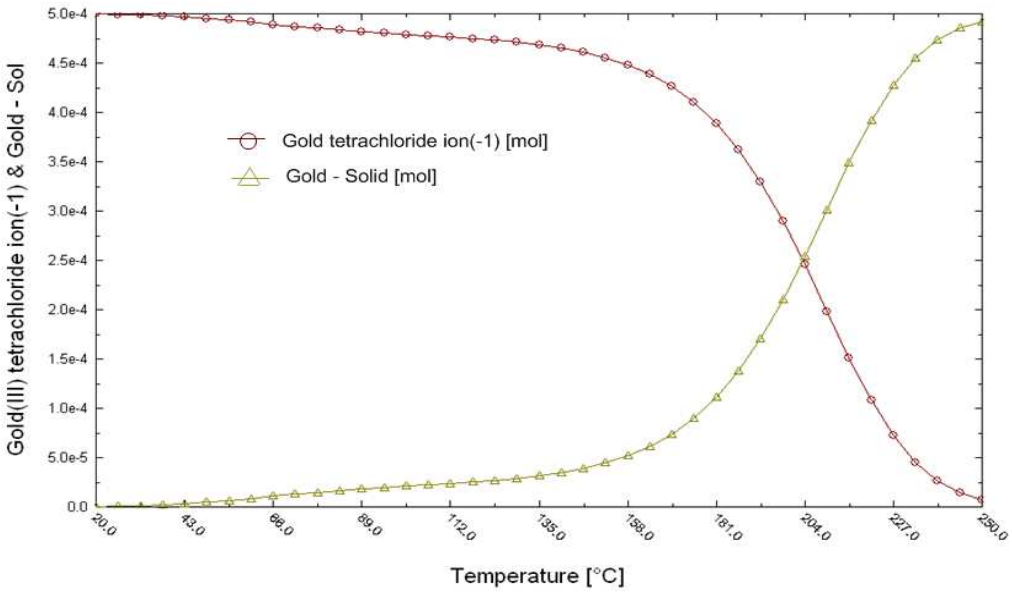

Figure 14: Thermodynamic prediction of gold products in the $AuCl_3$-HCl-H2O system with an initial $AuCl_3$ concentration of $5x10^{-4}$, a molar excess of 40 times chloride ions as a function of temperature

To further investigate the system, the solubility limit of the gold (III) chloride complex before metallic gold forms was determined using OLI for the case of a 0.0715M HCl solution. This HCl concentration is 143 times the standard gold concentration of 5x10-4 (or 100mg/L) Au. The results are plotted in Figure 14.

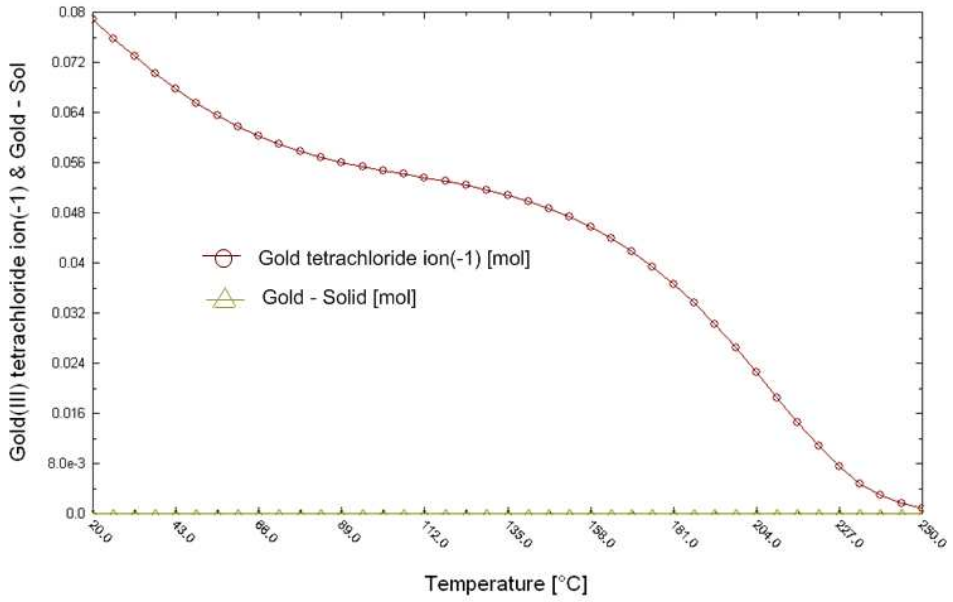

Figure 15: Solubility limit of gold (III) chloride in a 0.0715M solution as a function of temperature

As expected the solubility limit of gold (III) chloride decreases with temperature. At 227 °C the solubility limit corresponds to 100 mg/L of gold. In other words, according to these calculations it is theoretically possible to build up to 100 mg/L of soluble gold under these conditions (143 times molar excess of Cl^-), before gold is reduced to its metallic state. In real systems however this solubility limit can be affected by the presence of other reducing agents such as unreacted sulphides. Nevertheless, the aforementioned thermodynamic analysis serves to establish general trends and set the scene for the experimental program that was carried out.

2.5.2 Gold chloride complex adsorption

During the in-situ precipitation of iron oxides and iron arsenates in the POX autoclave or neutralization circuit, soluble species (cations or anions) may co-precipiate via adsorption [13]. In this section, the general adsorption phenomenon is discussed from the standpoint of possible co-precipitation of $AuCl_4^-$.

2.5.2.1 General adsorption theory

Adsorption occurs via physical or chemical mechanisms often referred to as physisorption and chemisorption. During chemisorption covalent bonds are created between the adsorbate ion and the substrate surface. The reaction has high activation energies and thus takes longer to occur than physical adsorption [53]. During physical adsorption the adsorbate is held to the surface via weak Van der Waals forces, thus ions are removed from solution rapidly in a reversible manner. Physical adsorption involves low enthalpies (under 20kJ/mol) and is always exothermic whereas chemisorption tends to have enthalpies in the range of -100 to -500kJ/mol [53]. However, unlike physisorption, chemisorption may also be endothermic in nature [53].

Oxides, like ferric oxides and other solids provide favorable surface characteristics for ion adsorption due to incomplete coordination of the surface atoms [13, 54]. As a result specific anion and cation sites develop on the surface of the oxide. Upon surface hydration and hydrolysis the non-fully coordinated sites give rise to a hydroxylated surface: $/XOH^{o}$. Chemisorption of cations or anions on this type of surface sites leads to the formation of surface complexes which are analogous to the formation of solution complexes. The formation of surface complexes on an oxide involving anions (as, for example, arsenate species [44] and $AuCl_4^-$) is described in Equation 23:

$$\overset{\square}{XOH^{o}} + A^{3-} + H^{+} \rightarrow \overset{\square}{XA^{2-}} + H_2O \qquad (23)$$

As it can be seen, an adsorption reaction as described above involves protons, in other words it is pH dependent. In general anion adsorption (as is the case for $AuCl_4^-$) is favored in the acidic pH and depends further on the mass or surface area of the precipitating oxides. The latter effect may be expressed as a molar ratio between iron (in the case of ferrihydrite or hematite) and the adsorbate (for example arsenic), i.e. Fe/As as in the case of arsenate adsorption on ferrihydrite [13].

2.5.2.2 Gold complex adsorption mechanisms

Studies have been performed on the adsorption of different gold complexes onto several surfaces such as goethite, hematite, pyrite, or activated carbon [2, 3, 55, 56]. The process of gold adsorption may involve the formation of a surface complex as described above or involve reduction of aurous or auric species or a combination of the two. For reductive adsorption to occur the adsorption substrate must be able to reduce the gold(III) or gold tetrachloride ion as is the case with activated carbon [57]. In the case of goethite, hematite and ferrihydrite it is not possible for this to occur as no reducing agents (ie. ferrous ions) are present. On the other hand, in the case of pyrite and by extrapolation arsenopyrite, reduction may occur but it has been reported that gold adsorbs first via the development of Au-S bonds [56] which is followed by an exchange of electrons with the substrate leading to the formation of metallic gold.

The adsorption of gold chloride on iron oxides/hydroxides via surface complexation has been described by Machesky *et al.* [2] for the case of goethite and by Nechayev *et al.* [3] for the case of hematite. Of the various Au-Cl-OH complexes (seen in Figure 16: Gold(III)-chloride speciation (I=0.01M) [Au=2*10^{-4}M] [Cl- =0.01 M]) Machesky *et al.* [2] reported $AuCl_2OHH_2O$ to have a greater affinity for adsorption to goethite and hematite as compared to gold tetrachloride. However, given that tetrachloride is the dominant complex up to a pH of 5 it is deduced that in the acidic region adsorption will occur through the gold tetrachloride complex.

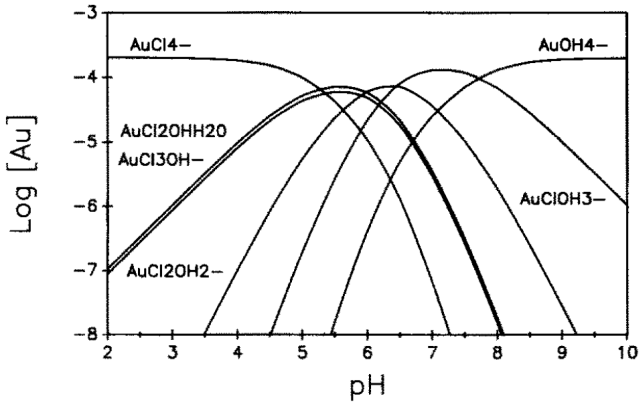

Figure 16: Gold(III)-chloride speciation (I=0.01M) [Au=2*10^{-4}M] [Cl- =0.01 M] [2]

$AuCl_4^-$ adsorption has been shown to be independent of ionic strength [56] thus suggesting that gold forms an inner sphere bidentate coordination with iron surfaces, i.e. covalently bonded surface complexes (chemisorption). This is further supported by the fact that gold chloride, much as phosphate, has a square planar coordination [2]. It has also been suggested [2] that sodium ions may play a role in the suppression of gold chloride adsorption although this has not been studied in great detail.

Chapter 3 Methods and Materials

This chapter deals with all that pertains to the methodology, set-up and execution of the experiments performed.

3.1 Chemicals

The chemicals, their grades and additional information, used throughout the course of the research are listed in Table 1. All solutions were prepared with deionized water which was produced with the use of a Biolab 2200 reverse osmosis apparatus.

Table 1: Information on chemicals used

Chemical	Formula	Supplier	Batch #	Assay
Iron (III) sulphate hydrate 97%	$Fe_2(SO_4)_3 \cdot xH_2O$	Sigma Aldrich	05517TS	21.6% Fe
Magnesium oxide heavy powder	MgO	Fisher Scientific	086318	59.2% Mg
Gold(III) chloride solution	$HAuCl_4$	Sigma Aldrich	41498PJ	17.5% Au
Arsenic (V) oxide hydrate	$As_2O_5 \cdot xH_2O$	Sigma Aldrich	07511DE	57.3% As
Hydrochloric acid reagent grade ACS pure	HCl	Fisher Scientific	n/a	36.5-38%
Sulphuric acid reagent grade ACS pure	H_2SO_4	Fisher Scientific	n/a	95-98%
Nitric acid reagent grade ACS pure	HNO_3	Fisher Scientific	n/a	68-70%
ICS-AES standard Au 1000mg/L	n/a	SCP Science	SC9027993	n/a
AA standard Fe 1000mg/L	n/a	SCP Science	SC8123833	n/a
AA standard As 1000mg/L	n/a	SCP Science	SC8105587	n/a
AA standard Na 1000 mg/L	n/a	SCP Science	SC5329269	n/a

3.2 Atmospheric neutralization/precipitation experiments

The various atmospheric pressure neutralization experiments were carried out according to the following general procedure. The experiments involved heating, as required, the appropriate volume (typically 250 mL per batch) of feed solution placed in a 800 mL beaker on a hot plate. A schematic of the experimental set-up is shown in Figure 17. Solutions were mechanically agitated using a plastic (PTFE) coated stirrer at an

agitation speed of 200 rpm. A plastic coated impeller was chosen over a metallic one in order to avoid gold cementation.

The chemical compositions of all the feed solutions used in this part of the work are summarized in Table 2. Iron feed solution preparation involved dissolving ferric sulphate into 250 mL deionized water into which HCl was added to give a total chloride concentration of 0.05M. To promote homogeneous mixing of all chemicals of the feed solution were placed in an ultrasonic bath for approximately 1-2 hours prior to transferring it into the 800 mL beaker. Finally 0.147 g of a gold (III) chloride stock solution (17.5 % Au in dilute HCl) was added to the ferric sulphate solution to provide for the target 100 mg/L Au ($5x10^{-4}$ M) in the feed solution.

Table 2: Chemical solution composition used in the various for neutralization experiments

	[Fe]	[As]	[Au]	Cl	pH
Experiment	**(M)**	**(M)**	**(M)**	**(M)**	
Prelim 3M MgO			5.08E-04	0.051	1.1
Prelim 0.3M MgO			5.08E-04	0.051	1.1
FeAu 22 °C 0.3M	0.300		5.08E-04	0.051	1.1
FeAu 22 °C 0.15M	0.150		5.08E-04	0.051	1.2
FeAu 22 °C 0.15M Rpt	0.150		5.08E-04	0.051	1.2
FeAu 22 °C 0.075M	0.075		5.08E-04	0.051	1.3
FeAu 57 °C 0.15M	0.150		5.08E-04	0.051	1.2
FeAu 90 °C 0.15M	0.150		5.08E-04	0.051	1.2
FeAu 90 °C 0.3M	0.300		5.08E-04	0.051	1.1
FeAs 4:1 22 °C	0.150	0.037	5.08E-04	0.051	0.90
FeAs 1:1 22 °C	0.150	0.150	5.08E-04	0.051	0.85
FeAs 4:1 60 °C	0.150	0.037	5.08E-04	0.051	0.90
FeAs 1:1 60 °C	0.150	0.150	5.08E-04	0.051	0.85
FeAs 4:1 90 °C	0.150	0.037	5.08E-04	0.051	0.87

FeAs 1:1 90 °C	0.150	0.150	5.08E-04	0.051	0.85
FeAs 1:1 90 °C (scorodite)	0.150	0.150	5.08E-04	0.051	0.67

For neutralization experiments involving both iron and arsenic (FeAs series) two 100mL volumetric flasks were filled with arsenic pentoxide and ferric sulphate solutions separately. The chloride (as HCl)-containing ferric sulphate solution was prepared the same way as already outlined above. The arsenic solution was prepared 2 days in advance and was allowed to homogenize by promoting complete dissolution in an ultrasonic bath at a temperature of 50 °C. The arsenic and iron solutions were mixed prior to the addition of gold chloride and it was made certain that no precipitates formed during this process. The beaker containing the solution was then placed on the hot plate and agitation was started.

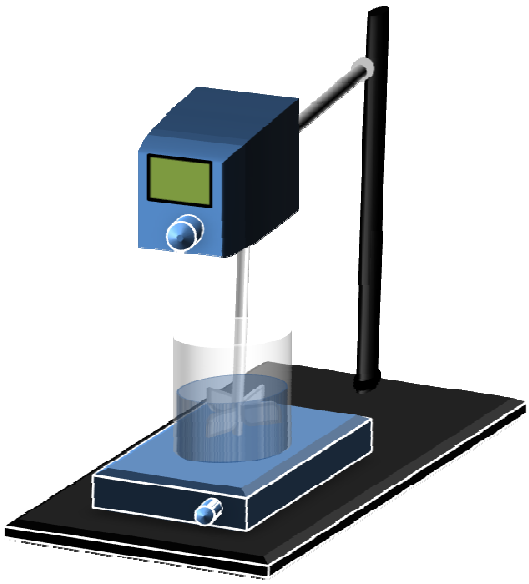

Figure 17: Schematic of equipment used for neutralization experiments. The glass beaker measures 4 inches in diameter and the plastic coated impeller measures 2 inches in diameter

For the experiments conducted at elevated temperatures a cover was placed on the beaker to minimize evaporation losses. Gold chloride was always added to the system

once the temperature had stabilized and not before in case precipitates formed during heating of the solution. Once gold was added, the feed solutions were sampled and analyzed. This signified the initial feed solution composition at time zero. The pH (its initial value ranged from 0.85 to 1.25) was then raised to the target pH of 4 using a 3M MgO (6 grams in 50 mL of deionized water) suspension added through a pipette, at a rate of 3 mL per minute. The base used in these experiments is a suspension of magnesium oxide, it is written as 3M for convenience. Once the pH had reached the target value of 4 the solution was allowed to stir for one hour. During this time samples were taken for analysis. Samples were passed through 0.22 μm disposable PTFE filters[1] prior to analysis.

At the end of each test (after one hour) agitation was stopped and the solution filtered using 0.22μm pore size Millipore MF-Millipore Mixed Cellulose Ester Membranes in a pressure filter at a pressure of 50 psi. The solution was allowed to filter alone once and then 1 L of deionized water was added to the pressure filter to rinse the solids. The solids obtained after pressure filtration were placed inside an oven at 40 °C overnight and then collected the following day for further characterization.

3.3 High temperature autoclave experiments

Initial tests planned for high temperature experiments involved employing a 2L titanium PARR autoclave equipped with a titanium agitator/impeller and thermowell plus a Pyrex liner. During experiments performed under these conditions gold was found to plate on the impeller and other titanium parts. A picture of the plating is seen in Figure 18.

[1] During the early stages of this research it was observed that gold chloride complexes would adsorb on the filters made of Nylon. This prompted a screening of different filters. PTFE filters (supplied by FisherScientific: Fisherbrand model) were found not present this problem. Thus if not otherwise specified, filtration in all experiments was performed using 0.22 μm disposable PTFE filters.

Figure 18: Gold deposits on titanium impeller blades used in 2L PARR autoclave

As a result of the cementation of gold on the titanium parts the experimental design needed to be changed. Thus the 2L autoclave was replaced with a custom-modified 300mL Parr titanium pressure vessel equipped with a Pyrex liner. However, to avoid the occurrence of cementation the following modifications were made. The Ti—made internal parts, impeller/stirring shaft and sampling tube, were removed. In order to have agitation in the system the vessel was placed on a hot plate capable of achieving temperatures of at least 300 °C. This allowed for a Teflon-coated magnetic bar to be used for stirring. Tests had to be performed to ensure the magnetic bar did not cause precipitation of gold from the solution or that it could withstand the maximum temperature applied, 250 °C. As for temperature monitoring the stainless steel thermowell was not allowed to be in contact with the solution by using a maximum of 75mL of it only. No sampling was possible. Hence for each experiment only the final solution and product were analyzed. A picture of the autoclave set-up is provided in Figure 19.

Ferric sulphate, arsenic pentoxide and hydrochloric acid stock solutions were prepared and mixed in the same fashion as in the neutralization experiments with the pH set at 1 using H_2SO_4. The exact solution make-up of the various autoclave experiments may be seen in Table 3. The feed solution (75 mL) after loading in the autoclave was typically held at the target temperature for one hour unless the test specifically called for another time. The starting time of the experiment was once the target temperature was

achieved. A 30 minute heat-up period was required until the solution reached the target temperature. This heat-up period is not included when speaking of retention time within the autoclave. When the experiment was over the hot plate was turned off and the autoclave quenched in tap water. After a few minutes the temperature was low enough to open the autoclave and collect the contents via filtration.

Table 3: Chemical solution composition used in the various autoclave experiments

		[Fe]	[As]	[Na]	[Au]	[Cl]
		M	M	M	M	M
Experiment	**Compound name**					
Fe 200 °C (30,60,90m)	Hematite	0.150			5.1E-04	0.051
Fe 225 °C	Hematite	0.150			5.1E-04	0.051
Fe 237 °C	Hematite	0.150			5.1E-04	0.051
Fe 250 °C	Hematite	0.150			5.1E-04	0.051
FeAs 1:1 200 °C	Scorodite+FAsH	0.150	0.150		5.1E-04	0.051
FeAs 1:1 225 °C	FAsH	0.150	0.150		5.1E-04	0.051
FeAs 4:1 225 °C	BFAS	0.150	0.0375		5.1E-04	0.051
Jarosite 200 °C (run #1,3,4)	Jarosite	0.150		0.060	5.1E-04	0.051

Figure 19: Experimental set up for autoclave tests: 300mL Parr Ti autoclave equipped with pressure monitor, release valve and temperature probe

3.4 Chemical analysis

Inductively Coupled Plasma Spectroscopy (ICP-OES) was used to determine the concentration of arsenic present in solutions or solid digestions. Samples were diluted to below 50 mg/L and standards of 0.5, 5 and 50 mg/L were prepared to calibrate the Thermo Jarrell Ash machine. Standard checks were performed after every 5 samples and the bracketing technique was used to account for machine drift over time. Atomic absorption was used to analyze solutions from neutralization and autoclave experiments as well as samples from the digestion tests in terms of iron, sodium and gold concentrations. Samples were diluted to <20 mg/L for gold samples and under 50 mg/L for iron samples. Standards of 0.5, 5 and 20 mg/L were prepared for gold and 0.5, 5 and 50 for iron. AA analysis was done using a Varian AA240FS Fast Sequential Atomic Absorption Spectrometer and CanLab gold lamp at 267.6nm, and Varian iron and sodium lamps at 372.2 and 589 nm respectively.

3.5 Solids Characterization

3.5.1 Diagnostic Leaching

In order to determine the amount and type of gold co-precipitated with the iron/arsenic solid products a small amount of the precipitates was dissolved (separately) in both 3M HCl and 3M *aqua regia* (AR). For neutralization experiment precipitates 0.5 g of solids were placed in a 100 mL volumetric flask and filled with the respective acid solutions till digestion in the respective solution was complete. The final solutions/residues were collected, filtered and sent to be analyzed for gold, iron and arsenic. The difference between the HCl and AR solutions was taken as being the amount of metallic gold in the solids. For autoclave experiments 0.05 g of solids were placed in sampling tubes and filled with 10 mL of respective acidic solutions. The digestion amounts were scaled down since there was less solid product obtained from the autoclave experiments. The sample tubes were placed on a rotating platform (see Figure 17) and shaken for 4-5 days since hematite dissolution was rather slow.

Figure 20: Shaking/rolling platform used to speed the process of hematite dissolution

Once the iron/arsenic precipitates were fully dissolved (except for any metallic gold that might be present in the HCl solution) they were filtered and sent for gold, iron and arsenic analysis.

3.5.2 Physical characterization

The morphological features of the produced precipitates were examined by scanning electron microscopy. In the case of the solids obtained from the neutralization experiments (poorly crystalline and relatively amorphous) a Hitachi S-3000N Variable Pressure Scanning Electron Microscope (VP-SEM) was used. Images were obtained at a working distance of 6 mm and a beam strength of 5kV to avoid charging. The samples were coated with carbon in an attempt to better reveal (if present) any gold grains using BSE imaging. This coating was required as, even operating under variable pressure mode, charging on the surface of particles would occur. To avoid any charging in the future it was decided to use the FEG-SEM for imaging as opposed to the VP-SEM. Surface images were obtained using an Everheart Thornley secondary electron detector.

The solids obtained from the autoclave experiments (all crystalline powders) were placed on double sided carbon tape and coated with a thin layer (~20nm) of gold/palladium. A Hitachi S-4700 Field Emission Gun Scanning Electron Microscope was

used to view the samples at multiple magnifications. A beam strength of 5kV was used at all times. All images were taken via secondary electron detection.

The surface area of the precipitates was determined by BET analysis. Samples were placed inside vials, which were degassed at 80 °C for two hours. Multi-point BET readings were taken using a Micromeritics TriStar Surface Area and Porosity Analyzer.

3.5.3 Phase identification

Identification of the various iron and arsenate phases precipitated was performed with the aid of XRD, ATR-IR and Raman spectroscopy. For XRD analysis solid samples were finely ground and placed in a metallic sample holder with the help of a glass slide in order to obtain a flat surface by pressing. The samples were analyzed using a Philips PW 1710 X-Ray Diffractometer with a 1.5405 A Cu-Kα source, operating at 20 mA and 40 kV. Samples were scanned from 5 to 100 degrees (2θ), the step size was 0.1 and the sampling time 47 minutes.

For ATR-IR analysis a small amount of solids (ground) were placed in a Perkin Elmer (Spectrum BX model) Fourrier Transform Infrared (FTIR) spectrometer with a Miracle single bounce diamond ATR cell.

Raman spectra were collected for identification of the autoclave precipitates with a Renishaw Invia microscope. A 514 nm polarized argon laser operating at 5% power at the microscope exit was used to obtain the readings.

Chapter 4: Gold behavior during atmospheric precipitation

Acidic leach solutions discharged from POX autoclaves are subjected to neutralization. Any soluble gold present in solution may interact with the precipitates that form as the pH is raised. For this reason, the behavior of gold (III) chloride ions during neutralization is investigated in this chapter. The effects of pH, temperature (22 to 90 °C), initial iron concentration (0.075 – 0.3M), iron/arsenic molar ratio (1 and 4) and the ensuing precipitate phases on gold (III) chloride stability are all considered.

4.1 Co-precipitation of gold (III) chloride with iron

4.1.1 Neutralization of iron-free solutions at 22 °C

According to the OLI thermodynamic calculations presented in Chapter 2, gold (III) chloride ions are thermodynamically stable if there is an excess of chloride ions. In order to verify that the theory holds true in a lab setting, neutralization tests were performed to determine whether gold would remain in solution over a wide pH range. Acid-base titration type tests were performed using an acidic gold (III) chloride solution (initial pH of approximately 1) of standard concentration (100mg/L or $5x10^{-4}$ M Au) plus excess chloride ions in the form of HCl set at a molar ratio of chloride ions to gold (III) chloride equal to 100. As base two different MgO suspension concentrations were used, more specifically 0.3M and 3M. The obtained results are shown in Figure 21. The amount of soluble gold lost during the addition of MgO is seen to be minimal and the concentration remains stable across the pH region of 2 to 8. This is true for both low and high concentration base solutions. This behavior was further verified with additional neutralization tests. Hence it can be concluded that the base itself does not cause gold (III) chloride to precipitate over the tested pH range.

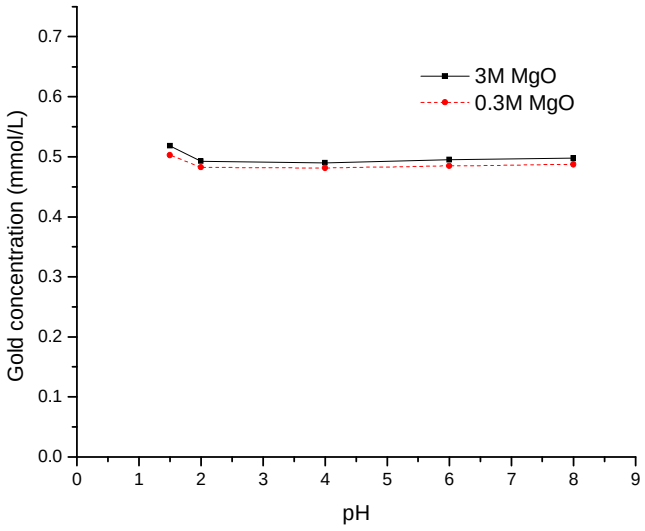

Figure 21: Effect of pH on the stability of the gold (III) chloride ion at room temperature with Cl /Au molar ratio equal to 100

4.1.2 The effect of Iron concentration on gold (III) chloride co-precipitation

During the neutralization of autoclave discharge solutions, base is added in order to precipitate the residual iron left in solution. During this process any soluble gold could react with the forming solids. In order to study the behavior of gold (III) chloride during precipitation of iron, various neutralization tests were performed. Initially, acidic solutions with various ferric (added as a sulphate salt) concentrations were treated. In all these solutions approximately $5x10^{-4}$ M (100mg/L) Au (as $HAuCl_4$) plus 0.05MHCl was added to provide for a Cl/Au molar ratio equal to 100. The tests involved a gradual increase of pH with the addition of MgO (3M) until the target precipitation pH (pH 4) was reached as per the procedure described in Chapter 3. The behavior of gold during a typical test with an initial iron concentration of 0.3M is shown in Figure 22. It can be seen that the gold concentration variation parallels that of iron. At low pH levels, before iron begins hydrolyzing (< 30 minutes) for all practical purposes gold can be said to remain in solution. That no gold precipitates when iron stays in solution was further verified by agitating a solution of pH 1.2 with 0.15M dissolved iron and the same Cl/Au content, for one hour. No gold concentration drop was observed.

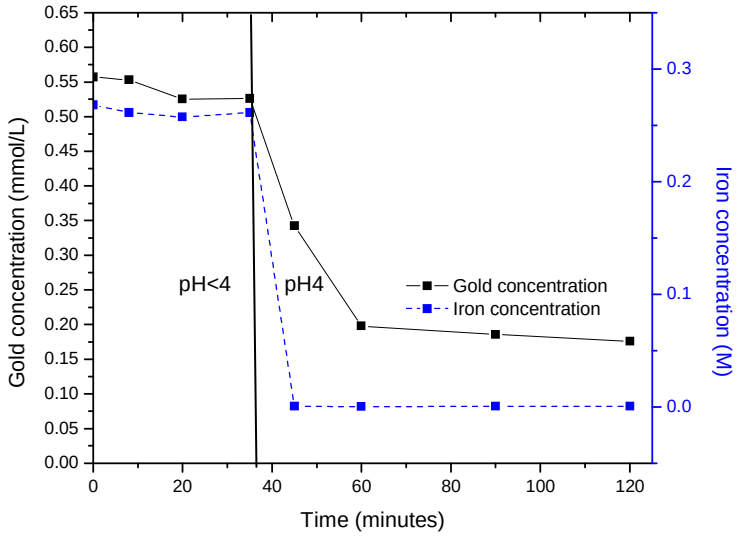

Figure 22: Iron and gold concentration profiles during co-precipitation experiment at pH 4. Vertical line represents the point at which the target pH was reached

However, upon reaching pH 4 (denoted by the vertical line in Figure 22) complete iron precipitation (apparently as ferrihydrite, this is described in the characterization section) occurred, accompanied by partial co-precipitation of gold (III) chloride. The gold uptake occurs over a short period of time and then plateaus at a gold concentration of 0.17 mmol/L . The mechanism by which gold co-precipitates could be attributed to either reduction of gold (III) into metallic gold, or adsorption of gold (III) chloride onto the surface of ferrihydrite or the incorporation of gold in the structure of ferrihydrite. As there are no other ions present in solution to act as reducing agents for gold (III) chloride the more likely mechanism for the loss of gold is via adsorption. The adsorption of gold (III) chloride to goethite via inner-sphere bidentate surface complex formation has been reported in literature [2]. The present results, as will be further substantiated in the characterization section, seem to suggest a similar mechanism takes place during the precipitation of ferrihydrite at pH 4.

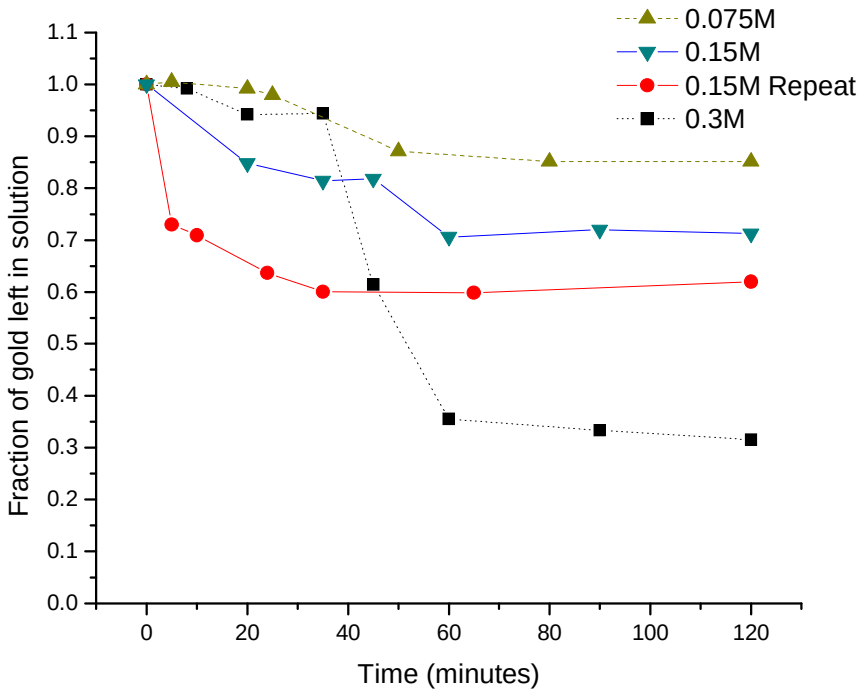

Figure 23: Fraction of gold (III) chloride left in solution during co-precipitation experiments at 22 °C with varying initial iron concentrations (0.075, 0.15 and 0.3M)

The effect of initial iron concentration on gold co-precipitation is reported in Figure 23. It can be seen that the fraction of gold co-precipitating with iron increases with increasing iron concentrations. When the initial iron concentration is lowered to 0.15M and 0.075M, the final gold fractions left in solution are around 0.7 (0.406 mmol/L) and 0.9 (0.457 mmol/L) (respectively) compared to 0.35 (0.177 mmol/L) for an initial iron concentration of 0.3M. The repeat experiment for the initial concentration of 0.15M does not follow the exact path as the original experiment. Experimental errors could explain the more rapid co-precipitation however the results still show the same trend in the effect of initial iron concentration. The fact that the amount of gold co-precipitating increases with an increasing iron concentration is consistent with the postulated adsorption mechanism. As the amount of iron precipitate increases, the surface area available does too thus allowing for more gold (III) chloride complex to be attached to the surface of ferrihydrite. Furthermore, as per supersaturation theory, the higher the

iron supersaturation becomes, precipitates with smaller particles form which possess higher surface areas.

To validate this assumption, BET surface area measurements were performed and co-precipitate gold concentrations (adsorption densities) were determined. The obtained results are compiled in Table 4 .

Table 4: BET surface area measurements on ferrihydrite produced during co-precipitation experiments at room temperature

Sample Name	BET Surface Area (m^2/g)	Error	Adsorption Densities ($mmol/m^2$)	BET equivalent particle size (nm)
0.3M	15.232	0.0696	0.737	98.47
0.15M	11.068	0.0574	0.884	135.52
0.075M	8.187	0.0645	1.140	183.21

As it can be seen, the surface area increases (or equivalently the primary particle size decreases, this is visually determined later via SEM characterization) with increasing iron concentration, as would be expected from a supersaturation theory point of view [13]. Furthermore, in agreement with our postulation that the mechanism for soluble gold co-precipitation is via adsorption, there exists a correlation between the relative surface area and the amount of gold (III) chloride removed from solution as shown in Figure 24. With increased surface area more sorption sites are available, as a result more gold is removed from solution. In terms of adsorption densities, the values vary from 0.7 to 1.1 $mmol/m^2$, significantly higher than those reported for goethite ($0.26mmol/m^2$)[2]. The reason for this difference in adsorption density between ferrihydrite and goethite may be due to the nature of the experiment and the iron phase involved. In the present study gold removal takes place during in-situ precipitation of iron (co-precipitation test) while the case of the goethite experiment [2] involved the addition of goethite particles into a gold (III) chloride containing solution (adsorption test). As it has been shown in the case of arsenate removal from solution, co-precipitation [49] is more effective than simple adsorption [44, 58]. The other difference between the two systems is the nature of the

ferric oxy-hydroxide phase. Ferrihydrite, because of its poorly crystalline and nano-structured characteristics [63], has a far larger number of non-fully coordinated surface sites suitable for adsorption than the crystalline goethite phase.

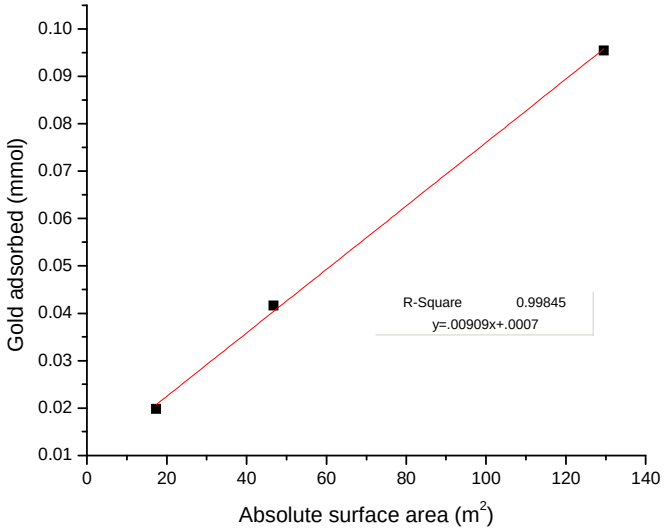

Figure 24: Plot of absolute surface area versus the amount of gold (III) chloride adsorbed during iron and gold co-precipitation experiments at 22 °C and pH 4

4.1.3 The effect of temperature on gold (III) chloride co-precipitation

The previous section detailed the effect that the initial iron concentration has on the amount of gold adsorbed at room temperature. The exit solution from pressure oxidation is hot and even if the solution is cooled before neutralization it may still be at an elevated temperature during the neutralization process. Elevated temperatures could affect the kinetics and equilibrium of adsorption or change the type of precipitate that forms.

Co-precipitation experiments employing the same procedure as in the previous section were performed at 60 and 90 °C. The terminal pH was again 4. As was the case with the room temperature tests, the initial iron concentration was found to affect the amount of gold removed from solution as shown in

Figure 25: Concentration of gold in solution during iron co-precipitation experiments at 90°C with varying initial iron concentrations (0.15M and 0.3M [Fe]). Although the difference between the amount of gold adsorbed during the 0.15 and 0.3M tests at 90 °C (

Figure 25) is less distinguished than in the case of room temperature tests (Figure 23) there is still a clear trend that more gold is adsorbed as the initial iron concentration is increased.

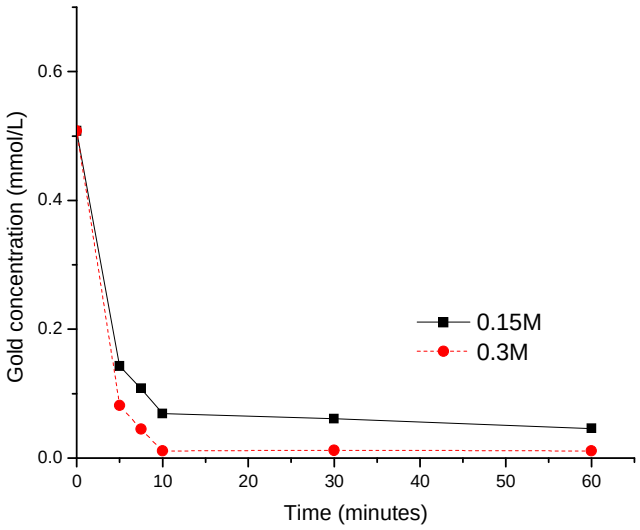

Figure 25: Concentration of gold in solution during iron co-precipitation experiments at 90°C with varying initial iron concentrations (0.15M and 0.3M [Fe])

The effect of temperature on gold co-precipitation at fixed iron concentration is reported in Figure 26. The plotted data reveals that the loss of gold increases with increasing temperature. The repeat experiment for 22 °C is not a perfect match to its predecessor however still confirms the aforementioned trend. Not only is the amount of gold removed affected (as deduced from the final gold concentration) but also the kinetics of gold co-precipitation, this is analyzed and discussed in the following section.

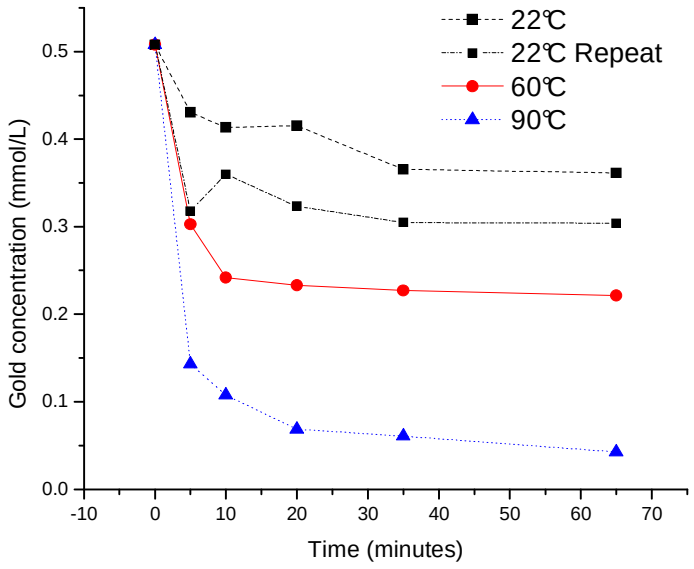

Figure 26: Effect of temperature on the gold (III) chloride concentration during iron precipitation (initial concentration of 0.15M) at pH 4

4.1.4 Kinetic considerations

The data presented thus far revealed that as the amount of iron in the system increases more gold is removed from the solution at a faster rate. This behavior was shown to correlate well to the surface area of the precipitated ferrihydrite (more on its characterization in the next section) in agreement with the postulated adsorption mechanism. In addition to this correlation, an attempt was made to establish an empirical rate equation expressing the initial rate of gold removal to the initial iron concentration. The initial rate of gold removed was taken as being the difference between the gold concentration at pH 4 and 5 minutes after the target pH was obtained. The empirical rate equation obtained from these rates corresponds to the following overall reaction:

$$Fe(SO_4)_{1.5} + AuCl_4^- + 3H_2O \rightarrow Fe(OH)_3 - AuCl_{3(ads)} + Cl^- + 1.5H_2SO_4 \quad (24)$$

$$\log(\text{rate}) = n \cdot \log([Fe]) + p \cdot \log([Au]) + \log(k)$$

According to this global reaction, iron hydrolyses and forms ferric hydroxide (ferrihydrite) on the surface of which gold (III) chloride adsorbs. Since the initial rate is far from the equilibrium position, an irreversible reaction chemical rate equation can be written as follows:

$$\text{rate} = k[Fe]^n [[Au]]^p \quad (25)$$

Further manipulation of the rate law allows for the results to be plotted and checked for linearity to determine the order of the reaction:

$$\log(\text{rate}) = n \cdot \log([Fe]) + p \cdot \log([Au]) + \log(k) \quad (26)$$

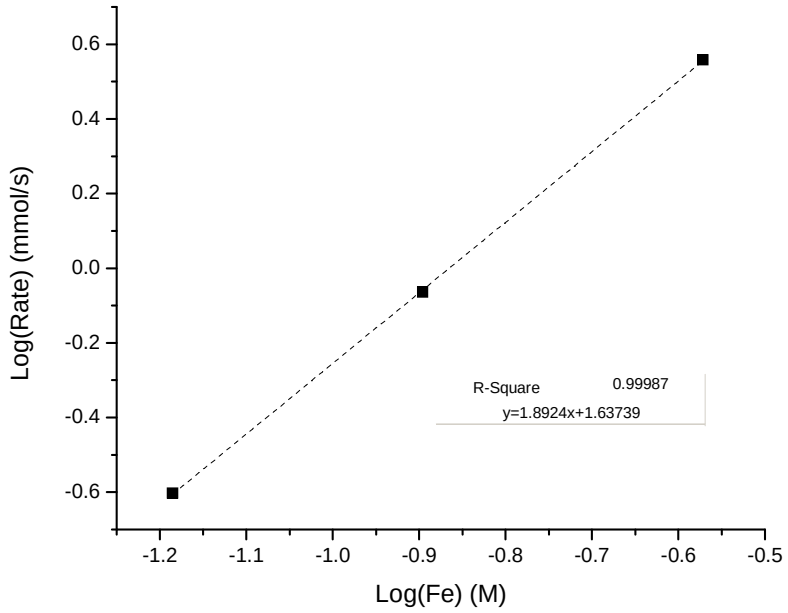

Figure 27: Log-log plot of the initial rate of gold (III) chloride precipitation versus the initial iron concentration in co-precipitation experiments at 22 °C

The log-log plot according to Figure $\log(\text{rate}) = n \cdot \log([Fe]) + p \cdot \log([Au]) + \log(k)$ (26 as it applies to the data of Figure 23 is shown in Figure Figure 27. From this plot the gold precipitation rate was found to have a second order dependency on iron concentration. This second order dependency may reflect the fact that gold chloride adsorption on iron oxy-hydroxides occurs via bidentate complex formation [2]. In other words for each gold (III) chloride complex there are two iron hydroxide surface sites involved. Notwithstanding the true underlying factor behind this second order dependency, this finding provides a useful quantitative measure of the effect of iron concentration on gold removal kinetics.

As reported, temperature has an effect on gold (III) chloride co-precipitation, as seen in Figure 26. By analyzing the initial precipitation rate with the aid of the second order rate Equation (27) and using the Arrhenius equation (Equation (28) $k = Ae^{-\frac{E_a}{RT}}$ (28)) the activation energy was determined via the plot presented in Figure 28.

$$rate = k[Fe]^{a} \tag{27}$$

$$k = Ae^{-\frac{E_a}{RT}} \tag{28}$$

$$\ln(k) = \ln(A) - \frac{E_a}{RT} \tag{29}$$

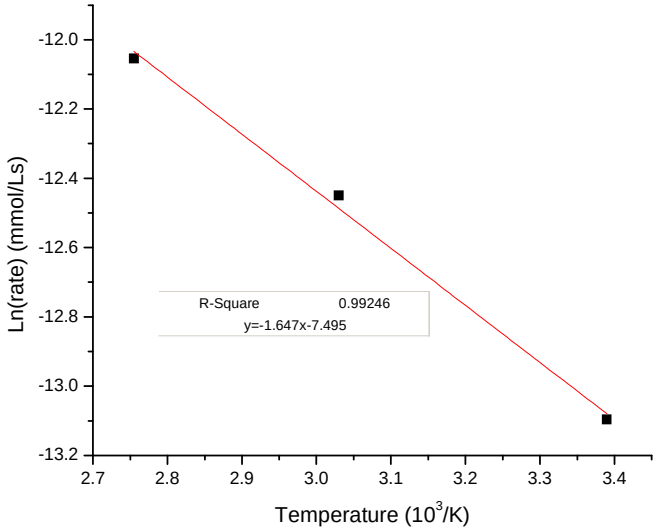

Figure 28: Arrhenius plot of the initial rate of gold (III) chloride versus temperature for 0.15M iron and gold co-precipitation experiments

Figure 28The slope obtained from the Arrhenius plot is -1.6476 which, when multiplied by the gas constant, yields an activation energy of 13.698 kJ/mol. It is accepted that activation energy of less than 15kJ/mol suggests mass transfer control [60]. This would imply that the chemical adsorption process is relatively fast especially as the temperature is increased and is controlled by the gold chloride complex's interfacial transfer to reach the adsorption sites.

4.1.5 Enthalpy of adsorption

In order to identify the type of adsorption that occurs a Van't Hoff plot of the gold (III) chloride equilibrium constant as a function of the inverse of temperature was constructed. The equilibrium constant was calculated from the equilibrium (final) concentration:

$$\equiv \mathbf{Fe} + \mathbf{AuCl_4^-} \rightarrow \equiv \mathbf{Fe} - \mathbf{AuCl_{3(ads)}} + \mathbf{Cl^-} \tag{30}$$

Where $\equiv$ depicts the surface adsorption sites on ferrihydrite particles. Using this adsorption reaction the equilibrium constant can be written:

$$K = \frac{[AuCl_4^-]_{surf}}{[AuCl_4^-]_{aq,eq}}, \qquad \ln(K) = \ln\left(\frac{[AuCl_4^-]_{surf}}{[AuCl_4^-]_{aq,eq}}\right), \qquad \ln(K) = -\ln\left([AuCl_4^-]_{aq,eq}\right) \tag{31}$$

Tha Van't Hoff equation is written below:

$$\log(K) = -\frac{\Delta H^\circ}{RT} + \frac{\Delta S^\circ}{R} \tag{32}$$

By plotting log(K) vs. 1/T for the data of Figure 26 the Van't Hoff plot is obtained as shown in Figure 29.

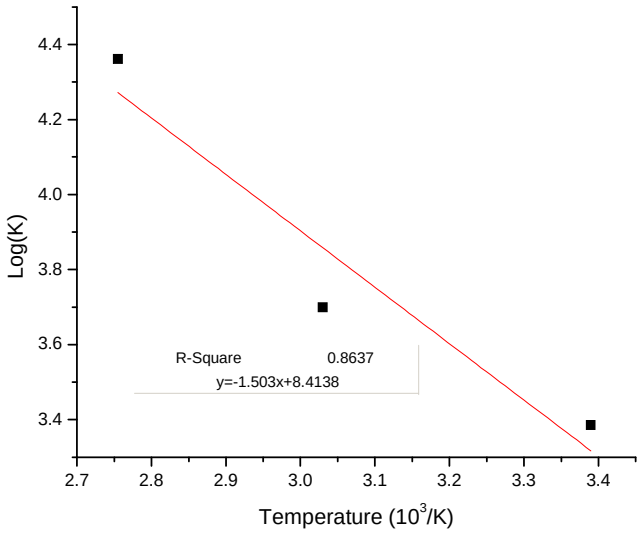

Figure 29: Van't Hoff isotherm of varying temperatures versus equilibrium concentration of gold (III) chloride during iron and gold co-precipitation experiments

From the Van't Hoff plot the enthalpy of adsorption was calculated to be 12.397kJ/mol. This suggests an endothermic reaction is taking place, which is to be expected as the results show a decrease in the equilibrium concentration as heat is added to the system. Typically physical adsorption (physisorption) is always exothermic whereas chemisorption at low temperatures is endothermic and at high temperatures is exothermic [53, 61]. Therefore the removal of gold (III) chloride during co-precipitation has the characteristics of chemisorption-in agreement with the postulated surface complexation mechanism.

4.1.6 Characterization

It has been reported that gold does co-precipitate during the precipitation of iron under varying conditions. It has been further postulated that the co-precipitation of gold occurs via adsorption of gold (III) chloride onto ferrihydrite. In this section the precipitates are characterized to validate this postulation.

In order to determine the mechanism by which gold co-precipitates, diagnostic leaching on the produced precipitates was performed. By independently digesting solids obtained from iron and gold co-precipitation experiments in a non oxidizing acid (3M HCl) and in *aqua regia* (AR) a distinction between metallic gold and adsorbed gold was made. Any metallic gold formed would dissolve solely in the AR solution. Therefore if metallic gold were present after co-precipitation the AR samples would yield higher concentrations than the HCl digestion samples. The diagnostic leaching results (in the form of dissolved gold concentration) are reported in Table 5. As it can be seen there is no difference in the gold concentration in HCl and AR. Therefore, as was hypothesized in the previous section, no reduction to metallic gold occurs during gold (III) chloride co-precipitation with iron.

Table 5: Diagnostic leaching results obtained from ferrihydrite samples of iron and gold co-precipitation experiments

	HCl	AR
Temperature	**(mmol/L)**	**(mmol/L)**
22 °C	0.067	0.066
60 °C	0.117	0.121
90 °C	0.129	0.127

It has been determined that gold co-precipitates with iron during batch neutralization experiments at pH 4. To this point we have assumed that the solids formed were ferrihydrite however for confirmation a closer look at the characterization of the solids is required. XRD patterns of the three iron precipitates obtained at 22 °C from various iron concentration solutions are shown in Figure 30. All patterns show the characteristics of 2-line ferrihydrite having two broad peaks centered at 2θ values of 34 and 61 degrees [45]. It may be further commented that the pattern of the precipitate obtained at low concentration (0.075 M) appears to have a higher degree of crystallinity than the other two precipitates, reflecting the effect of supersaturation on nucleation rate [13].

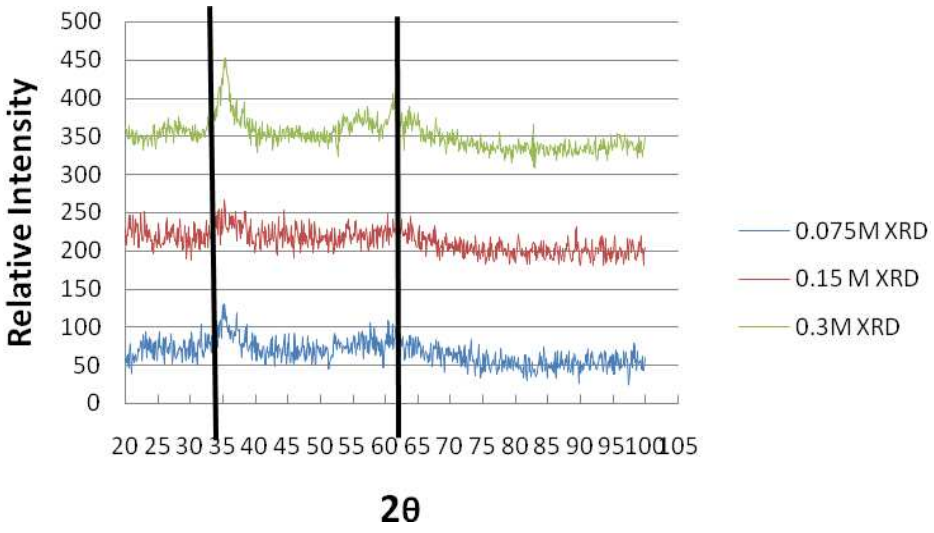

Figure 30: XRD patterns of ferrihydrite formed at pH 4 with initial iron concentrations of 0.075, 0.15 and 0.3M at 22 °C. The vertical lines represent the theoretical peaks for 2-line ferrihydrite

In Figure 31 the XRD patterns of the precipitates obtained at higher temperatures are presented. Once more the patterns suggest that the solids are in fact 2-line ferrihydrite. Comparing the relative height and breadth of the peak at 34 degrees of the three ferrihydrites of Figure 28 it becomes apparent that temperature elevation results in higher degree crystallinity for the produced 2-line ferrihydrite. Furthermore, it is interesting to note that BET measurements yielded a specific surface area of 307.3 m^2/g for the ferrihydrite product produced at 90 °C as opposed to 11 m^2/g of the corresponding precipitate at 22 °C. The equivalent primary particle sizes are 5 nm and 135 nm. The smaller particle size at higher temperatures is attributed to the faster homogeneous nucleation kinetics [13].

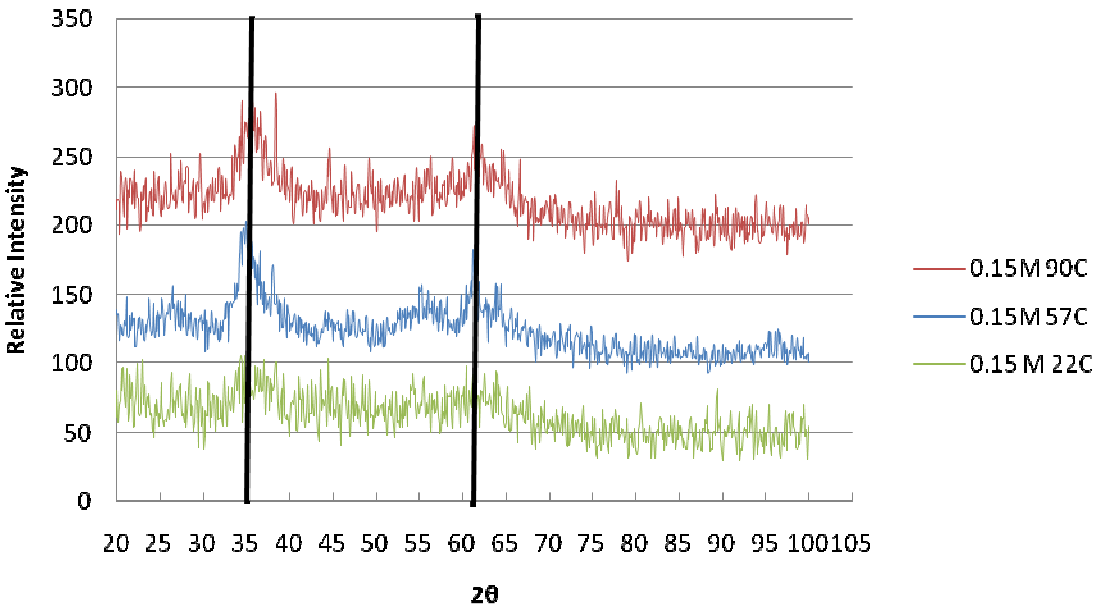

Figure 31: XRD patterns for ferrihydrite compounds formed at pH4 at 22, 57 and 90 °C during iron and gold co-precipitation experiments. The two vertical lines represent the theoretical peaks for ferrihydrite

The ferrihydrite precipitates were examined by SEM after drying to evaluate their morphological features. The relevant SEM images are presented in Figure 32. From these images we may deduce that the ferrihydrite precipitates are made from very fine nano-particles clustered together in larger aggregates. There is a trend for the particle size to decrease as the concentration increases. Although this is not quantified it correlates to the information collected via BET measurements. It was not possible to detect gold via EDS analysis of the particles due to the fact that gold is under the detectable limit of 1wt%.

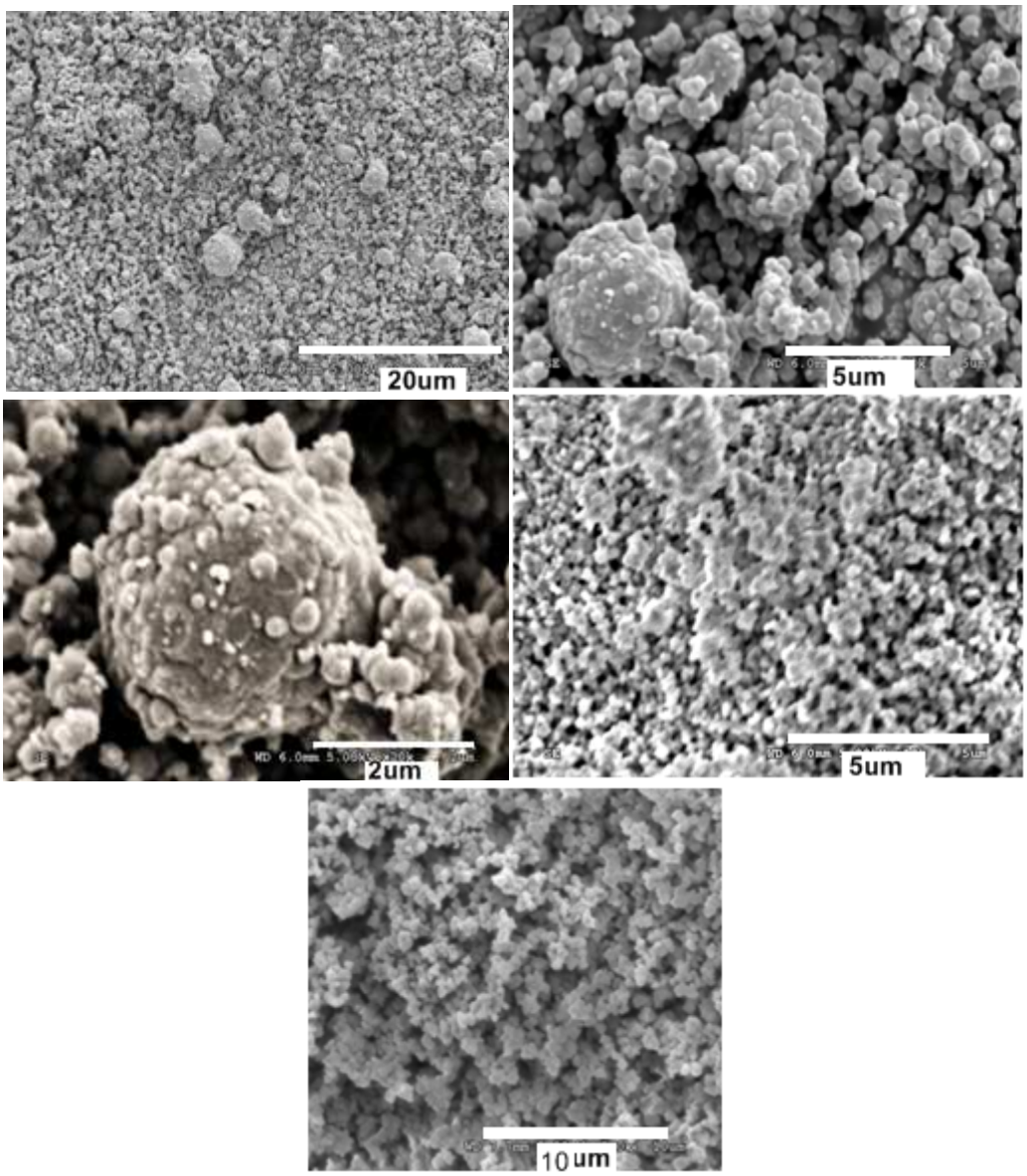

Figure 32: SEM images of ferrihydrite precipitates from iron and gold co-precipitation experiments (from top to bottom, left to right): 0.075M, 0.075M , 0.075M, 0.15M, 0.3M

4.1.7 Conclusions

Upon MgO slurry neutralization of variable ferric sulphate concentration solutions containing 100 mg/L Au and excess chloride at molar artio Cl/Au =100 to pH 4, it was observed that gold co-precipitates with iron. At pH 4 the precipitation of iron was complete under all conditions but the amount of gold co-precipitated increased with the

initial concentration of iron and temperature. It was determined that 0.0423 to 0.0689 mmol of gold (III) chloride to co-precipitate per mole of iron precipitated.

All the iron precipitates were determined to be 2-line ferrihydrite and gold (III) chloride was found to co-precipitate via adsorption. No evidence of reduction to metallic gold was found. The increased gold uptake with initial iron concentration was correlated to the available surface area of ferrihydrite. Estimation of the enthalpy of adsorption indicated an endothermic chemisorption reaction to occur. Finally according to kinetic analysis of the initial rates of gold co-precipitation the overall process exhibits second order dependence on initial iron concentration and mass-transfer rate limiting characteristics.

4.2 Co-precipitation of gold with iron and arsenic

The behavior of gold (III) chloride during iron precipitation has been investigated in the previous section and was found that gold follows iron to some extent via adsorption on the formed ferrihydrite. However, typical pressure oxidation/leaching processes deal with arsenic-containing ores and concentrates in the form of minerals like arsenopyrite in the case of gold POX or enargite in the case of copper pressure leaching. Autoclave discharge solutions may thus contain residual soluble arsenic along with iron that tends to precipitate during atmospheric neutralization. Depending on the temperature, Fe/As molar ratio and method of pH control, the arsenic may report in the precipitate as a complex amorphous product or as well crystallized scorodite. In this section the behavior of gold (III) chloride during atmospheric precipitation of iron and arsenic is investigated.

4.2.1 Precipitation of amorphous ferric arsenate/ferrihydrite

As discussed in the literature review chapter, to achieve effective arsenic removal during conventional neutralization the molar ratio of ferric/arsenate should be at least 3. This process, in the case of pH under 8, results in a mixed precipitate consisting of poorly crystalline ferric arsenate ($FeAsO_4 \cdot xH_2O$) plus arsenic-bearing ferrihydrite [45, 46, 49,

58]. The effect of arsenate ions on the co-precipitation behavior of gold (III) chloride with iron and arsenic is studied in this section.

4.2.1.1 The effect of arsenic on gold co-precipitation

The experimental procedure followed was the same as the one applied in the previous section. Essentially, iron sulphate solutions with 0.15 M Fe(III) concentration containing arsenic (as arsenate) at a molar ratio of 4 or 1 and the standard 100 mg/L Au and Cl/Au=100 molar ratio were neutralized via MgO slurry (3 M) addition to pH 4. The concentration profiles of Fe, As and Au for a typical test at 22 °C and Fe/As ratio of 4 are shown in Figure 33. As it can be seen upon raising the pH (from the initial 1.1 to 4) all iron and arsenic precipitate out of solution within 5 minutes.

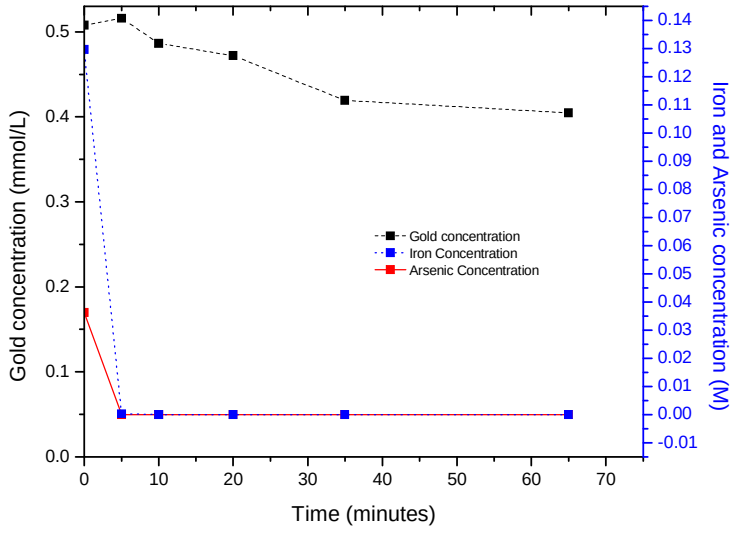

Figure 33: Iron, arsenic and gold concentration profiles during co-precipitation experiment at pH 4 and 22 °C

During the experiment approximately 20% of the soluble gold (III) chloride was removed from solution. The test was repeated with excellent reproducibility in terms of gold co-precipitation shown in Figure 34. It appears the co-precipitation of gold is not "instantaneous" but rather follows a slower kinetics path than the precipitation of iron

and arsenic as gold only begins to co-precipitate after iron and arsenic have precipitated out of solution.

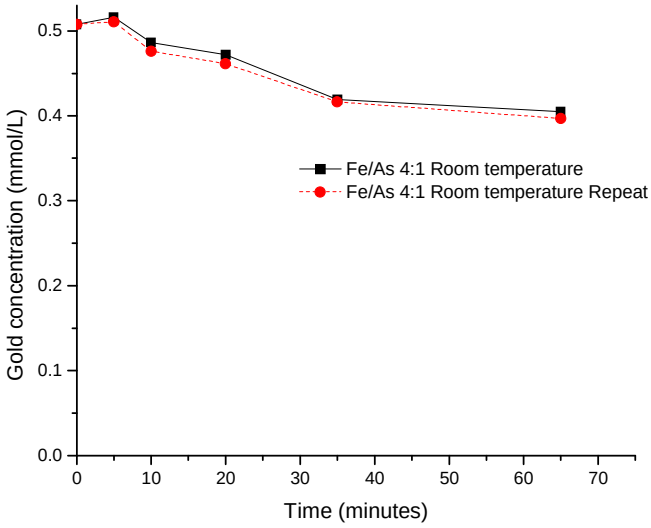

Figure 34: Gold concentration change during co-precipitation of iron (0.15M) and arsenic (4/1 ratio) at 22 °C and pH 4

Although gold (III) chloride was found to co-precipitate with iron and arsenic, a comparison with the data from the arsenic-free tests (Figure 23) shows the amount of gold removed to be lower. This is better illustrated with the data plotted in Figure 35. According to this graph, the extent of the reaction is dependent upon the initial arsenic concentration. Figure 35 demonstrates the percentage of gold lost as the arsenic concentration is increased from none to a 1/1 molar ratio of iron to arsenic.

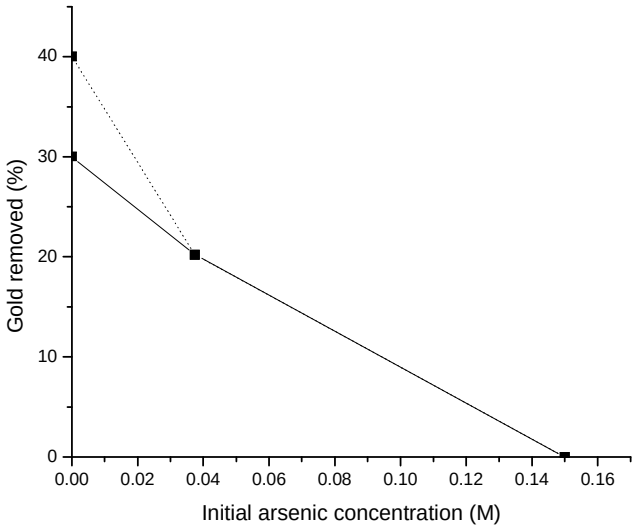

Figure 35: Effect of the initial arsenic concentration on the % gold (III) chloride removed from solution during iron, arsenic and gold co-precipitation: the dotted line is the results plotted using the repeat experiment for 0.15M Fe in the absence of arsenic at 22 °C

A clear trend is seen where less gold is removed from solution as the arsenic concentration is increased. As the most likely co-precipitation route for gold is via adsorption the increased amount of arsenic in solution may be thought to cause a competition between arsenate ions and gold (III) chloride ions on the surface of ferrihydrite. In the case of the experiment where the molar ratio of Fe/As is 1 ([As]=0.15M) apparently all the iron and arsenic combine to form the poorly crystalline ferric arsenate as reported by LeBerre *et al.* [63] with no ferrihydrite present hence the nil co-precipitation of gold (III) chloride. The characterization of the Fe(III)-AsO_4 co-precipitates is described in a subsequent section. The observed decrease in apparent gold chloride adsorption because of competition from arsenate ions is similar with the effect nitrate ions were reported to have on gold adsorption on goethite [2]. Similarly Jia and Demopoulos [44] found arsenate to hinder the adsorption of sulphate ions on ferrihydrite.

The same trend of arsenate causing a decrease in the co-precipitation of gold (III) chloride as its concentration increases was observed also at higher temperatures, namely 60 and 90 °C seen in Figure 36. It must be noted that the test carried out at 60 °C with no arsenic present was actually performed at 57 °C which may explain why the curve is slightly different than the other two temperatures. It was shown in section 4.1.3 that at higher temperatures more gold chloride tends to adsorb onto ferrihydrite.

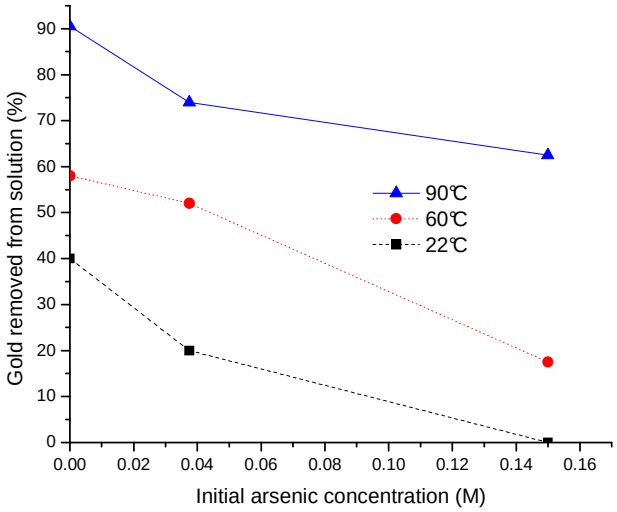

Figure 36: Effect of the initial arsenic concentration on the amount of gold (III) chloride removed from solution during iron (initial concentration of 0.15M), arsenic and gold co-precipitation experiments at various temperatures

If we assume that co-precipitation of gold chloride occurs via adsorption on ferrihydrite but not ferric arsenate an issue that arises is how gold is removed at higher temperature when the Fe/As ratio is 1, i.e. the concentration of arsenic is 0.15M. As discussed by Le Berre [62] and Le Berre *et al* [59], who studied the precipitation of poorly crystalline ferric arsenate from equimolar iron-arsenic solutions, with increasing temperature the solubility of ferric arsenate increases with a fraction of it converting to ferrihydrite. In other words the observed increase in gold removal with increasing temperature coincides with the increasing fraction of ferrihydrite as a result of incongruent precipitation/dissolution behavior on the part of ferric arsenate. Equation 33 shows the

dissociation reaction of poorly crystalline ferric arsenate to ferrihydrite in the pH range of 3 to 7.

$$FeAsO_4 \cdot (2+x)H_2O + OH^- \rightarrow FeOOH \cdot (1+x)H_2O + H_2AsO_4^- \quad (33)$$

4.2.1.2 Kinetic and equilibrium analysis

The concentration vs. time curves for the three temperature co-precipitation experiments (22, 60 and 90 °C) are shown in Figure 37. It can be seen that as the temperature of the system increases the amount of gold that co-precipitates with iron and arsenic increases as well. This trend is the same with that of gold co-precipitation with iron (section 3.1). This implies a similar mechanism, i.e. adsorption of gold (III) chloride on ferrihydrite.

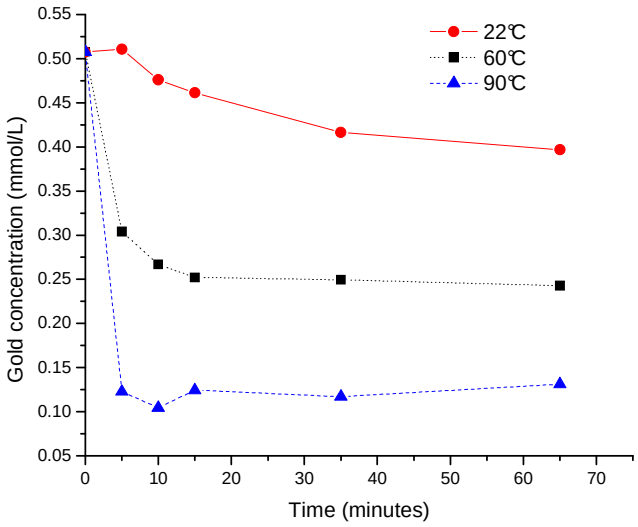

Figure 37: Effect of temperature on the gold (III) chloride concentration during iron (initial concentration 0.15M), arsenic (4/1 ratio) and gold co-precipitation experiments

Construction of the respective Van't Hoff plot (shown in Figure 38) confirmed the adsorption reaction system to be endothermic in nature.

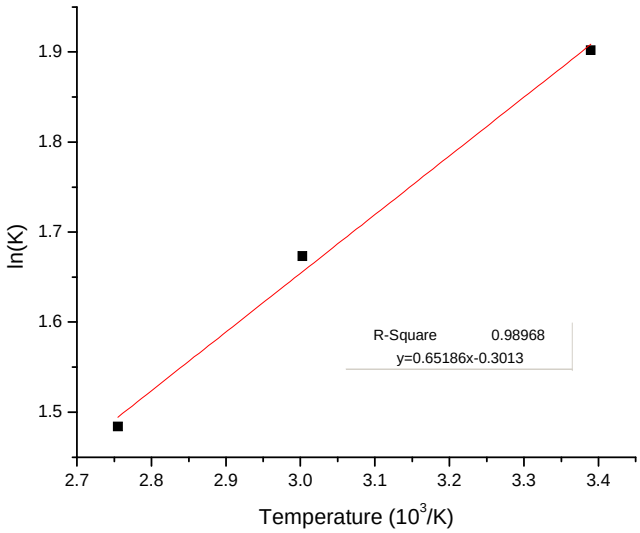

Figure 38: Van't Hoff plot of the gold (III) chloride equilibrium concentration versus temperature during iron, arsenic (4/1 ratio) and gold co-precipitation experiments

With the aid of the initial rates, the Arrhenius plot, seen in Figure 39, was built using the same method as was used in section 3.1 for the co-precipitation of gold with iron.

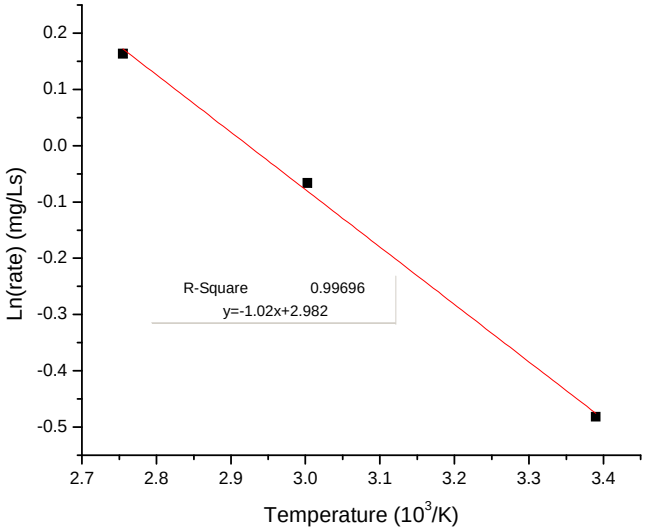

Figure 39: Arrhenius plot of the initial rate of gold (III) chloride co-precipitation versus temperature for the 4/1 iron/arsenic and gold co-precipitation experiments

The slopes for both the Arrhenius and Van't Hoff plots along with the respective activation energy and enthalpy of gold adsorption during iron and arsenic co-precipitation are tabulated in Table 6. As the activation energy value is low we may deduce, as before, that the adsorption process is mass transfer controlled. It is interesting to note that the activation energy and enthalpy values obtained from both plots are smaller than the values obtained when there was no arsenic present in solution. This is consistent with the findings that the presence of arsenic has a hindering effect on the rate and amount of gold (III) chloride co-precipitation.

Table 6: Information deduced from the Arrhenius and Van't Hoff plots of Figures Figure 38Figure 39

Plot	Slope	Activation energy/enthalpy	Interpretation
Arrhenius	-1.02	-8.48kJ/mol	Mass transfer Control
Van't Hoff	0.652	5.42kJ/mol	Chemisorption

4.2.1.3 Characterization

The XRD patterns of the co-precipitates generated from the 4/1 and 1/1 iron/arsenic experiments at 22 °C are shown in Figure 40. On the same figure the characteristic peaks of poorly crystalline ferric arsenate and 2-line ferrihydrite [45] are indicated with vertical lines. The peaks for the Fe/As molar ratio of 1 co-precipitate are stronger and less broad than the respective ones for the 4/1 co-precipitate. This implies that the crystallinity (or order) of the latter is lower than that of the former. The peaks of the 1/1 co-precipitate clearly match the peaks for poorly crystalline (amorphous) ferric arsenate, which are 28 and 58 degrees. The peaks of the 4/1 co-precipitate are very close to these values as well but judging from the low intensity and breadth of them we may consider them to comprise ferrihydrite, the latter being more amorphous (and hence less evident) than ferric arsenate itself. In the case of the 4/1 co-precipitate is impossible to have only ferric arsenate given the stoichiometry of the latter ([63,64]). At best 25% of the iron is present as ferric arsenate and 75% as ferrihydrite with some fraction of arsenate adsorbed on the latter.

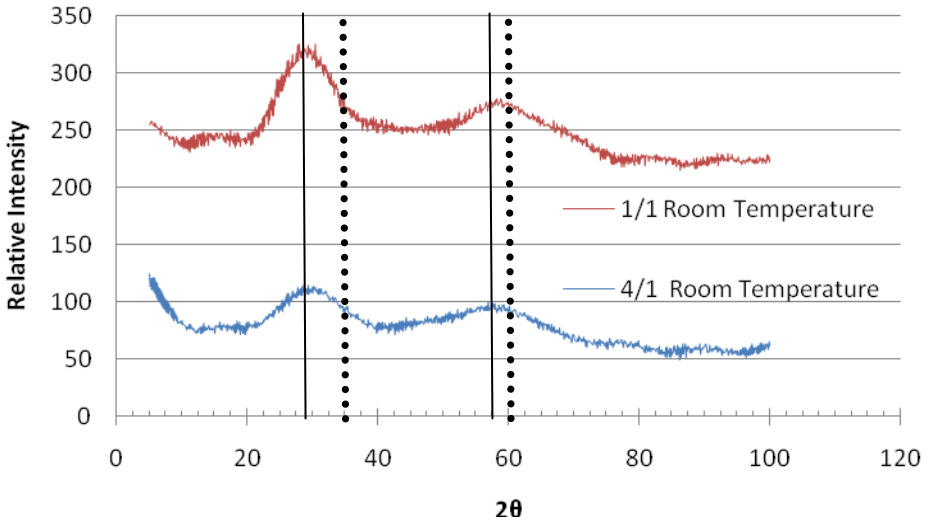

Figure 40: XRD patterns of iron-arsenic co-precipitates formed in experiments using 4/1 and 1/1 iron/arsenic molar ratios at 22 °C at pH 4. Solid vertical lines represent the reference peaks for poorly crystalline ferric arsenate, dotted vertical lines represent the reference peaks for ferrihydrite

The XRD patterns produced for the co-precipitates obtained from 4/1 iron/arsenic molar ratio experiments at 22 and 90 °C are seen in Figure 41. The characteristic peaks of poorly crystalline ferric arsenate (28 and 58) and ferrihydrite (34 and 61) are represented by vertical lines in the figure. As previously discussed, the peaks obtained for the 4/1 co-precipitate at 22 °C display characteristics of being a mixed co-precipitate: comprised of both poorly crystalline ferric arsenate and ferrihydrite. The peaks of the co-precipitate from the 4/1 experiment at 90 °C is a good match to the reference patterns of ferrihydrite. An increase in temperature has been shown by LeBerre *et al.*[62] to increase the amount of ferrihydrite and decrease correspondingly the amount of ferric arsenate formed from 1/1 iron/arsenic co-precipitation tests. This behavior, which arises from the incongruent dissociation of poorly crystalline ferric arsenate (seen in (Equation 33), is supported by the XRD pattern for the 4/1 experiment at 90 °C that matches the ferrihydrite pattern. Hence as mentioned earlier gold chloride co-precipitation was favored at higher temperature (Figure 37) is indeed due to the prevalence of ferrihydrite formation.

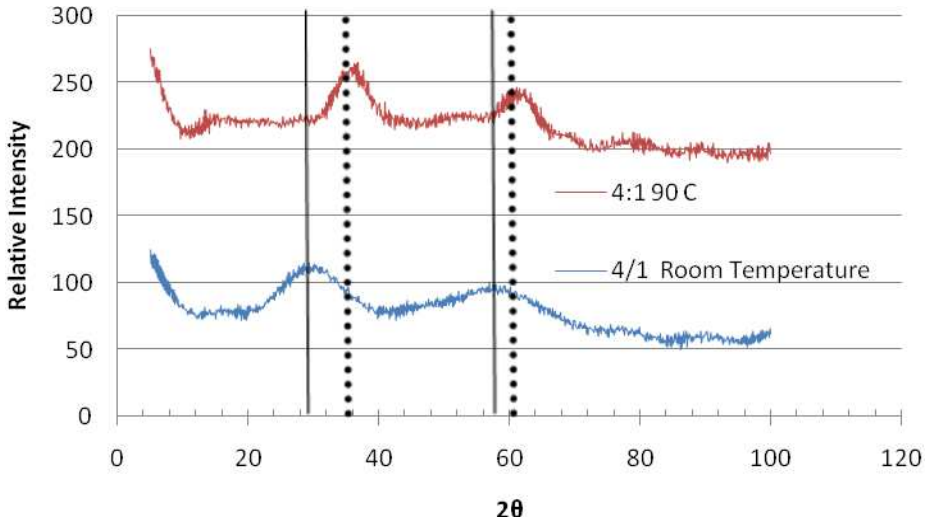

Figure 41: XRD patterns of iron-arsenic co-precipitates formed in experiments using a 4/1 molar ratio of iron/arsenic at 22 and 90 °C produced at pH 4. Solid vertical lines represent the reference peaks for poorly crystalline ferric arsenate, dotted vertical lines represent the reference peaks for ferrihydrite

4.2.2 Precipitation of crystalline scorodite

In the previous experiments the neutralization of the iron (III) sulphate-arsenic (V) solutions to pH 4 led to the precipitation of a mixture of poorly crystalline ferric arsenate and ferrihydrite. However, it is possible upon maintaining the pH below a certain critical value at a temperature above 80 °C and in the presence of seed as described by Demopoulos' research group [47, 48 64, 65, 66] to precipitate arsenic in the form of crystalline scorodite. It was decided to verify if gold (III) chloride would co-precipitate with scorodite.

Crystalline scorodite was precipitated heterogeneously using hydrothermal scorodite seed [66]. X-ray diffraction patterns were obtained for the powder produced from the heterogeneous co-precipitation experiment in order to ascertain the compound formed.

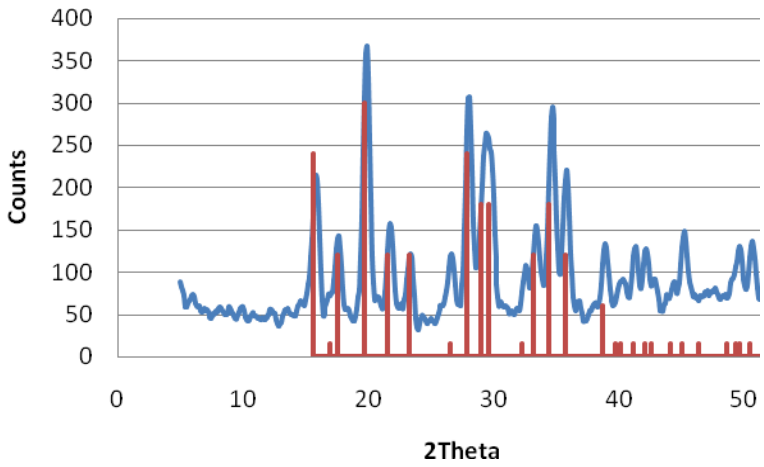

Figure 42: XRD pattern of scorodite produced heterogeneously along with reference pattern (red sharp lines)

The pattern obtained, shown in Figure 42, is an excellent match to the reference pattern and exhibits a very high degree of crystallinity. There was no evidence of amorphous (poorly crystalline) ferric arsenate. The well grown and crystalline scorodite precipitate had the morphology shown in Figure 43. This morphology shows similarities to the scorodite formed by Singhania *et al.* [66] suggesting the successful heterogeneous deposition of scorodite upon the seed.

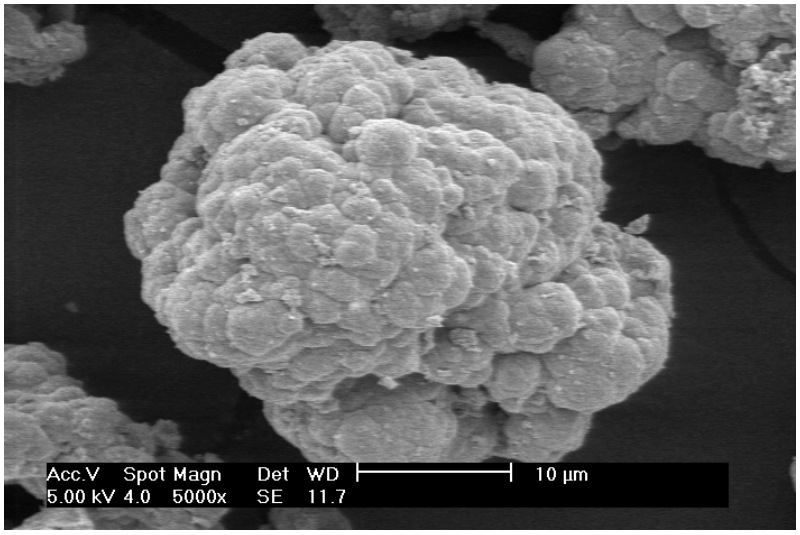

Figure 43: FEG-SEM image of scorodite precipitate obtained during 12 hour atmospheric heterogeneous precipitation at 90 °C

The precipitation of scorodite occurred over a period of twelve hours and the relevant concentration data is plotted in Figure 44.

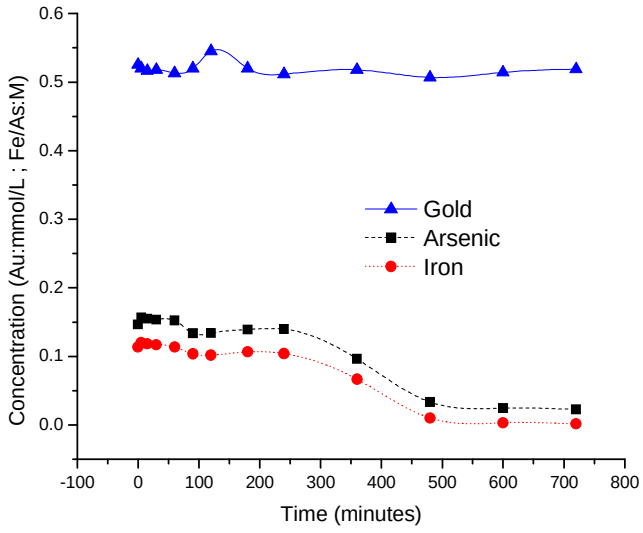

Figure 44: Gold, iron and arsenic concentrations during heterogeneous precipitation of scorodite using hydrothermal scorodite as starter seed

Figure 44 shows that there is a certain induction period before iron and arsenic begin to precipitate, following the same path afterwards. By the end of the experiment 98% of iron and 85% of the arsenic had precipitated. The molar ratio of precipitated amounts of iron and arsenic was essentially one in agreement with the stoichiometry of scorodite ($FeAsO_4 \cdot 2H_2O$) (0.06 moles arsenic vs. 0.055 moles iron precipitated). There was no gold (III) chloride co-precipitation occurring during the precipitation of scorodite as was the case with the poorly ferric arsenate formed at Fe/As=1 and 22 °C. This implies that gold (III) chloride cannot adsorb nor become incorporated via substitution of Au^{3+} for Fe^{3+} in the scorodite structure.

4.2.3 Conclusions

Gold (III) chloride was found to co-precipitate during the precipitation of amorphous ferric arsenate/ferrihydrite from mixed iron-arsenic solutions at pH 4. The presence of arsenic causes a reduction in the amount of gold that co-precipitates. At 22 °C and a Fe/As molar ratio equal to one gold was found to have co-precipitated. However, upon temperature elevation or an increase in the amount of Fe (Fe/As>1) the amount of gold that co-precipitated increased.

Finally, there was no decrease in gold concentration during atmospheric (90 °C) precipitation of scorodite. It was concluded that gold chloride cannot adsorb on ferric arsenate/scorodite or become incorporated via substitution. Instead any gold that co-precipitates with iron and arsenic occurs via its adsorption on ferrihydrite surfaces albeit at lower extent than in the absence of arsenic.

Chapter 5: Gold behavior during autoclave precipitation

During pressure oxidation pyrite and arsenopyrite are oxidized. As iron and arsenic are released into solution they immediately begin reacting with each other to form new "in-situ" compounds such as hematite, jarosite, scorodite and others. With the proper complexing agents, such as an excess of chloride ions, gold complexes may form as well, as per the discussion in the literature review chapter. It is of interest to know, if gold chloro-complexes are indeed present, how they would behave during in-situ iron and arsenic compound precipitation. Will they stay in solution, adsorb or become incorporated into these in-situ forming compounds or simply reduce to the metallic state? It is the scope of this section to investigate these questions. This investigation involved a selection of conditions in terms of temperature and solution composition favoring the formation of specific compounds and monitoring the co-precipitation behavior of gold chloride. The list of experiments performed along with the various conditions applied is given in Table 3 of Chapter 3.

5.1 Co-precipitation of gold with hematite

The precipitation of hematite is a common occurrence in many hydrometallurgical processes including the zinc, nickel, copper and gold industries. Hematite may precipitate in-situ during the refractory gold ore autoclave oxidation process.

Conditions were chosen so that the formation of hematite would be favored in order to observe its interaction with gold (III) chloride. On the basis of previous work performed at McGill [22] the conditions chosen involved the hydrolysis of a ferric sulphate solution with the initial pH set at 1 and an initial iron concentration equal to 0.15M. In addition the solution contained the standard 100 mg/L Au ($5x10^{-4}$ M $HAuCl_4$) plus 0.05 M HCl (Cl/Au molar ratio =100). After one hour (unless otherwise stated) of residence time at ≥ 200 °C the solution was analyzed for gold and iron content and the solids were subjected

to characterization. A heat up period of 30 minutes was required to reach the target temperature. This is not included in the reported residence times.

The formation of hematite was confirmed by XRD analysis. The XRD pattern of the precipitate produced at 200 °C is shown in Figure 45: XRD pattern of hematite precipitated at 200 °C for 60 minutes (30 minute ramp up time not included) with an initial iron concentration of 0.15M and hematite reference. Similar patterns were obtained at higher temperature. Chemical analysis by digestion showed the hematite precipitate to contain between 66.5 and 67.3 % iron. This value is comparable to values obtained by Cheng and Demopoulos [22] at similar conditions (63.3% at 0.2 M initial iron concentration).

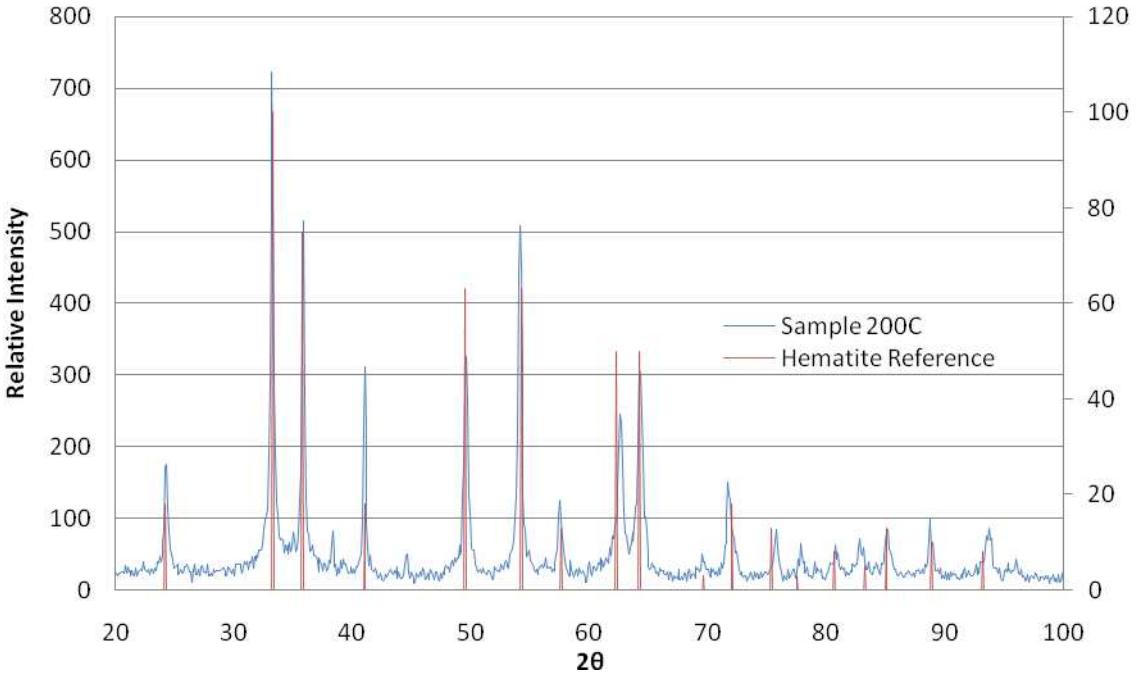

Figure 45: XRD pattern of hematite precipitated at 200 °C for 60 minutes (30 minute ramp up time not included) with an initial iron concentration of 0.15M and hematite reference

The concentration of gold in solution was measured prior to and after the precipitation of hematite to determine the deportment of gold. Three tests were performed at

increasing retention times at 200 °C, namely 30, 60 and 90 minutes. The results are plotted in Figure 46.

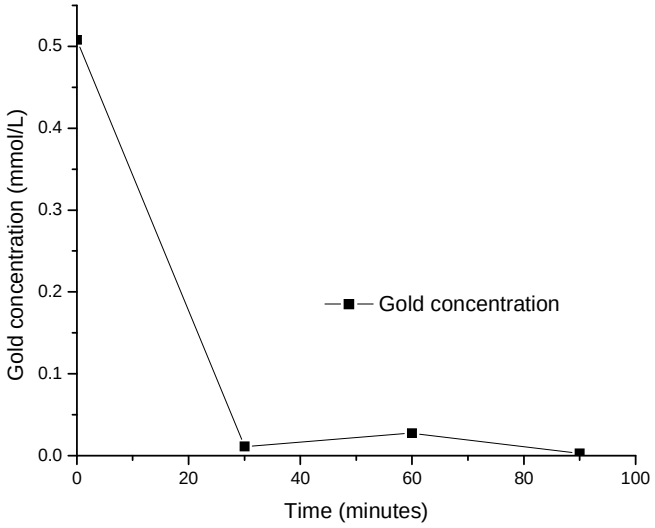

Figure 46: Gold concentration change with retention time (disregarding heat up) during hydrolytic precipitation of hematite at 200 °C

Figure 46 shows that gold does in fact co-precipitate with iron during the formation of hematite in the autoclave. Similar experiments were performed at higher temperatures to cover the whole POX temperature range and obtain additional confirmatory data. The collected data is summarized in Figure 47.

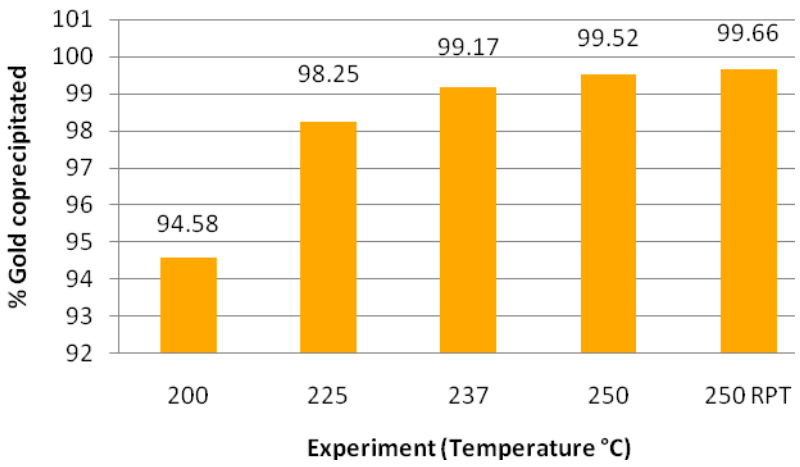

Figure 47: Percentage of gold that co-precipitated during formation of hematite at various temperatures after 1 hour plus 30 minutes of heating up

It can be seen that as the temperature is increased the amount of gold which reports to the forming hematite increases as well (Figure 47). However, given the unavoidable experimental error it can be said that for all practical purposes all gold co-precipitated at 225 °C.

As discussed in the previous chapter, the mechanism by which gold co-precipitates can be via adsorption (onto hematite [3] in the present case) or via reduction to metallic gold. To distinguish between the two forms of co-precipitated gold diagnostic leaching in HCl and *aqua regia* media was performed. *Aqua regia* provides the necessary oxidizing environment to dissolve metallic gold whereas simple HCl does not. The obtained data from the diagnostic leaching tests is summarized in Table 7. As it can be seen approximately half of the gold is present in metallic state and the other half in an adsorbed form.

Table 7: Nature of gold found in hematite precipitates at 200 °C

Experiment	Weight % Au (g/g) Adsorbed	Weight % Au (g/g) Metallic	Weight %Au (g/g) Total
200 °C 30min	0.246	0.349	0.596

200 °C 60min	0.332	0.213	0.546
200 °C 90min	0.280	0.245	0.526

The adsorption of gold chloride on hematite is envisioned to occur in a similar manner as it occurs on ferrihydrite. As discussed by Nechayev [3], gold chloro-complexes may adsorb onto the surface of hematite as per the following reaction:

$$\equiv FeOH + AuCl_4^- \rightarrow \equiv FeOHAuCl_3 + Cl^- \quad (34)$$

However, the mechanism responsible for the reduction of part of the gold chloride to metallic gold is still elusive. It is recalled per theoretical analyses presented in Chapter 2, that the stability (resistance to reduction) of gold tetrachloride ions decreases with increasing temperature on one hand and increase with increasing excess chloride ion concentration on the other. Thus as per theoretical data plotted in Figure 13 of Chapter 2, a 100mg/L Au (as $AuCl_3$) concentration is supposed to remain stable in solution at 200 °C when the excess chloride ion concentration is 100 as was the case with the tests of Table 7. The fact that gold was nevertheless reduced in the actual experiment may reflect error with the thermodynamic data on which the theoretical OLI calculations are based on. This is not unlikely given the inevitable uncertainty with high temperature data extrapolation. Another possible cause for this behavior may have been the presence of a reducing agent, such as ferrous ions. Given the small concentration of gold ($5x10^{-4}$ M) it would take three times as much iron, see Equation 35, to be present as ferrous, which corresponds to approximately 0.4-0.5% of the 0.15M ferric sulphate used, not an unrealistic scenario.

$$AuCl_4^- + 3Fe^{2+} \rightarrow Au + 3Fe^{3+} \quad (35)$$

5.2 Co-precipitation of gold with jarosite

Autoclave operating conditions are more complex than laboratory scale experiments can account for. There are several different impurities and non-metallic ions which are found

in solution from the waters used or from the ores themselves. For this reason another iron compound that often forms and needs to be investigated is jarosite. Of the various forms of jarosites, natrojarosite ($Fe_3Na(SO_4)_2(OH)_6$) formed in the presence of sodium is the most common type. In order to form natrojarosite, sodium was added in a proper molar ratio to that found in the expected solids at 200 °C (3/1 Fe/Na). Natrojarosite was indeed formed under these conditions as it is confirmed with the XRD pattern in Figure 49.

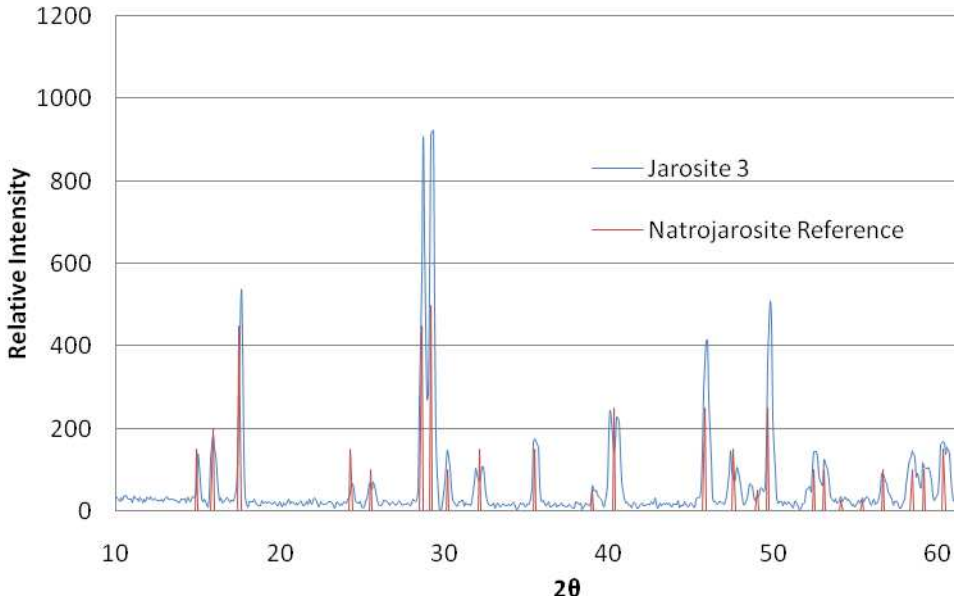

Figure 48: XRD pattern of natrojarosite formed at 200 °C and natrojarosite reference

The formation of jarosite was further supported by the Raman spectroscopic analysis as it can be verified with the results in Figure 49 below.

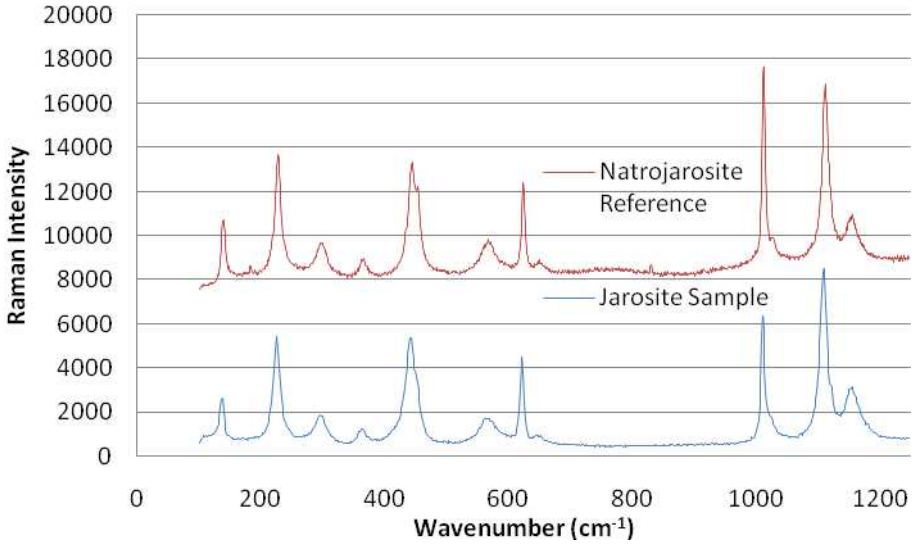

Figure 49: Raman spectra of natrojarosite precipitate formed at 200 °C and reference material

In contrast to hematite precipitation no gold was found to co-precipitate during the formation of natrojarosite at 200 °C. This is clearly seen with the data plotted in Figure 50. To be certain about this behavior, additional tests ("Jarosite 3" and "Jarosite 4")[2] were run with exactly the same results. Analysis of the jarosite solids via both HCl and *aqua regia* yielded a so very small an amount of gold that it was below the accepted detection limit, thus within experimental error essentially no gold was found. In other words in this case gold chloride neither adsorbed nor was chemically reduced.

[2] During "Jarosite 2" there was a pressure leak and thus the test was aborted

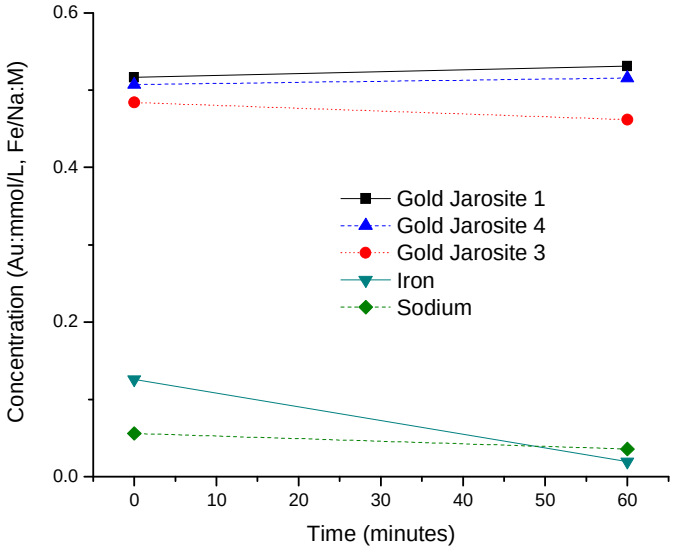

Figure 50: Gold, iron and sodium concentration profiles during triplicate natrojarosite precipitation tests at 200 °C

The lack of adsorption may arise from the different surface characteristics of jarosite like it happened with scorodite in Chapter 4. Likewise, it may be the sodium ions that hindered the adsorption of gold chloride ions onto the forming precipitate surface as it was observed by Machesky *et. al* [2] during adsorption tests involving gold chloride and goethite in the presence of sodium nitrate. However, as gold chloride remains in soluble form it suggests that there were no redox reactions occurring either. This effect remains a question since similar behavior as was observed with hematite (similar iron concentration and Cl/Au molar ratio used) would have been expected. The fact that no reduction of gold chloride to metallic gold was observed it may imply that as per Figure 13 the Cl/Au=100 ratio is sufficient to stabilize gold chloride and no significant amount of ferrous iron is present to cause reduction. The absence of reduction may suggest that a prerequisite for gold reduction is that gold chloride must first adsorb and that reduction is heterogeneous in nature. In other words it is postulated that upon adsorption, an alteration in surface gold chloride complex formation leads to lower stability and hence easier reduction. Further research will be required to verify this postulation.

5.3 Co-precipitation of gold with iron-arsenate phases

As stated, arsenic is often present in pressure oxidation feedstocks. The iron/arsenic system is more complex than the iron system under autoclave conditions. Several compounds may form depending on variables such as the iron/arsenic molar ratio and temperature as discussed in Chapter 2.

Three operating conditions were chosen with the goal of intentionally forming different ferric arsenate compounds: scorodite ($FeAsO_4 \cdot 2H_2O$) at 200 °C with a ratio of Fe:As of 1:1, ferric arsenate sub-hydrate (FAsH, ($FeAsO_4$ · 0.75H2O) at 225 °C with a ratio of Fe:As of 1:1) and finally basic ferric arsenate sulphate (BFAS, $(Fe[(AsO4)_{1-x}(SO4)_x(OH)_x] \cdot wH_2O)$ at 225 °C with a ratio of Fe:As of 4:1. Using a combination of XRD, IR and Raman spectroscopy the solids collected from these tests were identified as per reference spectra published by Gomez *et al.* [37].

5.3.1 Characterization of iron-arsenate precipitates

The XRD pattern of Figure 51 confirms that the test performed at 200 °C produced scorodite as intended. However, it can be seen that there exist some unidentified peaks or slight discrepancies, which suggest that possibly another phase is present. Referring to the Raman bands in Figure 52 we see evidence, as in the XRD, that scorodite is present. But in addition the presence of FAsH is evident as well. As it has been reported by Gomez *et al.* [36] scorodite is metastable at 200 °C converting to FAsH with time. It is obvious that the produced precipitate is more representative of a mixture of scorodite and FAsH, this similarity is shown with the reference spectrum labeled “FAsH+Scorodite” taken from Gomez [67].

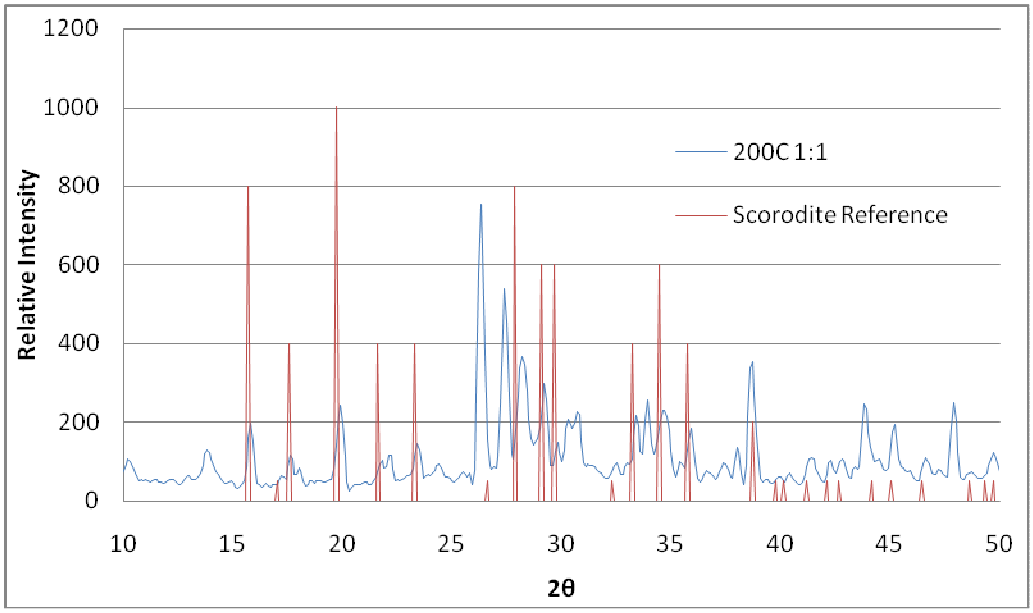

Figure 51: XRD pattern of scorodite precipitate produced from a 1:1 Fe(III)/As(V) solution heated at 200 °C for 1 hour plus a 30 minute ramp-up

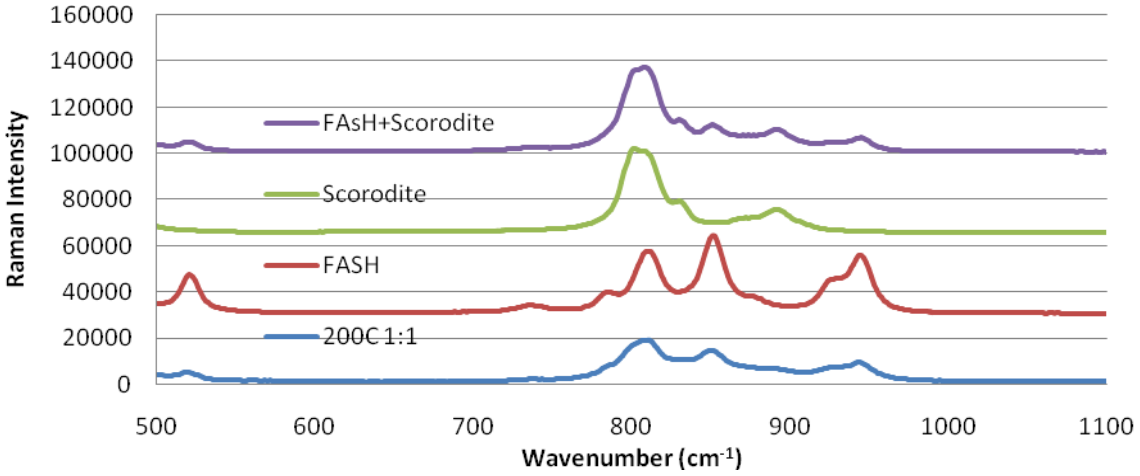

Figure 52: Raman spectra of 200 °C 1:1 Fe(III)/As(V) scorodite precipitate compared to scorodite and FAsH references

Upon temperature elevation to 225 °C, the precipitate collected from the 1:1 Fe:As experiment proved to be pure FAsH as expected. The respective FTIR and Raman spectra can be seen in Figure 53.

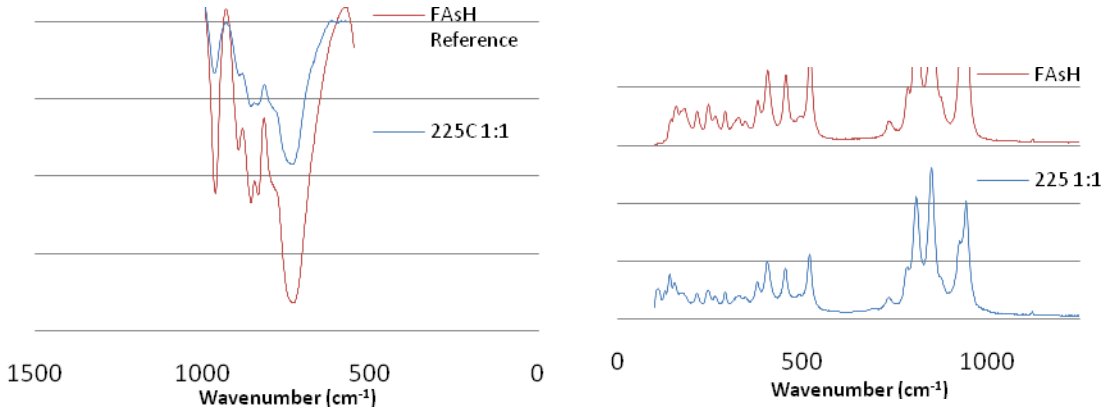

Figure 53: IR (left) and Raman (right) spectra for 225 °C 1:1 Fe(III)/As(V) FAsH precipitate and FAsH reference spectra

Finally the FTIR spectra in Figure 54 (left) confirms that the precipitate produced at 225 °C with 4:1 F/As molar ratio was BFAS. The Raman peaks in Figure 54 (right) also match the characteristic peaks of BFAS as determined by Gomez *et al*.[37].

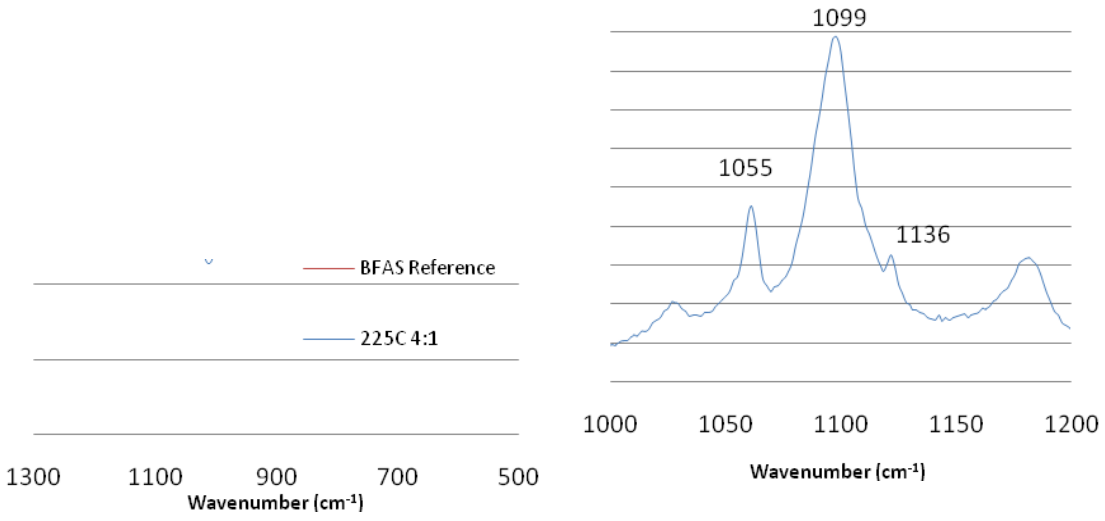

Figure 54: IR(left) and Raman(right) spectra for 225 °C 4:1 Fe(III)/As(V) BFAS precipitate and BFAS reference spectra

5.3.2 Deportment of gold

The behavior of gold (in terms of concentration change in solution) during precipitation of scorodite/FAsH at 200 °C is shown in Figure 55. Figure 55 reveals that essentially all of the gold co-precipitates with scorodite and FAsH. Similar results were produced at higher temperature and Fe/As ratio, conditions that favored the precipitation of FAsH and BFAS, as shown in Figure 56. These results are in agreement with the behavior of gold during hematite precipitation (Section 5.1) but do not agree with the scorodite test performed under atmospheric pressure at 90 °C (Section 4.3.2).

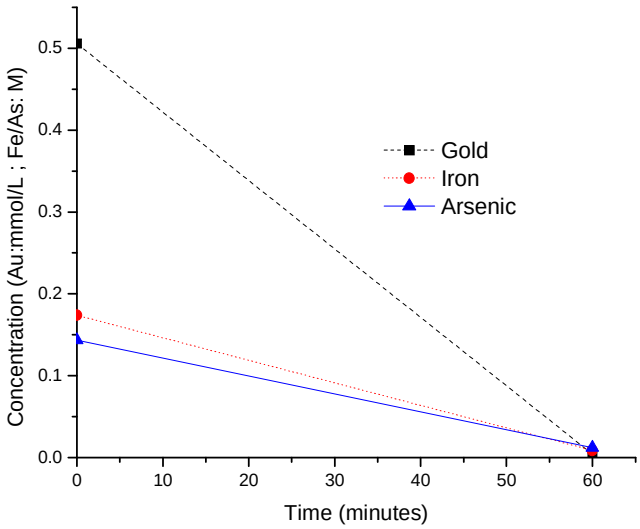

Figure 55: Gold, iron and arsenic concentration profiles during precipitation of scorodite/FAsH at 200 °C (Fe/As= 1:1)

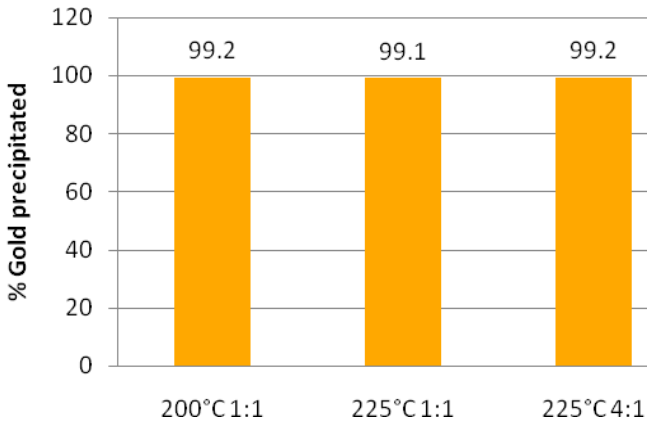

Figure 56: Percentage of gold that co-precipitates during formation of iron-arsenate phases (scorodite/FAsH at 200 °C, FAsH at 225 °C 1:1 and BFAS at 225 °C 4:1) at various temperatures after 1 hour hydrolysis ([Fe] initial= 0.15M, 100mg/L $HAuCl_4$, Cl/Au=100)

Diagnostic leaching on the produced precipitates generated the results summarized in Table 8: Distribution . There we can see gold to have co-precipitated in two forms, namely oxidized (i.e. Au^{3+} or $AuCl_3$) and metallic. These results should be considered semi-quantitative as the relative distribution of oxidized and metallic gold does not seem to provide a certain trend. Nevertheless it is clear that both forms of gold are present. Let us discuss the possible underlying mechanisms for the presence of oxidized and metallic gold in the iron-arsenate precipitates.

In terms of the oxidized gold we may have either adsorption of gold chloride on scorodite/FAsH/BFAS or incorporation in them via substitution of Au^{3+} for Fe^{3+}. During precipitation of crystalline scorodite at 90 °C (section 4.3.2) no co-precipitation of gold by either mechanism was observed. The difference between the two series of tests, atmospheric precipitation of scorodite and autoclave precipitation of scorodite/FAsH/BFAS, is that in the case of the former precipitation was heterogeneous in nature, involving seeding while in the latter precipitation took place through homogeneous nucleation. Since adsorption of gold (III) chloride was not observed during heterogeneous atmospheric precipitation of scorodite it is remotely possible that during

homogeneous precipitation in the autoclave some Au^{3+} becomes trapped in the iron-arsenate structure due to some apparent similarity with the trivalent ferric ion.

As for the formation of metallic gold this may be thought to occur via reduction of part of the substituted Au^{3+} due to reaction with trace amounts of Fe^{2+} or As^{3+} at least at 200 °C. At the elevated temperature (225 °C) additional reduction could have occurred by reaction with water due to inefficient excess Cl ion concentration (Cl/Au=100 as opposed to the required 143 ratio) as discussed in the literature review chapter.

Table 8: Distribution and nature of gold reported in autoclave iron-arsenate precipitates

Experiment/Precipitate	Weight% Au in precipitate Oxidized	Weight% Au in precipitate Metallic	Weight% Au in precipitate Total
200 °C 1:1/Sc+FAsH	0.0936	0.0977	0.1914
225 °C 1:1/FAsH	0.1608	0.0317	0.1925
225 °C 4:1/BFAS	0.0943	0.2549	0.3493

5.4 Conclusions

At elevated temperatures and pressures several precipitates form depending on the autoclave operating conditions. Gold chloride was found to exhibit different co-precipitation behavior depending on the phase and condition of precipitation. In the case of hematite formation 96% of the soluble gold was found to co-precipitate at 200 °C and above 99% at 225, 237 and 250 °C. Approximately half of the gold chloride adsorbs on the surface of hematite and the other half is reduced to metallic state. Similar results were observed in the case of the three iron-arsenate phases: scorodite, FAsH and BFAS although in this case substitution rather than adsorption is suspected. The partial reduction to metallic gold may have involved trace amounts of ferrous or arsenite impurities or inadequate amounts of excess chloride ions required to stabilize gold chloride. Finally, as an exception to the general trend listed above, if sodium and

iron form natrojarosite there is no loss of gold from solution neither via adsorption nor by reduction.

Chapter 6: Global Conclusions

In this thesis the behavior of gold (III) chloride during precipitation of iron and arsenate under hydrothermal processing (i.e. pressure oxidation, 200-250 °C) or neutralization (using 3M MgO slurry) of acidic solutions (22-90 °C) has been investigated. In particular the co-precipitation of gold chloride via adsorption, substitution or reduction was examined via the treatment of solutions with variable iron (III) sulphate concentrations (with or without arsenate present). All solutions contained 100 mg/L Au ($5x10^{-4}$ M as $HAuCl_4$) and an excess of chloride ions equal to Cl/Au molar ratio of 100. The major conclusions drawn from this research work are given in this Chapter.

Initial neutralization of iron-free acidic water containing 100 mg/L ($5x10^{-4}$ M) Au with a molar ratio of Cl/Au of 100 over the pH range of 2 and 8 showed the gold tetrachloride complex to be stable in solution. Upon MgO slurry neutralization to pH 4 and agitation for 60 min the various (arsenic-free) ferric sulphate solutions resulted in ferrihydrite precipitation over the entire temperature (22-90 °C) and concentration range (0.075, 0.15, 0.3M). Along with ferrihydrite it was found that various amounts of gold chloride co-precipitated via adsorption. No evidence of reduction of the gold chloride complex to metallic gold was found. The amount of gold co-precipitated increased with the initial concentration of iron and temperature. The increased gold uptake with initial iron concentration was correlated to the available surface area of ferrihydrite. Estimation of the enthalpy of adsorption indicated an endothermic chemisorption reaction to occur. Finally according to kinetic analysis of the initial rates of gold co-precipitation the overall process was found to exhibit second order dependence on initial iron concentration and mass-transfer rate limiting characteristics.

Similar experiments to the aforementioned neutralization tests were performed with solutions containing varying initial iron/arsenic molar ratios. In this case poorly crystalline ferric arsenate was found to form at ambient temperature when the Fe/As

ratio was 1. Upon elevation of the Fe/As ratio to 4 the excess iron precipitated as ferrihydrite. At higher temperatures (60-90 °C) there was a decrease in the amount of ferric arsenate forming and an increase in ferrihydrite even at Fe/As equal to one due to incongruent dissolution of the former. The co-precipitation of arsenate (either as ferric arsenate or arsenical ferrihydrite) was found to interfere or completely hinder the co-precipitation of gold chloride. Thus at 22 °C and a Fe/As molar ratio equal to one no gold was found to have co-precipitated. However, upon temperature elevation or an increase in the amount of Fe (Fe/As>1) the amount of gold that co-precipitated increased but this was lower than that co-precipitated under the same conditions in the absence of arsenic. There was an apparent correspondence between the amount of gold removed by adsorption (again no metallic gold was present) and the formation of ferrihydrite.

It was further found that during atmospheric (90 °C) heterogeneous (on seed) precipitation of crystalline scorodite from Fe/As equal to one solutions no gold chloride co-precipitation takes place. It was concluded that gold chloride cannot adsorb on ferric arsenate/scorodite or become reduced to metallic gold under the applied conditions (Cl/Au=100).

The behavior of gold (III) chloride in solution was further investigated by observing its co-precipitation behavior under high temperature, autoclave conditions. Several precipitates were formed by choosing specific solution chemistries with each solution containing the standard 100 mg/L Au and the Cl/Au molar ratio of 100. In the case of hematite formation 96% of the soluble gold was found to co-precipitate at 200°C and above 99% at 225, 237 and 250°C. Approximately half of the gold chloride was found to adsorb on the surface of hematite and the other half to be reduced to metallic state. Similar results were observed in the case of the three iron-arsenate phases: scorodite, ferric arsenate sub-hydrate (FAsH) and basic ferric arsenate sulphate (BFAS). The partial reduction to metallic gold may have involved trace amounts of ferrous or arsenite impurities, inadequate amounts of excess chloride ions required to stabilize gold chloride (e.g. at 225 °C) or simply reduction of gold chloride stability due to complex

alteration upon adsorption. Finally, as an exception to the general trend of gold chloride behavior during autoclave phase precipitation, it was determined that if sodium and iron form natrojarosite there is no loss of gold from solution neither via adsorption nor by reduction.

Given the above findings it becomes apparent that gold chloride complexes that may form[3] during pressure oxidation or pressure leaching (like the CESL process) operations may either stay in solution and report to the neutralization solids (as adsorbed species), if the Cl/Au ratio> 150, or precipitate in situ in the autoclave. In the latter case part of the gold may be in metallic form hence recoverable in the subsequent cyanidation step. However the remaining gold (as adsorbed or incorporated via substitution) may be lost if not properly diagnosed and recovered.

Finally, further research will be required to elucidate the true underlying factor(s) responsible for the complex behavior of gold chloride during autoclave precipitation. In addition tests involving pressure oxidation of pyrite/arsenopyrite in the presence of gold chloride under various conditions should be undertaken to evaluate if the findings from this work can be applied to actual pressure oxidation situations.

[3] The formation of such complex, as discussed in Chapter 2, will depend on the Cl/Au ratio and the prevailing oxidizing conditions in the autoclave.

Appendix A. Additional experimental data

In this section additional data collected during the experiments described in Chapters 4 and 5 is presented. These figures and information are presented here to provide additional insight into the behavior of the systems described during the co-precipitation of gold (III) chloride.

A.1 Data from ambient pressure neutralization experiments

During the precipitation of iron and arsenic in co-precipitation experiments at 22 °C there is a relatively complete removal of both iron and arsenic ions from solution. Figure 57 shows that after 5 minutes at pH 4 there is nothing left in solution except for a very small amount of arsenic (approximately 0.01M).

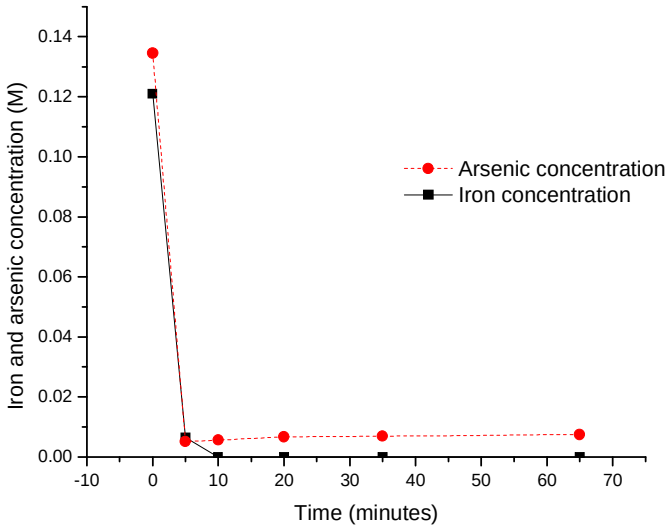

Figure 57: Concentration profiles for iron and arsenic concentration during iron and arsenic co-precipitation at a 1/1 molar ratio (0.15M) at 22 °C

This matches very well the precipitation behavior of iron and arsenic at 90 °C where again after 5 minutes there is no iron left in solution and a very small amount of arsenic, as seen in Figure 58.

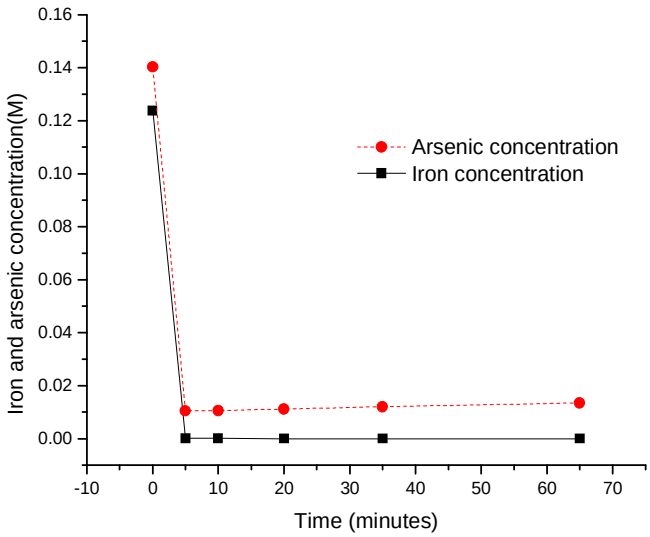

Figure 58: Concentration profiles for iron and arsenic concentration during iron and arsenic co-precipitation at a 1/1 molar ratio (0.15M) at 90 °C

In Chapter 4, heavy consideration was given to the amount of gold (III) chloride there was in solution during the course of co-precipitation experiments. One example, showing the quick precipitation of iron and arsenic after 5 minutes, was provided to exemplify the phenomena. Further data is provided in Figure 59 and Figure 60.

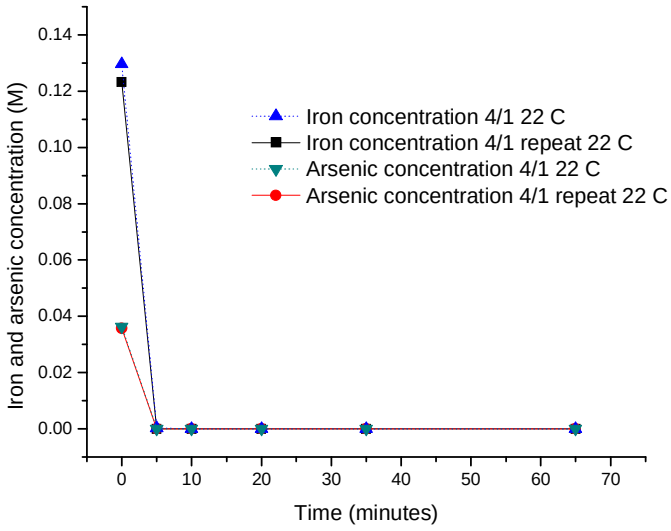

Figure 59: Concentration profiles for iron and arsenic concentration during iron (0.15M) and arsenic co-precipitation at a 4/1 molar ratio at 22 °C

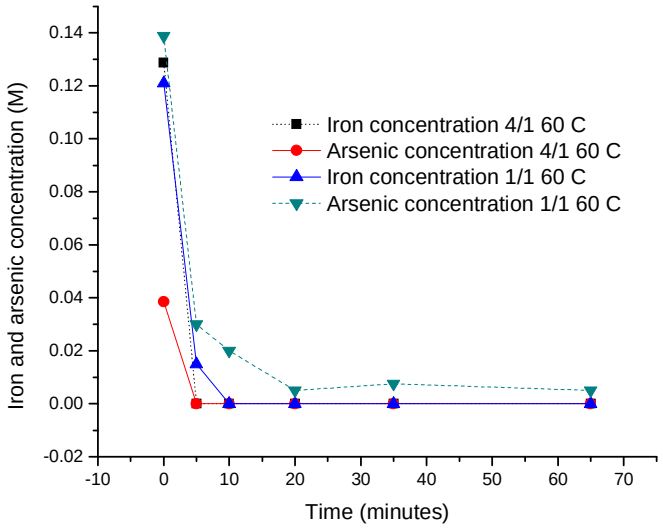

Figure 60: Concentration profiles for iron (0.15M) and arsenic concentration during iron and arsenic co-precipitation experiments at a 4/1 and 1/1 molar ratio at 60 °C

A.2 Data from autoclave experiments

During the precipitation under autoclave conditions of iron-arsenate products, data was collected via diagnostic leaching to ascertain the contents. From this characterization the solids content was found in terms of arsenic and iron content. These results are tabulated in Table 9. The most important type of information in this table are the results for the iron-arsenate tests (Scorodite+FAsH, FAsH and BFAS). These results show that there is a molar excess of iron (up to 20%) in each of these cases. As the products should form a 1:1 molar ratio (or 4:1 molar ratio) of iron to arsenic we can conclude that there must be some systematic error with the performed analysis or that hematite may have formed during these experiment. The latter was not observed by Gomez and Demopoulos [36] who had studied this system extensively, thus it is rather unlikely.

Table 9: Iron and arsenic content of precipitates formed during autoclave precipitation experiments

	Weight %		**Molar equivalent**	
	Fe	**As**	**Fe**	**As**
Precipitate				
Hematite 30m	67.40		1.207	
Hematite 60m	67.15		1.202	
Hematite 90m	66.56		1.192	
Jarosite 1	38.42		0.688	
Jarosite 3	35.25		0.631	
Jarosite 4	35.05		0.628	
Scorodite+FAsH	27.33	29.69	0.489	0.396
FAsH	26.81	31.35	0.480	0.418
BFAS	31.57	9.43	0.565	0.126

References

1. Garofalo, D., *Aemtoday: Agnico-Eagle Mines-Limited 2009 Annual Report*. 2009, Agnico Eagle Mines: Toronto, Canada.
2. Machesky, M., Andrade, W.O., Rose, A.W, *Adsorption of gold(III)-chloride and gold(I)-thiosulfate anions by goethite.* Geochemica et Cosmochimica Acta, 1990. 55: p. 769-776.
3. Nechayev, Y. A, *The effects of solution composition on the adsorption of gold(III) complexes on hematite.* Geochem. Int., 1984. 21(4): p. 87-93.
4. Marsden, J., House, I. *The chemistry of gold extraction*. 2nd ed. 2006: Ellis Horwood. New York, NY
5. Cabri, L.J., Chryssoulis, S.L., de Villiers, J.P.R., Laflamme, J.H.G., Buseck, P.R, *The nature of "invisible" gold in arsenopyrite.* The Canadian Mineralogist, 1989. 27: p. 353-362.
6. Cabri, L.J., Newville, M., Gordon, R.A., Crozier, E.D., Sutton, S.R., McMahon, G., Jiang, D.T, *Chemical speciation of gold in arsenopyrite.* The Canadian Mineralogist, 2000. 38: p. 1265-1281.
7. Benzaazoua, M., Marion, P., Robaut, F., Pinto, A, *Gold-bearing arsenopyrite and pyrite in refractory ores: analytical refinments and new understanding of gold mineralogy.* Mineralogical Magazine, 2007. 71(2): p. 123-142.
8. Maddox, L.M., Bancroft, G.M., Scaini, M.J., Lorimer, J.W, *Invisible gold: comparison of Au deposition on pyrite and arsenopyrite.* American Mineralogist, 1998. 83: p. 1240-1245.
9. Demopoulos, G.P., Papangelakis, V.G., *Recent Advances in Refractory Gold Processing.* CIM Bulletin, 1989. 82(931): p. 85-91.
10. Defreyne, J., Grieve, W., Jones, D.L., Mayhew, K., ed. *The Role of Iron in the CESL Process*. Iron control technologies, ed. J.E. Dutrizac, Riveros, P.A. 2006, CIM: Montreal, Canada. 205-221.
11. Barr, G., Grieve, W., Jones, D., Mayhew, K. *The new CESL gold process*. in *ALTA 2007 Copper*. 2007 .eds. Perth, Australia: ALTA Metallurgical Services.
12. Haque, K.E., *Gold Leaching from Refractory Ores—Literature Survey.* Mineral Processing and Extractive Metallurgy Review, 1987. 26(3-4): p. 235-253.
13. Demopoulos, G.P., *Aqueous precipitation and crystallization for the production of particulate solids with desired properties.* Hydrometallurgy, 2009(96): p. 199-214.
14. Nyvlt, J., *The Oswald rule of stages.* Cryst. Res. Technol., 1995. 30(4): p. 443-449.

15. Cheng, T.C.-M., Demopoulos, G.P. *Analysis of the hematite precipitation process from a crystallization point of view*. in *EPD Congress 1997*. 1997. B. Mishra. eds. Warrendale, Pa: TMS. 599-617.

16. Posjnak, E., Merwin, H.E, *The Fe_2O_3 - SO_3 - H_2O system.* Journal of American Chemical Society, 1922. 44: p. 1965-1994.

17. Cheng, T., *Production of hematite in acidic zinc sulphate media*, .Ph.D Thesis. Materials Engineering: McGill University. 2002,Montreal, Quebec

18. Umetsu, Y., Tozawa, K., Sasaki, K, *The hydrolysis of ferric sulphate solutions at elevated temperatures.* Canadian Metallurgy Quarterly, 1977. 16: p. 111-117.

19. Tozawa, K., Sasaki, K. *Effect of coexisting sulphates on precipitation of ferric oxide from ferric sulphate solutions at elevated temperatures*. in *Symposium on Iron Control in Hydrometallurgy*. 1986. J.E. Dutrizac, Monhemius, A.J .eds. Montreal, Canada: CIM. 454-476.

20. Tozawa, K., Sasaki, K., Umetsu, Y. *The effect of the second dissociation of sulfuric acid on hydrometallurgical processes: the electrical conductivity of sulfuric acid-containing electrolytes and the hydrolysis of ferric sulfate solutions at elevated temperatures*. in *3rd international symposium on hydrometallurgy*. 1983. K. Osseo-Asare, Miller, J.D .eds. Warrendale, PA: TMS. 375-387.

21. Voight, B., Gobler, A. *Formation of pure hematite by hydrolysis of iron (III) salt solutions under hydrothermal conditions.* Cryst. Res. Technol., 1986. 21: p. 1177-1183.

22. Cheng, T., Demopoulos, G.P, *Hydrolysis of Ferric Sulfate in the Presence of Zinc Sulfate at 200 °C:Precipitation Kinetics and Product Characterization* Ind. Eng. Chem. Res., 2004. 43(20): p. 6299–6308.

23. Dutrizac, J.E., Chen, T.T, *Surface and structural impurity incorporation in iron precipitates*. in *Emerging Separation Technologies for Metals and Fuels*. 1993. V.I. Lakshmanan, Bautista, R. G., Somasundaran, P .eds. Warrendale, PA, USA: TMS. 183-198.

24. Dutrizac, J.E. *Overview of iron precipitation in hydrometallurgy*. in Crystallization and Precipitation. 1987. Strathdee G.L., Klein M.O. and Melis L.A. eds. New York, NY: Pergamon Press. 259-283.

25. Randolph, A.D., Williams, R.D., Milligan, D.A, *Hydrolysis of iron on a retained crystal bed.* Fundamentals Aspects of Hydrometallurgical Processes, 1978. Chapman, T.W .eds. 74(173): AIChE Symposium Series, New York, NY p. 89-96.

26. Das, G.K., Archarya, S., Anand., S., Das, R.P, *Jarosites: A review.* Mineral Processing and Extractive Metallurgy Review, 1996. 26(3-4): p. 185-210.

27. Rosato, L., Agnew, M.J, *Iron disposal options at Canadian Electrolytic Zinc* in *Iron control and disposal: second international symposium on Iron control in hydrometallurgy*. 1996. Dutrizac, J.E., Harris, G.B, .eds. Montreal, QC: CIM. 281-286.

28. Arregui, V., Gordon, A.R., Steintveit, G. *The Jarosite Process--Past, Present and Future*. in *Lead--Zinc--Tin '80*. 1980. M.H. Jha, Hill, S.D .eds. Warrendale, Pa: TMS. 97-123.

29. Won, C.W., Paik, Y.H, *Precipitation kinetics of hydronium jarosite at elevated temperatures.* Taehan Kumsok Hakhoe Chi, 1982. 20(7): p. 594-602.

30. Dutrizac, J.E., *The effect of seeding on the rate of precipitation of ammonium jarosite and sodium jarosite.* Hydrometallurgy, 1996. 42: p. 293-311.

31. Bolorunduro, S.A., Dreisinger, D.B., Van Weert, G, *Fundamental study of silver deportment during the pressure oxidation of sulphide ores and concentrates.* Minerals Engineering, 2003. 16: p. 695-708.

32. Papangelakis, V.G., Demopoulos, G.P, *Acid pressure oxidation of arsenopyrite: part I, reaction chemistry.* Canadian Metallurgy Quarterly, 1990. 29(1): p. 1-12.

33. Papangelakis, V.G., Demopoulos, G.P, *Acid pressure oxidation of arsenopyrite: part II, reaction kinetics.* Canadian Metallurgy Quarterly, 1990. 29(1): p. 13-20.

34. Swash, P.M., Monhemius, A.J. *Hydrothermal precipitation from aqueous solutions containing iron(III), arsenate and sulphate* in *Hydrometallurgy '94*. 1994. I.o.M. Metallurgy. eds. London, UK: Chapman and Hall. 177-190.

35. Dutrizac, J.E., Jambor, J.L, *Characterization of the iron arsenate–sulphate compounds precipitated at elevated temperatures.* Hydrometallurgy, 2007. 86: p. 147-163.

36. Gomez, M., Becze, L., Bluteau, M.C., Le Berre, J.F., Demopoulos, G.P. *Autoclave precipitation and characterization of Fe(III) - AsO_4 - SO_4 phases* in *Hydrometallurgy 2008*. 2008. C.A. Young, Tay, P.R., Anderson, C.G., Choi, Y. eds. Littleton, CO: SME. pp 1078.

37. Gomez, M., Assaaoudi, H., Becze, L., Cutler, J.N., Demopoulos, G.P, *Vibrational spectroscopy study of hydrothermally produced scorodite (FeAsO4·2H2O), ferric arsenate sub-hydrate (FAsH; FeAsO4·0.75H2O) and basic ferric arsenate sulfate (BFAS; Fe[(AsO4)1−x(SO4)x(OH)x]·wH2O).* Journal of Raman Spectroscopy, 2010: p. 212-221.

38. Mayhew, K., Parhar, P., Salomon-de-Friedberg, H. *CESL process as applied to enargite-rich copper concentrates*. in *Copper 2010*. 2010. Harre,J .eds. Hamburg, Germany: GDMB. 1983-1998.

39. Tsuchida, N., Ozaki, Y., Nakai, O., Kobayashi, H. *Development of process design for coral bay nickel project*. in *International Laterite Nickel Symposium 2004*. 2004. W.P. Imrie, Lane, D.M. eds. Warrendale, PA: TMS. 151-160.

40. Demopoulos, G.P., Zinck, J., Kondos, P.D. *Production of super dense sludges with a novel neutralization process*. in *Waste processing and recycling in mineral and metallurgical industries II*. 1995. S.R. Rao, Amaratunga, L.M., Richards, G.G., Kondos, P.D. eds. Montreal, QC: CIM. 401-412.

41. Jambor, J.L., Dutrizac, J.E, *Occurrence and Constitution of Natural and Synthetic Ferrihydrite, a Widespread Iron Oxyhydroxide.* Chemical Reviews, 1998. 98(7): p. 2549–2586.

42. Cornell, R.M., Schwertmann, U, *The Iron Oxides: Structure, properties, reactions, occurances and uses*. 2nd ed. 2003: Wiley.

43. Cudennec, Y., Lecerf, A, *The transformation of ferrihydrite into goethite or hematite, revised.* Journal of Solid State Chemistry, 2006. 179(3): p. 716-722.

44. Jia, Y., Demopoulos, G.P, *Adsorption of Arsenate onto Ferrihydrite from Aqueous Solution: Influence of Media (Sulfate vs Nitrate), Added Gypsum, and pH alteration.* Environ. Sci. Technol., 2005. 39: p. 9523-9527.

45. Jia, Y., Demopoulos G.P, *Observation of Surface Precipitation of Arsenate on Ferrihydrite.* Environ. Sci. Technol., 2006. 40(10): p. 3248-3253.

46. Chen, N., Jiang, D.T., Cutler, J., Kotzer, T., Jia, Y.F., Demopoulos, G.P., Rowson, J.W, *Structural characterization of poorly-crystalline scorodite, iron(III)-arsenate co-precipitates and uranium mill neutralized raffinate.* Geochim. Cosmochim. Acta, 2009. 73: p. 3260-3276.

47. Singhania, Q., Wang, D., Fillipou, D., Demopoulos, G.P, *Acidity, valency and third-ion effects on the precipitation of scorodite from mixed sulphate solutions under atmospheric-pressure conditions.* Metall. Mater. Trans, 2006. 37B: p. 189-197.

48. Fillipou, D., Demopoulos, G.P, *Arsenic Immobilization by controlled scorodite precipitation.* JOM, 1997: p. 52-55.

49. Jia, Y., Demopoulos, G.P, *Coprecipitation of arsenate with iron(III) in aqueous sulfate media: Effect of time, lime as base and co-ions on arsenic retention.* Water Research, 2008. 42: p. 661-668.

50. Jia, Y., G.P, *Infrared spectroscopic and X-ray diffraction characterization of the nature of adsorbed arsenate on ferrihydrite.* Geochemica et Cosmochimica Acta, 2007. 71: p. 1643-1654.

51. Henley, R.W., *Solubility of gold in hydrothermal chloride solutions.* Chemical Geology, 1973. 11: p. 73-87.

52. Lide, D.R., *CRC Handbook of chemistry and physics (*90th edition (Internet version 2010) ed. 2010, Boca Raton, USA: CRC Press/Taylor and Francis

53. Laidler, J., Sanctuary, B, *Physical Chemistry*. 4 ed. 2002, New York: Houghton Mifflin. 1060.

54. Dzombak, D.A., Morel, F.M.M., *Surface complex modelling: hydrous ferric oxide*. 1990, New York: J. Wiley and Sons.

55. Sun, T.M., Yen, W.T, *Kinetics of gold chloride adsorption onto activated carbon.* Minerals Engineering, 1993. 6(1): p. 17-29.

56. Schoonen, M., Fisher, N.S., Wente, M, *Gold sorption onto pyrite and goethite: A radiotracer study.* Geochemica et Cosmochimica Acta, 1992. 56: p. 1801-1814.

57. McDougall, G., Hancock, R.D, *Gold complexes and activated carbon.* Gold Bull., 1981. 14(4): p. 138-153.

58. Jia, Y., Demopoulos, G.P., Chen, N., Cutler, J.N., Jiang, D-T. *Preparation, characterization and solubilities of adsorbed and co-precipitated iron (III)-arsenate solids*. in *Hydrometallurgy 2003*. 2003. C. Young .eds. Warrendale, USA: TMS. 1923-1936.

59. Le Berre, J.-F., Gauvin, R., Demopoulos, G.P, *A study of the crystallization kinetics of scorodite via the transformation of poorly crystalline ferric arsenate in weakly acidic solution.* Colloids and Surfaces A: Physicochemical and Engineering Aspects, 2008. 315(1-3): p. 117-129.

60. Da Silva, G., Dlugogorski, B.Z., Kennedy, E.M, *Water-in-oil: emulsion foaming by thiourea nitrosation: reaction and mass transfer.* AIChE, Wiley Interscience, New York, NY 2006. 52(4): p. 1558-1565.

61. Smith, J.M., *Chemical Engineering Kinetics*, 1981, New York, NY: McGraw-Hill Science/Engineering/Math.

62. LeBerre, J.-F., *Synthesis, characterization and stability of arsenate-bearing materials*, in *Mining, Metals and Materials Engineering*. Ph.D Thesis. 2007, McGill University: Montreal, Canada. p. 223.

63. LeBerre, J.-F., Gauvin, R., Demopoulos, G.P, *Characterization of Poorly-Crystalline Ferric Arsenate Precipitated from Equimolar Fe(III)-As(V) Solutions in the pH Range 2 to 8.* Metallurgical and materials transactions B, 2007. 38(5): p. 751-762.

64. Dabekaussen, R., Droppert, D., Demopoulos, G.P, *Ambient pressure hydrometallurgical conversion of arsenic trioxide to crystalline scorodite.* CIM Bulletin, 2001. 94(1051): p. 116-122.

65. Demopoulos, G.P. *On the preparation and stability of scorodite*. in *Arsenic Metallurgy*. 2005. R.G. Reddy, Ramachandran, V .eds. Warrendale, USA: TMS. 25-50.

66. Singhania, S., Wang,Q., Filippou, D., Demopoulos, G.P, *Temperature and Seeding Effects on the Precipitation of Scorodite from Sulfate Solutions under Atmospheric-Pressure Conditions.* Metallurgical and Materials Transactions B, 2005. 36B: p. 327-333.

67. Gomez, M., Personal Communication. McGill Hydrometallurgy Group ,2010: Montreal, Quebec.